COLLECTIVE DIPOLE INTERACTION IN ATOM ARRAYS AND ENSEMBLES

by

Deepak Aditya Suresh

A Dissertation

Submitted to the Faculty of Purdue University

In Partial Fulfillment of the Requirements for the degree of

Doctor of Philosophy

Department of Physics and Astronomy

West Lafayette, Indiana

December 2024

THE PURDUE UNIVERSITY GRADUATE SCHOOL
STATEMENT OF COMMITTEE APPROVAL

Dr. Francis J. Robicheaux, Chair

Department of Physics and Astronomy

Dr. Chen-Lung Hung

Department of Physics and Astronomy

Dr. Qi Zhou

Department of Physics and Astronomy

Dr. Jukka I. Vayrynen

Department of Physics and Astronomy

Approved by:

Dr. Gabor A. Csathy

ACKNOWLEDGMENTS

This endeavor would not have been possible without my parents and grandparents, whose nurturing guidance and unwavering belief in me gave me the courage to pursue my interests. I'm extremely grateful to my wife, Sanjana, for her steadfast support and encouragement. She has been a constant source of strength and comfort throughout this journey.

I am immensely thankful to my advisor, Prof. Francis Robicheaux, for his incredible mentorship. His approach of giving structured guidance at the start and gradually allowing more independence as I developed was instrumental to my growth and success. I am also grateful to the members of my research group for their support, advice, and engaging conversations.

I extend my gratitude to my committee members Prof. Chen-Lung Hung, Prof. Qi Zou, and Prof. Jukka Vayrynen. I would especially like to thank Prof. Chen-Lung and his students for offering collaboration opportunities that broadened my perspectives, allowing me to gain a more interdisciplinary view of my field.

Finally, I thank my friends and family, near and far, for their constant support and encouragement. Their friendship and connection have been a source of strength and joy throughout this journey.

TABLE OF CONTENTS

LIST OF FIGURES

ABSTRACT

Collective dipole interaction has recently emerged as a powerful tool in controlling light-matter interactions. Ordered atomic arrays, in particular, enhance cooperative responses and are promising for applications in coherent control and quantum information. This thesis examines three distinct phenomena associated with collective dipole interactions. First, we study the recoil effects resulting from subradiant and superradiant emissions in sub-wavelength atom arrays. Second, we analyze the photon statistics of the emitted light in different directions and modes in the low-intensity regime. Finally, we explore the collective behavior of atoms confined near a nanophotonic micro-ring resonator, where the interplay of chiral cavity interactions and free space dipole-dipole coupling leads to novel subradiant and superradiant states.

1. INTRODUCTION

Collective dipole emissions have recently been used in many novel and interesting applications in the control of the interaction between light and matter. Reference [1] showed that when an ensemble of atoms interacts and radiates collectively, the dynamics are altered due to the interference of the outgoing light waves. This has led to abundant research investigating a wide variety of concepts including subradiance, superradiance, and collective Lamb shifts [2]–[12]. These concepts are also being used in establishing a link between atoms separated by more than their resonant wavelength [13]–[15].

Placing the atoms in uniformly spaced arrays will enhance the co-operative response resulting in increased coupling between the atoms and radiation field [16]–[24]. Recent experiments have achieved the realization of arrays of atoms with a high level of filling efficiency [25]–[31]. Closely packed atom arrays, where the atom separation is less than the wavelength of the light, have been found to have highly reflective properties due to the cooperative dipole interactions [18], [19], [31]. Reference [32] showed that atomic arrays can be used to coherently focus or steer light by individually varying the detuning of the atoms. Such arrays have also been suggested to be efficient options for photon storage [33]–[35].

Non-linear interactions to facilitate coupling between individual photons show exciting potential [36]–[40]. The scattering of two photons with the help of interaction with other systems has been explored in Refs. [41]–[45]. The collective interaction between emitters has been harnessed to facilitate this, especially in the more controllable case of emitters coupled to waveguides [46]–[57].

There has been significant progress in engineering nanophotonic interfaces for versatile control over light-matter interaction. The interaction between atoms has been experimentally implemented using nanofibers [14], [58]–[64], photonic crystals [65], [66], and slot waveguides [67], [68]. Since the atoms are usually trapped close to dielectric surfaces, the complexities of modeling the interactions have been explored in Refs. [35], [69]–[71].

Collective dipole interactions have found many applications in quantum information [15], [28], [72], [73]. Reference [13] described a system using distant atom arrays to form highly subradiant states which can be used as Bell states to perform computations. As such,

quantum information processing requires an extremely high degree of fidelity and coherence. Many proposals ignore the effect of the recoil during the photon atom interactions. However, the recoil impulse to the atoms can cause the information in the internal states to entangle with the vibrational states of the atomic motion, leading to a loss of coherence in the many atom electronic states. The subsequent motion can also affect the dynamics of the internal states of the system. Thus, the atom recoil can affect the overall robustness of the quantum system and introduce avenues for decoherence. The depth of the trapping potential required in experiments will be determined by this recoil and having a depth that is too low could escalate this problem. But, the role of the photon recoil may be counter intuitive. For example, the authors of Ref. [31] discussed that their experiments showed that increasing the depth beyond a certain level resulted in a reduced cooperative response. This raises the question of an optimal potential depth in experiments. Reference [74] also proposed to utilize atomic arrays to drive opto-mechanical systems and the recoil energy would play a large role in such interactions. Hence, it is imperative to accurately model the recoil force effects in such cases.

1.1 Outline of Thesis

In Chapter 2, the recoil due to the collective interactions in the atomic systems interacting with lasers are studied using density matrix calculations. It expands on the work done in Ref. [75] and studies the emergence of patterns of excitation and recoil in atomic arrays. The calculations are done under the slow oscillation approximation which assumes that the timescales of the atomic vibration are much larger than the timescales of the atomic internal state dynamics. This means that the atoms can be considered as almost stationary and the forces due to the interactions can be considered as impulses. Hence this model will be referred to as the 'impulse model' in this report. Several numerical methods to calculate the recoil during a decay process and in a steady state system are described.

The eigenstates of excitations of an atomic array and its effects on the recoil are studied. In particular situations, the recoil deposited on the array was found to be proportional to the lifetime of the electronic excitation. The recoil in the highly subradiant system

described in Ref. [13] was calculated and the results show a surprisingly high amount of recoil energy deposited on the atom array. But this abnormal result needed to be verified because the large lifetimes of the highly subradiant state will no longer satisfy the slow oscillation approximation.

In Chapter 3, the recoil is calculated by quantizing the vibrational states of the atoms. This method is not limited by the slow oscillation approximation and allows for the exploration of the regime beyond. Hence the results can be compared with the impulse model and the validity of the slow oscillation approximation can be tested. The effects of the trap frequency and the contributions to the recoil from the different terms of the Lindblad superoperator and the Hamiltonian are studied.

In Chapter 4, we study the photon statistics of the emitted light from collectively interacting dipole systems in the low-intensity limit using the double excitation states. We investigate how the eigenstates of the double excitation manifold relate to the eigenstates of the more accessible single excitation eigenstates. We also study how the lifetimes of these states can affect the initial time photon correlation $g^{(2)}(\tau = 0)$ of the emitted light under different detection schemes. By using two interfering beams of light that can address different eigenmodes of the system, we can constructively or destructively control the two-excitation probabilities and hence control the emission photon statistics.

In Chapter 5, we simulate the collective effects in atom ensembles and arrays trapped near a nanophotonic micro-ring resonator. This is a collaboration with the experimental group of Prof C. L. Hung from Purdue University. The atoms trapped near the resonator can interact with each other through two channels, free space and the chiral resonator cavity. The different properties of the two interaction channels can facilitate interesting combinations of subradiant and superradiant states with the potential to achieve "selective radiance" [35]. We simulate the current experiment using randomly distributed atom clouds to investigate the dynamics under pulsed and steady-state excitation. Further, we explore the potential of ordered atomic arrays, which are planned for implementation in the next phase of the experiment.

1.2 Theoretical Introduction to Collective Dipole Interactions in Atomic ensembles

In this thesis, we study how monochromatic light interacts with N two-level systems with average nearest neighbor separation less than a wavelength of the light. We use a semiclassical treatment, where the light is treated as classical EM waves interacting with quantized energy levels to describe the atom.

When light is incident on an atom with a frequency corresponding to a two-level transition, the atom absorbs the photon and gets excited to a higher energy level. This excited atom is usually unstable and can spontaneously emit a single photon, returning to the ground state. This spontaneous emission causes an exponential decay of the excitation and is decoherent, implying that the photon is emitted at a random time. The direction of emission is also random, but the probability of emitting into different directions depends on the orientation of the dipole. The emission pattern can be described by the equation governing the electric field due to a dipole and is shown in Fig. 1.1(a).

$$\mathbf{E}(\mathbf{r}) = \frac{1}{4\pi\epsilon_0}\left\{k^2((\mathbf{n}\times\mathbf{d})\times\mathbf{n}\frac{\mathrm{e}^{\mathrm{i}kr}}{r} + [3\mathbf{n}(\mathbf{n}\cdot\mathbf{d}) - \mathbf{d}]\Big(\frac{1}{r^3} - \frac{\mathrm{i}k}{r^2}\Big)\mathrm{e}^{\mathrm{i}kr}\right\} \tag{1.1}$$

where $\mathbf{d}$ is the dipole moment, $\mathbf{n}$ and r are the unit vector and magnitude of $\mathbf{r}$.

We consider the atoms to be two-level systems with ground state $|g\rangle$, and excited states $|\mathrm{e}\rangle$. The energy difference corresponding to this transition will be given by ω_0. When N such emitters are located very close to each other (separation $<$ resonant wavelength λ_0) the spontaneous emission from each atom can constructively or destructively interfere and increase the rate of emission. This constructive or destructive interference is known as superradiance or subradiance respectively.

This was first discovered by Dicke [1] where he studied the emission from an ensemble of atoms confined to a radius much smaller than the resonant wavelength. When all the atoms are excited (inverted ensemble) the emission is bolstered in proportion to the number of atoms in the system. There is a momentary burst of emission followed by a quick drop in the emission rate.

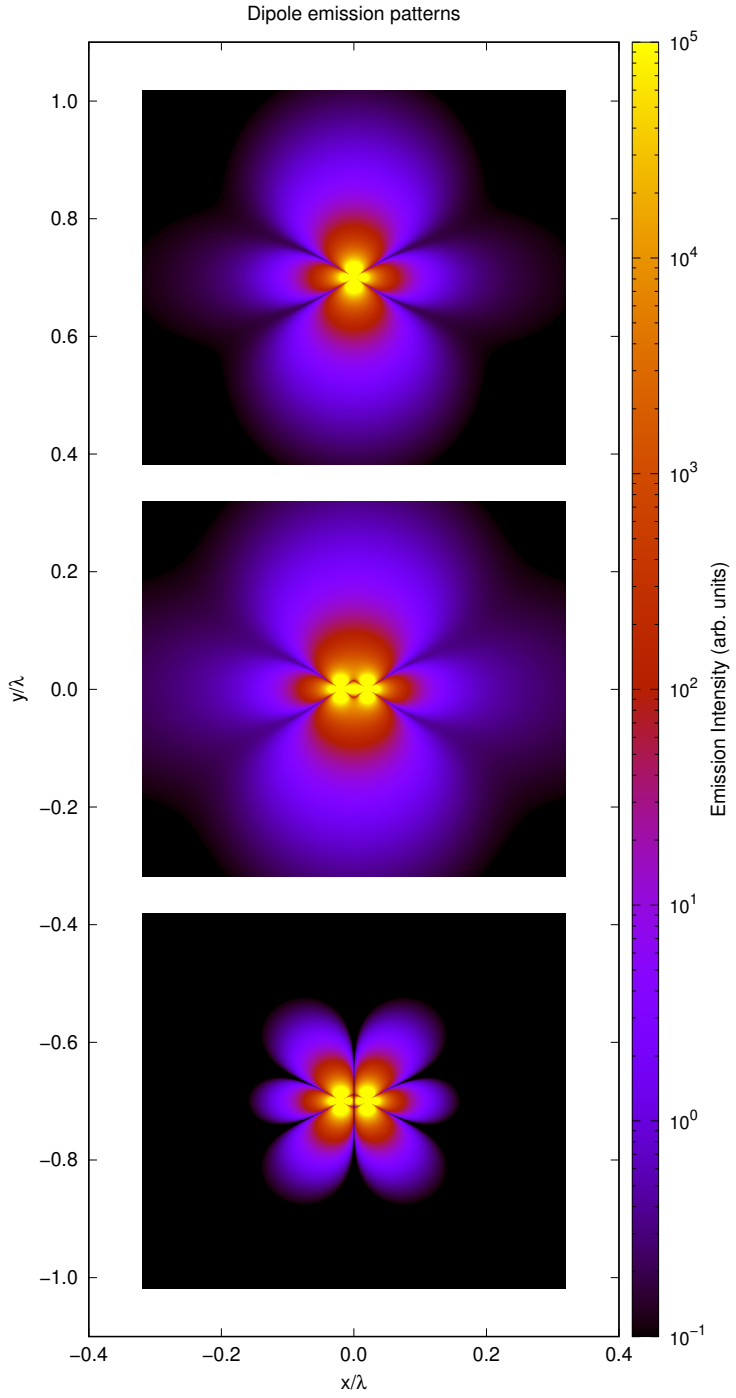

Figure 1.1. The dipole emission pattern for (a) single dipole, (b) and (c) two dipoles separated by $d = 0.04\lambda$. (b) has the dipoles excited in phase resulting in constructive interference and superradiance. (c) has the the dipoles excited out of phase resulting in destructive interference and subradiance. The emission intensity is plotted on a logarithmic scale.

This interference can also work when there is only a single excitation in the system. The single excitation can be spread over the ensemble, where there is a superposition of each atom being excited at a time. The emission wavefunction of each atom can then interfere to give collective effects. When two atoms, with each having an emission pattern shown in Fig.1.1(a), are close to each other with the same (or opposite) phases, the resulting emission pattern would look like Fig.1.1(b) (or Fig.1.1(c)). Thus, the spontaneous emission from the collective decay of atoms can increase or decrease depending on the circumstances. However, when there are many atoms placed in ordered lattices, we get interesting effects such as perfect reflection.

Another way to understand this is through the addition or subraction of the single and collective effects. While the single atom emission cannot be altered, the collective two atom emission can either add or subtract the single atom emission wavefunction, thereby causing superradiance or subradiance.

1.2.1 Laser interaction

The interaction between lasers and atoms can be studied as perturbations in the system due to oscillating electric fields. When there is an incoming EM radiation with frequency ω incident on the atoms, we can use time-dependent perturbation theory to describe the dynamics of the excitation. This will give us Rabi oscillations and a characteristic Rabi frequency with which the excitation oscillates between the atom and the EM field. This Rabi frequency is dependent on both the transition dipole moment and the intensity of the incident light, and is given by,

$$\Omega = \frac{\langle \mathrm{i}|e\mathbf{r}\cdot\mathbf{E}_0|\mathrm{j}\rangle}{\hbar} \tag{1.2}$$

where $\mathbf{r}$ is the position of the electron with respect to the center of mass and $-e\mathbf{r}$ is the electric dipole moment for the transition from state $\mathrm{i} \rightarrow \mathrm{j}$ and $\mathbf{E}_0$ is the amplitude of the oscillating electric field of the EM radiation.

For most cases, the frequency of the light is close to the frequency of the two-level system, i.e., the detuning is very small ($\Delta = \omega - \omega_0 \ll \omega_0$). This means that the rapidly oscillating terms in the time dynamics (counter-rotating terms with frequencies $\omega+\omega_0$) can be neglected.

This is called the Rotating Wave Approximation and is crucial to simplify and extend the range of calculations possible. This approximation will breakdown when (a) the intensity becomes too large, or (b) the detuning becomes too large.

The interaction with the laser is a coherent process and can be described by the Rotating Wave approximation Hamiltonian

$$\hat{H}_L = \hbar \sum_{\mathrm{j}} \left[-\Delta \hat{\sigma}_{\mathrm{j}}^{+} \hat{\sigma}_{\mathrm{j}}^{-} + \left(\frac{\Omega}{2} \hat{\sigma}_{\mathrm{j}}^{+} \mathrm{e}^{\mathrm{i}\mathbf{k}_0 \cdot \mathbf{r}_{\mathrm{j}}} + h.c. \right) \right] \tag{1.3}$$

where Ω is the Rabi frequency, Δ is the detuning, $\mathbf{r}_{\mathrm{j}}$ is the position of the j^{th} atom, and $\mathbf{k}_0 = k\hat{\mathbf{z}}$ is the initial wavevector of the incoming photons. $\hat{\sigma}_{\mathrm{j}}^{+}$ and $\hat{\sigma}_{\mathrm{j}}^{-}$ are the raising and lowering operators of the electronic excitation of the j^{th} atom.

1.2.2 Lindblad Operator

In the semiclassical treatment, the Electromagnetic degrees of freedom are traced out and will be considered as the environment. The spontaneous emission of photons into the environment will be a decoherent process with randomness involved and cannot be described by a Hamiltonian alone. The typical methods to simulate such dynamics are Quantum Trajectory [76]–[78], Wavefunction Monte-Carlo [79]–[82], or Lindblad operator with density matrices [83], [84].

In this thesis, we primarily use the density matrix representation to describe the spontaneous emission dynamics. Using the density matrix method provides several advantages. The density matrix describes the average ensemble of the system, making it easy to calculate expectation values directly from the density matrix. The off-diagonal terms can be used to understand the coherence involved in the system. It also allows for the representation of mixed states, unlike the wavefunction picture which can only describe pure states. The scaling of the size with the number of atoms for the density matrix is worse than the wavefunction methods. Nevertheless, since the density matrix directly works on ensemble averages instead of requiring random sampling, it performs better for a relatively limited number of atoms.

We consider the effects of collective interaction in the Low-intensity Limit, where only a single photon interacts with the system at a time. We assume that the incoming laser light has such low intensities that the rate of incoming photons is low enough that the previous excitation decays before the next photon is incident on the atoms. This also greatly helps with simplifying the calculations because the size of the density matrix only grows linearly with the number of atoms present.

To properly study the interaction of light with the emitters, the light field has to be quantized. While this works well in single mode systems like cavities, it becomes tedious to describe the infinite modes present in the spontaneous emission into free space. Hence, we use a Green's function approach to decompose the dynamics into a Lindblad operator form. To arrive at this form, we need to start with the full density matrix which includes the N atoms as well as the infinite dimensional Fock states that are associated with the EM field bath. Using second-order perturbation theory and then tracing out the EM field by integrating over all k, gives a reduced density matrix and corresponding master equation that uses a Lindblad term to describe the decoherent spontaneous emission process. This has been derived for a general situation in the thesis of T. Sutherland [85].

This description is only valid under the Markovian approximation, where the system does not hold memory and the dynamics of the past do not contribute to the dynamics of the present. This is relevant to our situation because the timescales of the internal state dynamics are much longer than the timescales that bring about memory effects. Using this approximation, the dependence of the Green's function response on the frequency can be ignored. Another limitation is that this cannot be used in the strong coupling regime where the EM field can cause changes to the energy level of the emitters (as we will see in Chapter 5).

In the Low-intensity limit, the Hilbert space of the atom excitations can be simplified to $N + 1$ states. The state where all the atoms are in the ground state is represented by $|g\rangle$

and the states where only the atom 'j' is excited will be represented by $|\mathrm{e_j}\rangle = \hat{\sigma}_\mathrm{j}^+|g\rangle$. The density matrix will be represented by,

$$\begin{aligned}\rho = \rho_{gg}|g\rangle\langle g| + \sum_\mathrm{j} \rho_{g\mathrm{e_j}}|g\rangle\langle \mathrm{e_j}| \\ + \sum_\mathrm{j} \rho_{\mathrm{e_j}g}|\mathrm{e_j}\rangle\langle g| + \sum_{\mathrm{i,j}} \rho_{\mathrm{e_i e_j}}|\mathrm{e_i}\rangle\langle \mathrm{e_j}|\end{aligned} \tag{1.4}$$

where the coefficients in the diagonal describe the populations and the off-diagonal terms describe the coherences between the corresponding states.

The Lindblad term for the evolution of atoms with dipole interactions from $m = 0$ to $m = \pm 1$ will be given by

$$\mathcal{L}(\hat{\rho}) = \sum_{\mathrm{i,j}} \left[(g(\mathbf{r_{ij}}) + g^*(\mathbf{r_{ij}}))\hat{\sigma}_\mathrm{i}^- \hat{\rho}\hat{\sigma}_\mathrm{j}^+ - g(\mathbf{r_{ij}})\hat{\sigma}_\mathrm{i}^+\hat{\sigma}_\mathrm{j}^-\hat{\rho} - \hat{\rho}\hat{\sigma}_\mathrm{i}^+\hat{\sigma}_\mathrm{j}^- g^*(\mathbf{r_{ij}}) \right] \tag{1.5}$$

There are two key components to the Lindblad super-operator. The first is the component that describes the hopping of the excitation between atoms, without any photon being emitted. These are the second and third terms in Eq. (1.5) and can also be represented as a commutator of the density matrix with a complex operator. These do not cause a change in the number of excitations in the system. On the other hand, we have the 'quantum jump' operator that transfers the population from the excited state to the ground state when a photon is being emitted. This takes the form of two operators surrounding the density matrix as seen in the first term of Eq. (1.5).

The coefficients of the Lindblad operator are determined by the dyadic Green's function of the interaction between two atoms. This Green's function is the fundamental solution of the EM wave equation. In the case of dipoles interacting in free space, it will simply be determined by the electric field due to a dipole at the position of the other:

$$g(\mathbf{r_{ij}}) = \frac{\Gamma}{2}\left[h_0^{(1)}(kr_\mathrm{ij}) + \frac{3(\hat{r_\mathrm{ij}}\cdot\hat{q})(\hat{r_\mathrm{ij}}\cdot\hat{q}^*) - 1}{2} h_2^{(1)}(kr_\mathrm{ij}) \right] \tag{1.6}$$

where $\hat{q}_\mathrm{i}$ is the dipole orientation of the i^{th} atom, $r_\mathrm{ij} = |\mathbf{r}_\mathrm{ij}|$ is the norm of $\mathbf{r}_\mathrm{ij}$, $\hat{r}_\mathrm{ij} = \mathbf{r}_\mathrm{ij}/r_\mathrm{ij}$ is the unit vector along $\mathbf{r}_\mathrm{ij}$, Γ is the decay rate of a single atom and $h_l^{(1)}$ are the outgoing spherical Hankel function of angular momentum l. $h_0^{(1)}(x) = \mathrm{e}^{\mathrm{i}x}/(\mathrm{i}x)$ and $h_2^{(1)}(x) = \mathrm{e}^{\mathrm{i}x}(-3\mathrm{i}/x^3 - 3/x^2 + \mathrm{i}/x)$.

It is important to note that the description of Green's function used in this thesis is $-\mathrm{i}$ times the Green's function generally described in the literature. The real part of Green's function will describe the lifetime and decay dynamics, while the imaginary part will describe the energy shift.

The density matrix can be evolved in time using the master equation,

$$\frac{d\hat{\rho}}{dt} = -\frac{\mathrm{i}}{\hbar}[\hat{H}, \hat{\rho}] + \mathcal{L}(\hat{\rho}) \tag{1.7}$$

Since there is decoherence in the time evolution, the differential equation can be time evolved using simple second-order Runge-Kutta methods.

While in some cases the atoms have been assumed to be fixed in lattice positions, there are situations discussed in this thesis where the atoms are in a cloud with random positions. To simplify the integration of the position of the atoms over the cloud wavefunction, we perform Monte Carlo integration. The positions of the atoms are generated randomly according to the corresponding probability distribution and are repeated many times until the results converge.

2. RECOIL IN THE SLOW OSCILLATION APPROXIMATION

The contents of this chapter were published as Deepak A. Suresh and F. Robicheaux (2021), Photon-induced atom recoil in collectively interacting planar arrays, Phys. Rev. A 103, 043722 [86].

2.1 Introduction

This chapter continues the exploration of the role of recoil in atomic ensembles conducted in Ref. [75]. We study the recoil energy when photons interact with atomic ensembles, more specifically, ordered planar atomic arrays with sub-wavelength interatomic spacing. See Fig. 2.1 for a schematic drawing. We describe a method to determine the recoil momentum and energy deposited in such cases using density matrix master equations. We focus on the regime where the periods of the atomic vibrations are much larger than the lifetimes of the internal excited states and the duration of the light pulse. We also work in the low light intensity regime, limiting the system to have one excited state at most, to reduce the computational complexity.

Reference [75] treated simplified cases where the array size was considered near-infinite, ignoring the effects of the edges and assuming that most of the bulk of the array experiences a recoil to the same degree as the center atom. In the present work, we explore the role of finite array size and situations where the excitation of an atom strongly depends on its position in the array. Calculations for the individual atoms of the array show that the finiteness of the array has pronounced effects. We study the recoil and reflectance of the array when the atoms are driven by a pulsed excitation and a steady state excitation.

When all the atoms of the array are uniformly illuminated by light, interesting patterns arise in the recoil distribution as well as in the distribution of the excitation itself. This is due to the interference of the different eigenmodes of excitation, each associated with a modified lifetime and energy shift. We study these eigenmodes which leads to an understanding of the patterns, as well as the relation between the decay lifetimes and the recoil energies deposited in individual atoms. We also investigate the case where two nearly planar arrays act as a

cavity, which have been proposed as interesting elements for connecting distant qubits. The prolonged lifetimes of cavities lead to enhanced recoil.

The chapter is structured as follows. Section 2.2 describes the methods used for the calculations. Section 2.3 presents results from a variety of situations. Section 2.4 presents the conclusions followed by the Appendices 2.A and 2.B.

2.2 Methods

The calculations are done for an ensemble of N atoms arranged in a planar array with sub-wavelength interatomic spacing, d. The atoms have two internal energy levels which couple to each other through collective dipole-dipole interactions and with an external light field. The array lies in the x-y plane (with minor deviations in the z-direction when using curved arrays) and the direction of propagation of the incident laser light is chosen to be the z-direction ($\mathbf{k}_0 = k\hat{\mathbf{z}}$) (Fig. 2.1). The light is circularly polarized in the $\hat{\mathbf{e}}_+ = -(\hat{\mathbf{x}} + \mathrm{i}\hat{\mathbf{y}})/\sqrt{2}$ direction and the dipoles are also oriented in the $\hat{\mathbf{e}}_+$ direction. The circular polarization is chosen to form symmetric patterns in the array but the main conclusions should remain valid for other polarizations. Bold fonts denote vectors.

To describe the dynamics of the collective dipole emissions, we use the density matrix formalism where the density matrix evolves according to

$$\frac{d\hat{\rho}}{dt} = -\frac{\mathrm{i}}{\hbar}[\hat{H}, \hat{\rho}] + \mathcal{L}(\hat{\rho}) \tag{2.1}$$

where $\hat{\rho}$ is the density matrix of the system, $\hat{H}$ is the effective Hamiltonian and $\mathcal{L}(\hat{\rho})$ is the Lindblad super-operator which describes the lossy collective dipole emissions. They shall be discussed subsequently.

To perform density matrix calculations for a large number of atoms, we adopt a few simplifications. We work in the low intensity limit where only the singly excited states are relevant, meaning only one atom can be excited at any time. In this limit, the density matrix dimensions scales more slowly with increasing number of atoms. This simplification allows us to perform calculations up to $N = 300$ for the effects studied below.

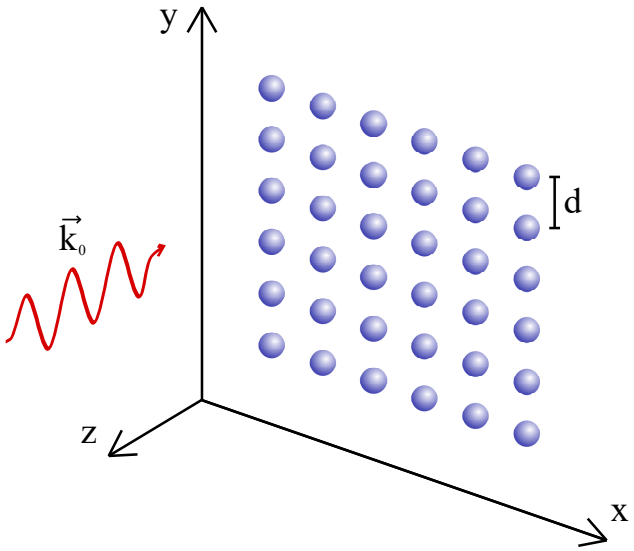

Figure 2.1. A schematic of the system considered. The atoms are the blue spheres and are placed in an ordered array in the x-y plane with interatomic separation d. The incoming light (red wavy arrow) is in the $\hat{\mathbf{z}}$ direction with wavevector $\mathbf{k}_0$

The ground state of the system which corresponds to all the atoms being in the electronic ground state, is represented by $|g\rangle = |g_1\rangle \otimes |g_2\rangle \otimes ...|g_N\rangle$, where $|g_\mathrm{j}\rangle$ denotes the electronic ground state of atom j. The raising and lowering operators of j^{th} atom are represented by $\hat{\sigma}_\mathrm{j}^+$ and $\hat{\sigma}_\mathrm{j}^-$ respectively. The state where only the j^{th} atom is excited is represented by $|\mathrm{e_j}\rangle = \hat{\sigma}_\mathrm{j}^+|g\rangle$. The density matrix describes both the internal degrees of freedom and the positional dependence of the atoms. The positional dependence is based on the atoms' coordinates $\mathbf{r}_\mathrm{j}$ and the density matrix is represented as

$$\begin{aligned}\hat{\rho} \quad = \quad & \rho_{gg}(\mathbf{r}_1, \mathbf{r}_2, ...\mathbf{r}_N; \mathbf{r}'_1, \mathbf{r}'_2, ...\mathbf{r}'_N)|g\rangle\langle g| \\ & \sum_\mathrm{i} \rho_{\mathrm{e_i}g}(\mathbf{r}_1, \mathbf{r}_2, ...\mathbf{r}_N; \mathbf{r}'_1, \mathbf{r}'_2, ...\mathbf{r}'_N)|\mathrm{e_i}\rangle\langle g| \\ & \sum_\mathrm{j} \rho_{g\mathrm{e_j}}(\mathbf{r}_1, \mathbf{r}_2, ...\mathbf{r}_N; \mathbf{r}'_1, \mathbf{r}'_2, ...\mathbf{r}'_N)|g\rangle\langle \mathrm{e_j}| \\ & \sum_\mathrm{i,j} \rho_{\mathrm{e_i e_j}}(\mathbf{r}_1, \mathbf{r}_2, ...\mathbf{r}_N; \mathbf{r}'_1, \mathbf{r}'_2, ...\mathbf{r}'_N)|\mathrm{e_i}\rangle\langle \mathrm{e_j}|\end{aligned} \tag{2.2}$$

where i, j go from 1 to N. The coefficients describe the spatial dependence of the density matrix and are functions of $6N$ positional coordinates.

Since operators acting on the left and right sides of the density operator will act on different indices, we define the following convention

$$\mathbf{r}_\mathrm{ij} \equiv \mathbf{r}_\mathrm{i} - \mathbf{r}_\mathrm{j}; \qquad \mathbf{r}'_\mathrm{ij} \equiv \mathbf{r}_\mathrm{i} - \mathbf{r}'_\mathrm{j}; \qquad \mathbf{r}''_\mathrm{ij} \equiv \mathbf{r}'_\mathrm{i} - \mathbf{r}'_\mathrm{j} \tag{2.3}$$

The effective Hamiltonian of the system will have (i) The laser interaction, (ii) the collective dipole interaction and (iii) the center of mass motional Hamiltonian consisting of the kinetic energy and the trapping potential of each atom. For the laser interaction, we work in the rotating wave approximation with

$$\hat{H}_L = \hbar \sum_\mathrm{j} \left[-\delta \hat{\sigma}_\mathrm{j}^+ \hat{\sigma}_\mathrm{j}^- + \frac{\Omega}{2} \hat{\sigma}_\mathrm{j}^+ \mathrm{e}^{\mathrm{i}\mathbf{k}_0 \cdot \mathbf{r}_\mathrm{j}} + \frac{\Omega^*}{2} \hat{\sigma}_\mathrm{j}^- \mathrm{e}^{-\mathrm{i}\mathbf{k}_0 \cdot \mathbf{r}_\mathrm{j}} \right] \tag{2.4}$$

which describes the Hamiltonian for a plane wave incident laser with Ω as the Rabi frequency, δ as the detuning and $\mathbf{k}_0 = k\hat{\mathbf{z}}$ as the initial wavevector of the incoming photons. The collective dipole emission also participates in the effective Hamiltonian based on the imaginary part of the Green's function ($Im\{g(\mathbf{r}_{ij})\}$) and is given by

$$\hat{H}_{dd} = \hbar \sum_{i \neq j} Im\{g(\mathbf{r}_{ij})\} \hat{\sigma}_i^+ \hat{\sigma}_j^- \tag{2.5}$$

where the $g(\mathbf{r}_{ij})$ is the free space dyadic Green's function given by Eq. (5.11). When calculating the commutator of the effective Hamiltonian ($\hat{H} = \hat{H}_L + \hat{H}_{dd}$) with the density matrix $\hat{\rho}$ in Eq. (4.2), indices of the position vector must be carefully implemented. When right-multiplying $\hat{\rho}$ with $\hat{H}$, the corresponding primed indices must be used ($\mathbf{r}'_j$ for $\hat{H}_L$ and $\mathbf{r}''_{ij}$ for $\hat{H}_{dd}$).

The decay effects of the collective dipole interaction will be captured by the Lindblad term

$$\mathcal{L}(\hat{\rho}) = \sum_{i,j} \left[2Re\{g(\mathbf{r}'_{ij})\} \hat{\sigma}_i^- \hat{\rho} \hat{\sigma}_j^+ - Re\{g(\mathbf{r}_{ij})\} \hat{\sigma}_i^+ \hat{\sigma}_j^- \hat{\rho} - Re\{g^*(\mathbf{r}''_{ij})\} \hat{\rho} \hat{\sigma}_i^+ \hat{\sigma}_j^- \right] \tag{2.6}$$

where the i = j terms are the usual single atom decay part of the Lindblad operator. The Green's function $g(\mathbf{r}_{ij})$ is given by

$$g(\mathbf{r}_{ij}) = \frac{\Gamma}{2} \left[\frac{3(\hat{r}_{ij} \cdot \hat{q}_i)(\hat{r}_{ij} \cdot \hat{q}_j^*) - (\hat{q}_i \cdot \hat{q}_j^*)}{2} h_2^{(1)}(kr_{ij}) + (\hat{q}_i \cdot \hat{q}_j{}^*) h_0^{(1)}(kr_{ij}) \right] \tag{2.7}$$

where $\hat{q}_i$ is the dipole orientation of the i^{th} atom, $r_{ij} = |\mathbf{r}_{ij}|$ is the norm of $\mathbf{r}_{ij}$, $\hat{r}_{ij} = \mathbf{r}_{ij}/r_{ij}$ is the unit vector along $\mathbf{r}_{ij}$, Γ is the decay rate of a single atom and $h_l^{(1)}$ are the outgoing spherical Hankel function of angular momentum l. When i = j, that is when $\mathbf{r}_{ij} = 0$, the imaginary part of the function becomes undefined, while the real part is defined. Hence, we redefine $g(\mathbf{r}_{ij})$ to be

$$\begin{aligned} g(\mathbf{r}_{ij}) &= g(\mathbf{r}_{ij}) \qquad for \quad i \neq j \\ &= Re\{g(\mathbf{r}_{ij})\} \quad for \quad i = j \end{aligned} \tag{2.8}$$

2.2.1 Slow Oscillation approximation

In this chapter, the calculations are primarily in the limit where the timescales of the atomic motion in the trap are much slower than the timescales for the evolution of the internal states. This means that during the evolution of the internal states, the position of the atom does not change. This also implies that the photon recoil can be considered as impulsive forces. This is a sudden approximation and allows us to drop the motional Hamiltonian with the kinetic energy and trapping potential. The recoil imparted by the photons and collective interactions can then be described by calculating the change in momentum ($\Delta\mathbf{p}$) and change in kinetic energy ($\Delta\mathbf{K}$) of the atoms. Typically, the frequencies of the trapping potentials will be around a few 10s of KHz and are much slower than the decay rates which are usually of the order of MHz. We also assume that the spread of the initial center of mass position is small compared to the separations. This will allow using the perfect position of the atoms in the calculations.

In the calculations where the system settles in the ground state, at infinite time, only the ρ_{gg} term is left non-zero and its spatial dependence will be of the form

$$\rho_{gg}(\mathbf{r}_1, \mathbf{r}_2, ...; \mathbf{r}'_1, \mathbf{r}'_2, ...) = \rho_0(\mathbf{r}_1, \mathbf{r}_2, ...; \mathbf{r}'_1, \mathbf{r}'_2, ...) \times F(\mathbf{r}_1, \mathbf{r}_2, ...; \mathbf{r}'_1, \mathbf{r}'_2, ...) \tag{2.9}$$

where ρ_0 is the spatial dependence at the initial time and F describes the evolution of the ground state spatial dependence. To calculate the momentum and kinetic energy change of the atoms, we take the expectation value of the corresponding operator using the density matrix.

$$\begin{aligned} \langle \mathbf{p}_\mathrm{j} \rangle &= \frac{\hbar}{\mathrm{i}} \int [\hat{\nabla}_\mathrm{j} \rho_{gg}] \delta(\mathbf{r}'_{11}) \delta(\mathbf{r}'_{22}) ... d\mathbf{r}_1 d\mathbf{r}'_1 d\mathbf{r}_2 d\mathbf{r}'_2 ... \\ &= Tr[\hat{\mathbf{p}}_\mathrm{i}(\rho_0 F)] = \langle \mathbf{p}_\mathrm{j} \rangle_0 + \Delta\mathbf{p}_\mathrm{j} \end{aligned} \tag{2.10}$$

where $\hat{\nabla}_{\mathrm{j}} = \hat{\mathbf{x}}\frac{\partial}{\partial x_{\mathrm{j}}} + \hat{\mathbf{y}}\frac{\partial}{\partial y_{\mathrm{j}}} + \hat{\mathbf{z}}\frac{\partial}{\partial z_{\mathrm{j}}}$ is the momentum operator of the j^{th} atom. The term $\langle \mathbf{p}_{\mathrm{j}} \rangle_0$ denotes the initial expectation value of the momentum and derives from ρ_0. Hence, the change in momentum can be calculated from the function F using

$$\begin{aligned} \Delta \mathbf{p}_{\mathrm{j}} &= \frac{\hbar}{\mathrm{i}} \int [\rho_0(\hat{\nabla}_{\mathrm{j}} F)] \delta(\mathbf{r}'_{11}) \delta(\mathbf{r}'_{22}) ... d\mathbf{r}_1 d\mathbf{r}'_1 d\mathbf{r}_2 d\mathbf{r}'_2 ... \\ &= Tr[\rho_0(\hat{\mathbf{p}}_{\mathrm{i}} F)] \end{aligned} \tag{2.11}$$

For the Kinetic energy, we follow a similar reasoning and use the KE operator $\mathbf{K}_{\mathrm{j}} = \mathbf{p}_{\mathrm{j}}^2/(2m)$ to get

$$\begin{aligned} \Delta \mathbf{K}_{\mathrm{j}} &= -\frac{\hbar^2}{2m} \int [\rho_0(\hat{\nabla}_{\mathrm{j}}^2 F)] \delta(\mathbf{r}'_{11}) \delta(\mathbf{r}'_{22}) ... d\mathbf{r}_1 d\mathbf{r}'_1 d\mathbf{r}_2 d\mathbf{r}'_2 ... \\ &= Re\{Tr[\rho_0(\hat{\mathbf{K}}_{\mathrm{j}} F)]\} \end{aligned} \tag{2.12}$$

The density matrix is propagated in time using the Runge-Kutta second order integration until the system completely decays into the ground state. This ground state density matrix coefficient is used to evaluate $F(\mathbf{r}_1, \mathbf{r}_2, ...; \mathbf{r}'_1, \mathbf{r}'_2, ...)$. This is in turn used to calculate the $\Delta\mathbf{p}$ and $\Delta\mathbf{K}$ in three dimensions using Eq. (2.11) and Eq. (2.12) by using symmetric 2-point and 3-point differentiation. To calculate the derivatives ∇_{j}, the positions of either the primed ($\mathbf{r}_{\mathrm{j}}$) or the unprimed coordinates ($\mathbf{r}'_{\mathrm{j}}$) are shifted by a small distance δr and evaluated. For a more detailed explanation of the methods followed, refer to Section II of Ref. [75].

2.2.2 Interatom distance

The process of subradiance can be thought of as the destructive interference of the wavefunctions of the light emitted by spontaneous decay of excited atoms. For example, when there are two atoms close together to the point of overlap ($d \to 0$), the wavefunctions of the emitted light will cancel out if they have opposing phases. This results in a prolonged lifetime for the excited state. For two atoms, the out of phase state remains as the subradiant state until the separation of $d \sim \lambda/2$. As the separation goes beyond half a wavelength, the light acquires an extra phase of $\boldsymbol{\pi}$ which causes the in-phase states to be subradiant until $d \sim \lambda$. This behavior continues as we increase d and oscillates with a period of $\lambda/2$. The

maximum effect of subradiance and superradiance possible decreases with increasing d and becomes small beyond $d \sim \lambda$.

This behavior carries over to the periodically placed atoms in arrays. For interatomic distances less than $\sim \lambda/2$, the subradiant states have adjacent atoms out-of-phase, while the superradiant states have them in-phase. Between $\lambda/2$ and λ, the subradiant states have adjacent atoms in-phase. Since we want to primarily focus on subradiant states, and exciting atoms with adjacent atoms being in-phase is easier to experimentally realize, we choose the range of interatomic distance to be between 0.5λ and 1.0λ.

2.3 Photon Recoil Energy and Momentum

When a photon is absorbed or emitted by a single atom, the photon imparts a momentum kick $\hbar k$ and recoil kinetic energy $E_r = \hbar^2 k^2/(2m)$. But when there is an ensemble of atoms and collective dipole interactions take place, Ref. [75] showed that the energy deposited is different and depends on collective decay dynamics. We delve deeper into this topic and discuss the directional properties of the kicks and its relation to the decay properties of the collective ensemble. Since a single photon undergoing perfect reflection on an atom imparts $2\hbar k$ momentum, the $\Delta p_z/(2\hbar k)$ serves as a good measure of reflectance.

The two different factors that contribute to the kicks have slightly different effects. In the out-of-plane direction, the collective dipole emissions emit light symmetrically on both sides and hence contribute to no net momentum kick in this direction, but will still contribute to the recoil energy deposited. In the in-plane direction, the atoms exchange photons among each other and, hence, the momentum and energy deposited will depend on the position of the atom within the array. The contribution from the laser will only be in the out of plane direction and has non-zero contributions to both momentum and kinetic energy deposition.

2.3.1 Eigenstates

Reference [2] discussed the interference of many eigenmodes of the system which contributes to the cooperative emission. To get an understanding of the effect of the decay rate on the recoil energy, we analyze the photon recoil momentum and energy deposited when

the initial state is an eigenstate of the excitation. When there is no driving interaction with the laser, the eigenstate of the excitation is the eigenstate of the dyadic Green's function in free space. They are eigenstates of a complex symmetric matrix which means that they maintain the distribution pattern of the excitation among the atoms while the magnitude of the total excitation in the system decays exponentially. We define the Green's tensor $G_{\mathrm{ij}} = g(\mathbf{r}_{\mathrm{ij}})$ which is an N×N-dimensional matrix, and $\mathbf{V}_\alpha$ is an N-dimensional vector. The eigenvalue equation is

$$\sum_{\mathrm{j}} G_{\mathrm{ij}} \mathbf{V}_{\mathrm{j}\alpha} = \mathcal{G}_\alpha \mathbf{V}_{\mathrm{i}\alpha} = (\frac{\gamma_\alpha}{2} + \mathrm{i}\Delta_\alpha)\mathbf{V}_{\mathrm{i}\alpha} \tag{2.13}$$

where i,j are atom indices and α denotes the index for the eigenstate. $\mathcal{G}_\alpha$ is the eigenvalue and $\mathbf{V}_\alpha$ is the corresponding eigenvector. The rate of decay is given by the real part of the eigenvalue, γ_α, and the shift in energy is given by the imaginary part, Δ_α. Since the Green's function is not Hermitian, the regular orthogonality conditions do not apply. Therefore, the vectors $\mathbf{V}_\alpha$ have to be normalized to satisfy,

$$\sum_{\mathrm{i}} \mathbf{V}_{\mathrm{i}\alpha} \mathbf{V}_{\mathrm{i}\alpha'} = \delta_{\alpha,\alpha'} \tag{2.14}$$

This relation should be used with care when there are degenerate eigenstates in the system. Each set of degenerate vectors must be orthogonalized to follow this condition. These eigenstates form interesting and symmetric patterns on the array and exhibit similarities to TEM modes of light. As noted earlier in Section 2.2.2, the adjacent atoms in the subradiant modes tend to be in-phase while the superradiant modes have the adjacent atoms out-of-phase in the specified range of d.

The array is initialized to one of the eigenstates, β, leading to the electronic part of the density matrix starting as $\rho(t = 0) = \mathcal{N}_\beta |\mathbf{V}_\beta\rangle\langle\mathbf{V}_\beta|$, where the ket $|\mathbf{V}_\beta\rangle = \sum_{\mathrm{i}} \mathbf{V}_{\mathrm{i}\beta} |\mathrm{e_i}\rangle$ and $\mathcal{N}_\beta = (\sum_{\mathrm{i}} |\mathbf{V}_{\mathrm{i}\beta}|^2)^{-1}$ is a normalizing factor to have only one excitation at the initial time; note the magnitude in the definition of $\mathcal{N}_\beta$. The system is evolved in time until it completely reaches the ground state, at which point, the $\Delta\mathbf{p}$ and $\Delta\mathbf{K}$ of each atom are calculated.

The total kinetic energy deposited in the array for each eigenstate is inversely proportional to the decay rate of that state. This implies that highly subradiant states will have very high

photon recoil energies. Another trend observed was that the kick on each individual atom was roughly proportional to the excitation probability of that atom. This, while being an expected result, allows for an easier way to look at the distribution of the energy deposition over the array. Commonly, the most subradiant mode at this range of interatomic distances is similar to a Gaussian distribution (TEM_{00} like) on the array. This implies that the deposition of the recoil is concentrated near the center, while the atoms close to the edges have relatively low recoil.

When the system is initialized to its eigenstates, it is possible to analytically obtain an expression to calculate the recoil after the system has decayed to the ground state. This expression can then be used to find the recoil in any arbitrary initial state configuration by decomposing it into its eigenstates. The coefficient of the ground state density matrix at infinite time will be

$$\rho_{gg}(\infty) = \sum_{\alpha,\alpha'} \sum_{\mathrm{j,j'}} 2R\mathrm{e}\{g(r'_{\mathrm{jj'}})\} \mathbf{V}_{\mathrm{j}\alpha} \mathbf{U}^*_{\mathrm{j'}\alpha'} \frac{C_{\alpha,\alpha'}(0)}{\mathcal{G}_\alpha + \mathcal{G}''^*_{\alpha'}} \tag{2.15}$$

where $\mathcal{G}''_{\alpha'}$ and $\mathbf{U}_{\mathrm{j}\alpha'}$ are the eigenvalue and eigenvector of the tensor $G''_{\mathrm{ij}} = g(\mathbf{r}''_{\mathrm{ij}})$. The contribution of each eigenstate is given by $C_{\alpha,\alpha'}(0) = \sum_{\mathrm{jj'}} \mathbf{V}_{\mathrm{j}\alpha} \mathbf{U}^*_{\mathrm{j'}\alpha'} \rho_{\mathrm{e_j e_{j'}}}(0)$. If the initial state is an eigenstate β, then it is given by $C_{\alpha,\alpha'}(0) = \mathcal{N}_\alpha \delta_{\alpha\beta} \sum_{\mathrm{i}} \mathbf{V}^*_{\mathrm{i}\beta} \mathbf{U}^*_{\mathrm{i}\alpha'}$. and the term where $\alpha = \alpha' = \beta$ will be the most dominant. The derivation can be found in Appendix 2.A.

When initialized to eigenstates, this expression can be used to calculate the momentum and kinetic energy kicks using Eqs. (2.11) and (2.12). The calculation using Eq. (2.15) is much easier than solving for large density matrices over extended times and it also provides intuition towards the trends observed. The denominator of the dominant term, $\mathcal{G}_\beta + \mathcal{G}''^*_\beta \approx 2R\mathrm{e}\{\mathcal{G}_\beta\} = \gamma_\beta$ explains why the kicks are inversely proportional to the decay rates of the eigenstates. The term $\mathbf{V}_{\mathrm{j}\beta} \mathbf{U}^*_{\mathrm{j'}\beta}$ also explains why the kicks on each atom is proportional to their excitation probabilities.

An expression for kick in the out-of-plane direction can be obtained to express the ΔK_z depending only on the decay rate of the eigenvector (γ_α). The derivation can be found in Appendix 2.A.1.

$$\frac{\Delta K_z}{E_r} = \frac{2}{5}\frac{\Gamma}{\gamma_\alpha} \tag{2.16}$$

This was a surprising result because there is no photon mediated atom-atom interaction in the z-direction and there is just a single photon emitted. Hence one might expect the $\Delta K_z/E_r$ to be independent of the lifetime of the excited state. However, the results from Eq. (2.16) show that when there is spontaneous emission, the decay lifetimes play an important role in the recoil of the atoms in the array.

Figure 2.2 shows the results for the net $\mathbf{\Delta K}$ deposited in the out-of-plane and in-plane directions with respect to the decay lifetimes of the eigenstates using full density matrix calculations. While the out-of-plane kicks are highly proportional, the in-plane kicks have a more complicated dependence and are only roughly proportional.

This section has discussed the recoil momentum and energy calculation for the case when the system is in either an eigenstate or an arbitrary excited state and allowed to decay into the ground state. This is a simplified case in which there are no incoming photons and it is highly unlikely to be experimentally seen. Nevertheless, it provides insight into how the lifetimes of the state affect the recoil.

2.3.2 Cavity

The degree of subradiance can be further increased by trapping the light between two arrays and forming a cavity. By slightly curving the arrays, the cavity formed can greatly improve light retention, in turn making the system more subradiant. Reference [13] have proposed to utilize such curved mirrors to couple distant qubits, under the simplification of the atoms being fixed in space. This simplification may not be reasonable because the states are so subradiant that they give rise to enormous kicks on individual atoms. Hence in this section, we calculate the recoil experienced by the atoms in such highly subradiant cavities.

The system consists of $2N$ atoms making up two arrays each with N atoms. The arrays are separated by a distance L. This is similar to the system described in Fig. 1 of Ref. [13]. To find the most efficient cavity mode, we find the eigenstates of the Green's function for the cavity and find the most subradiant mode. We vary the separation L and the curvature

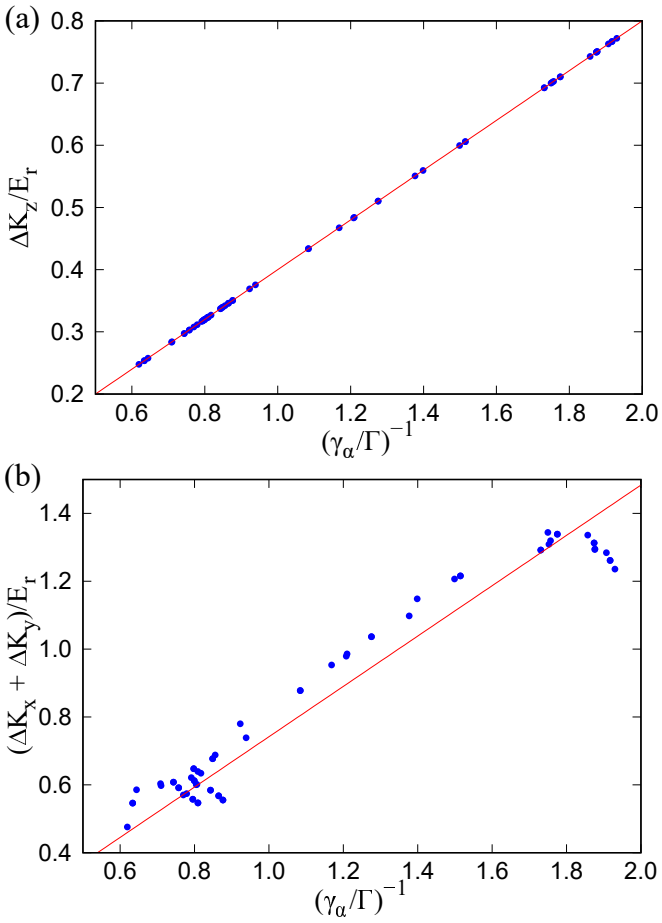

Figure 2.2. The net kinetic energy kick and the linear fit for an array of 8×8 array, initially in an eigenstate, with respect to the inverse of the decay rate of the eigenvalue. Blue dots denote the calculated plot points and the red line denotes the linear fit of the data. (a) denotes the kick in the out-of-plane direction which is proportional to the lifetime with slope 2/5, as expected from Eq. (2.16). (b) denotes the net kick in the plane of the array.

of the array until we find the optimal parameters for maximum subradiance. The imaginary part of the eigenvalue also provides the detuning at which the cavity mode should be driven.

The large lifetimes of the subradiant states prevent the calculation of the kick in all the atoms of the array within reasonable computation time using the density matrix method. Hence we use the second method described in Sec. 2.3.1 to calculate the recoil.

To characterize the light retention capacity of the cavity, we calculate the finesse of the cavity. In this case, we define the finesse using the intensity distribution of the cavity. The cavity is driven using lasers of fixed detuning, while scanning the separation of the arrays. The finesse, $\mathcal{F}$, will be defined as the free spectral range, $\lambda/2$, divided by the full width at half maximum in the separation of the intensity:

$$\mathcal{F} = \frac{\lambda/2}{\delta L_{FWHM}} \tag{2.17}$$

This gives an estimate of the number of times a photon bounces in the cavity before decaying.

In the following sections, we discuss the results calculated for a few typical cavities with different decay rates. The cavities are initialized into their most subradiant eigenstate with a single excitation and evolved until they reach the ground state, similar to Sec. 2.3.1. The results are also compared with the finesse of the cavity. In each case, we take a 11×11 array and the separation has been optimized around $L = 20\lambda$.

Spherical Mirrors

Reference [13] utilizes a set of spherically curved atom arrays to form highly subradiant states. Since light trapped in a cavity will have a Gaussian intensity profile, spherically curved mirrors match the spherical wavefront of the light and provides good energy retention. The mirrors are placed confocally. Following similar parameters to Ref. [13], with $d = 0.75\lambda$, separation $L = 19.75\lambda$, we attain the most subradiant mode to be extremely subradiant, with decay rates reaching $\sim 10^{-4}\Gamma$. The finesse of this particular configuration was found to be 1250. The kick the center atom experiences was calculated to be around $920E_r$ in the out-of-plane direction and $33E_r$ in the in-plane directions. This progressively reduces as we go closer to the edge in the shape of a Gaussian (See Fig. 2.3). This trend is expected because

the most subradiant eigenmode is typically a TEM_{00} mode (as noted in the supplementary of Ref. [13]). The atoms in the corner received a total of only $1.5 \times 10^{-3} E_r$. The net kick on the array leads to an energy increase of $\sim 10364 E_r$.

Unfortunately, this result is not completely valid because the decay rate is too small for the slow oscillation approximation to be satisfied. If the duration of the force on the array is of the order of the oscillation period, the impulsive nature of the recoil force will not be valid. In this timescale, the exact nature of the way fields interact with the atoms is not precisely known. A fully quantum mechanical treatment considering the motion of the particles as quantum oscillators is required to get a better understanding of the dynamics. While such a calculation would be very difficult, the enormous size of the kicks from our simplified treatment suggests that an attempt should be made.

Parabolic Mirrors

Another typical type of mirrors used in cavities are parabolic mirrors. Confocal cavities are only marginally stable and any small errors in the positions of the mirrors will cause destabilization. Hence, we use a cavity in the region between confocal and concentric to provide some room for errors. This configuration, with $d = 0.8\lambda$, parabolic focus $f = 15\lambda$ and separation $L = 19.694\lambda$, while not as subadiant as the previous case, has a decay rate of $\sim 10^{-3}\Gamma$. This decay rate also is at the edge of the slow oscillation approximation. The finesse for this cavity was calculated to be 263. The center atoms experienced $62 E_r$ recoil in the z-direction and $9.3 E_r$ in the x and y direction. A similar trend of decreasing kick in the edge atoms is seen and a total of only $8.3 \times 10^{-4} E_r$ was deposited in the corner atom. The total energy deposited on the whole array in this decay process is $\sim 774 E_r$

Plane mirrors

Curving a plane array of atoms as required in the above cases may prove to be complicated. Hence, to compare, we discuss the case where a cavity is formed by two plane mirrors. In this configuration, with $d = 0.8\lambda$ and separation $L = 20.045\lambda$, the decay rates reach $\sim 10^{-2}\Gamma$. The finesse was calculated to be approximately 14. The center atom received

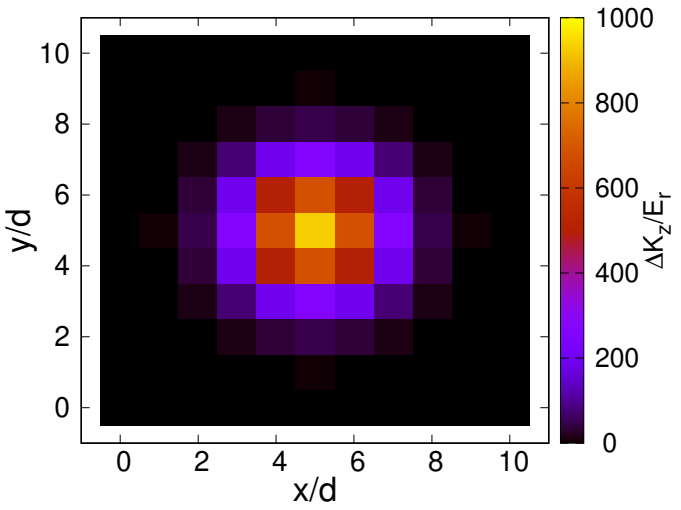

Figure 2.3. The recoil energy deposited in the z-direction on one array of a cavity with two 11×11 curved arrays with $d = 0.75\lambda$ and $L = 19.75\lambda$ corresponding to the system in Sec. 2.3.2. Each cell denotes one atom in the array. Note the center atom has a kick of $\sim 900E_r$.

a total of $0.61E_r$, while the corner atom received a total of $0.007E_r$. The array as a whole, received a kick of $10E_r$ in the out-of-plane direction and $12E_r$ in the in-plane directions.

2.3.3 Pulsed Laser

To simulate the effects of a single photon interacting with the array, a low intensity pulse of light is incident on it. A planar array with N atoms is initially in the ground state and a laser pulse with a Gaussian time profile is incident. The atoms are then evolved until they reach ground state. The $\Delta\mathbf{K}$ and $\Delta\mathbf{p}$ of each atom are calculated in this time frame and are compared to the probabilities of excitation of each atom. The Gaussian time profile of the light pulse of the form

$$\Omega(t) = \Omega_0 \mathrm{e}^{-t^2/t_w^2} \tag{2.18}$$

with peak Rabi frequency Ω_0 and pulse width t_w. The Ω_0 is kept low enough to not go beyond the single excitation limit. We see that like the trend in the previous section, the recoil is proportional to the integral of the excitation probabilities of each atom. That is, the excitation patterns are similar to the recoil distribution pattern in the array.

This calculation is similar to in Ref. [75], except that Ref. [75] assumes that there is a nearly uniform excitation of the atoms in the array and only calculates the dynamics of the central atom. By calculating the kicks in each atom of the array, we see patterns arise that vary with the detuning of the laser. Figure 2.4 shows the comparison between the excitation pattern and the recoil distribution in the array. Figure 2.4(a) shows the time integrated excitation probability of each atom, while Fig. 2.4(b) depicts the ΔK_z deposited on each atom. There is significant variation in the amount of energy deposited on the atoms and the corner atoms experienced only half the recoil energy of the atoms with the maximum recoil. These patterns are a combination of the eigenstates of the excitation as seen in Section 2.3.1. The selection of the eigenstates depends on both the pattern as well as the detuning of the incoming light.

Experimentally, achieving a 100% filling fraction for the array is difficult. Hence, the effects of the array missing a single atom have been studied. The scale of the disturbance caused by a missing atom depends on the contribution it would have made if present. If an atom is missing where the excitation is naturally weak, it has less effect on the excitation pattern and recoil (Fig. 2.5a). However, if the atom is missing where the excitation is large, there is a more substantial effect seen spanning a few nearby atoms (Fig. 2.5b). The recoil in the in-plane direction for the neighboring atoms will also change. The recoil they experience in the direction towards the missing atom will be increased.

As explained in Section 2.2.2, we have chosen the range of d between 0.5λ to 1.0λ so that coupling subradiant modes, which have adjacent atoms in-phase, will be easier with uniform illumination. For other experiments that prioritize working with superradiant states, the interatomic distance could be chosen in the range $d < 0.5\lambda$ for easy coupling with uniform light.

2.3.4 Steady State

So far, we have studied the recoil received after the system has completely relaxed to the ground state at infinite time. But in most experiments and applications, it is also important to understand the behavior of these kicks when there is a steady state involved. Instead of

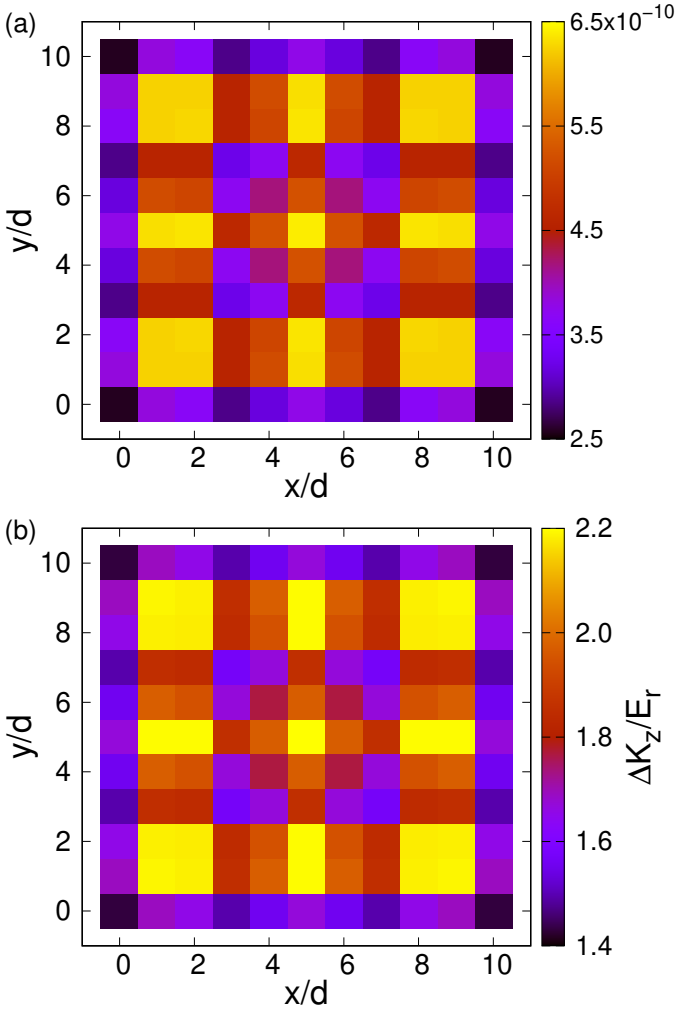

Figure 2.4. The excitation and recoil distribution pattern on a 11×11 atom array with $d = 0.68\lambda$ when excited by a laser pulse with peak Rabi frequency $\Omega_0 = 0.02\Gamma$ and pulse width $t_w = 16/\Gamma$ at zero detuning. Each cell denotes one atom in the array. (a) shows the integral of the excitation probability in time for each atom in arbitrary units and (b) shows the $\Delta K_z/E_r$ deposited on each atom of the array per photon incident on the atom.

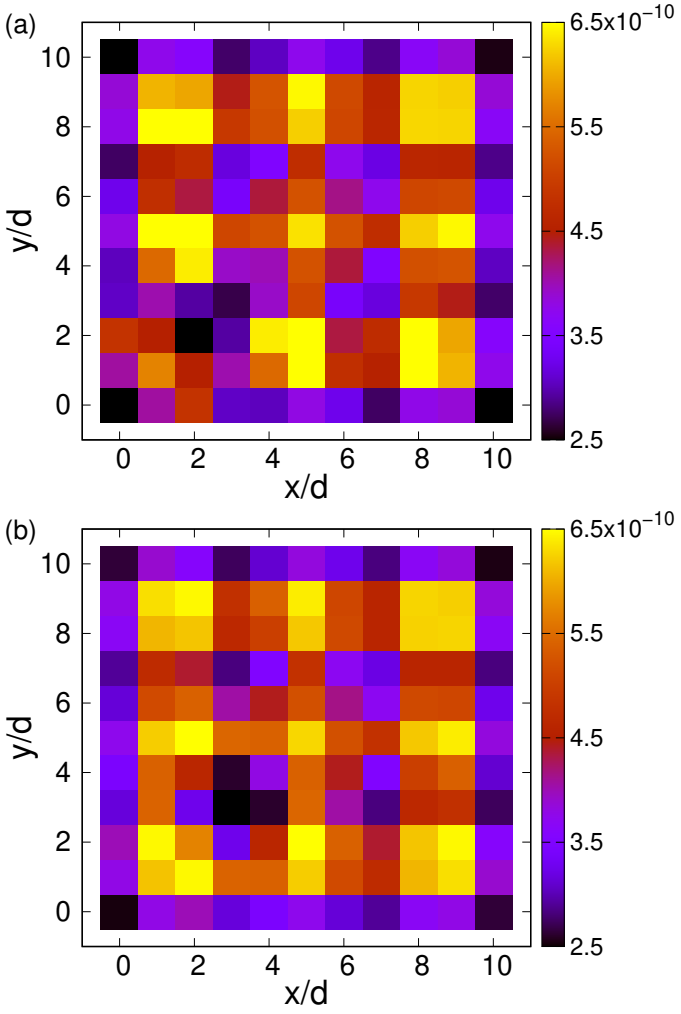

Figure 2.5. The effects of an atom missing from an array of 11×11 atoms with $d = 0.68\lambda$ and pulsed light illumination with no detuning. The plots show the total integrated probability of excitation of each atom in arbitrary units. Compare with Fig. 2.4(a) which is the case where no atoms are missing. (a) has atom at coordinate (2,2) missing. It has a larger impact and affects up to second nearest neighbour atoms. (b) has atom at coordinate (3,3) missing. It has a smaller impact and only affects the immediate neighbours.

finding the total momentum and energy deposited, a more useful quantity will be the rate of energy deposited in each atom in steady state.

The methods described earlier as well as in Ref. [75] describe the process in which the final state of the system is the ground state. Hence we developed a different method to determine the rate of momentum and energy deposited. When the system has reached steady state, we can approximate that up to the first order in time, all the density matrix elements except the ground state coefficient reaches equilibrium. This means that the only linear time dependent term will be the ground state density matrix coefficient (ρ_{gg}). Taking the positional derivatives on $\dot{\rho}_{gg}$ similar to Eq. (2.11) and Eq. (2.12) yields the rate of the momentum and energy kicks. The density matrix can be evolved until steady state is reached and the $\dot{\rho}_{gg}$ can be calculated. Alternatively, the master equation can be solved analytically to obtain an expression for $\dot{\rho}_{gg}$.

$$\begin{aligned}\dot{\rho}_{gg}(t) = &- \mathrm{i}\sum_{\mathrm{j}} \frac{\Omega^*(\mathbf{r}_\mathrm{j})}{2}\rho_{\mathrm{e_j}g} + \mathrm{i}\sum_{\mathrm{j}} \frac{\Omega(\mathbf{r}'_\mathrm{j})}{2}\rho_{g\mathrm{e_j}} \\ &+ \sum_{\mathrm{ij}} 2R\mathrm{e}\{g(\mathbf{r}'_{\mathrm{ij}})\}\rho_{\mathrm{e_i e_j}}\end{aligned} \tag{2.19}$$

where $\Omega(\mathbf{r}_\mathrm{j})$ describes the spatial profile of the incoming laser as well as carrying a phase factor $\mathrm{e}^{-\mathrm{i}\mathbf{k_0}\cdot\mathbf{r}_\mathrm{j}}$. The derivation and the procedure to calculate the density matrix terms at steady state are discussed in Appendix 2.B. For this approximation to have good accuracy, it is important that we stay within the low intensity limit and use low Rabi frequencies.

The momentum and the energy deposited increase as a function of Ω^2 which is expected as it is proportional to the number of incoming photons. To calculate the number of photons incident on an atom, we can integrate the intensity arriving on the area corresponding to one atom (d^2) per unit time and divide by the energy of a single photon ($\hbar c/\lambda_0$). The number of photons incident on each atom in one lifetime of a single atom is

$$\nu_\Gamma = \frac{2\pi}{3}\left(\frac{d}{\lambda}\right)^2\left(\frac{\Omega}{\Gamma}\right)^2 \tag{2.20}$$

The recent experimental work of Ref. [31] to measure the reflectance of a subradiant atomic mirror with around 200 atoms can be simulated. For a 14×14 array at peak resonance, with $d = 0.68\lambda$ and an influx of 1.8×10^{-4} photons per lattice site in one lifetime of a single atom, the calculations show that the average total energy deposited is $4.4E_r$ per incoming photon. Each individual atom experienced a total recoil ranging from $2.6E_r$ to $5.6E_r$ per photon incident on each atom. The total average momentum imparted on each atom is $1.7\hbar k$ per incoming photon, which corresponds to a reflectance of 85%.

Reference [18] discussed a null transmission situation for an infinite plane array with $d = 0.8\lambda$. Figure 8 of Ref. [75] also showed that the reflectance is near unity for an infinite array and estimates the same for a 11×11 array using the Δp_z of the center atom. The emergence of the excitation patterns implies that this will be an overestimation for non-infinite arrays. Performing the recoil calculations on all the individual atoms shows that the reflectance only reaches 80% for a 11×11 array when taking the average over all the atoms. The atoms at the edges couple less with the incoming light, decreasing the reflectance of the array. Re-calculating the average ignoring the edge atoms increases the reflectance to 95%.

By altering the detuning and the incident laser's transverse spatial profile, we can excite individual eigenmodes of the array. This would be impossible to experimentally implement for most states because of the high density of the atoms and the interatomic spacing being comparable to the resonant wavelength. The momentum imparted by the laser when exciting individual eigenmodes was inversely proportional to the eigenmode's decay rate. This is the result of the altered absorption rate of the incoming light. When the system is at steady state, the absorption rate must match the decay rate of that eigenmode. The energy deposited due to the collective dipole interaction followed a similar trend to the previous discussions and is also inversely proportional to the decay rate. This can be seen by the presence of the eigenvalue $\mathcal{G}_\alpha$ in the denominator of the dominant terms in the analytical solutions (Eq. (2.42)).

When driving with lasers, the detuning plays a role in deciding the contribution of the different eigenmodes as specified in Section 2.3.3. The eigenmodes closest to the symmetric Dicke state ($(\sum_i |e_i\rangle)/\sqrt{N}$) will couple better with the uniform incoming light. Since each eigenstate is associated with an energy shift ($Im\{\mathcal{G}_\alpha\} = \Delta_\alpha$), matching the detuning also

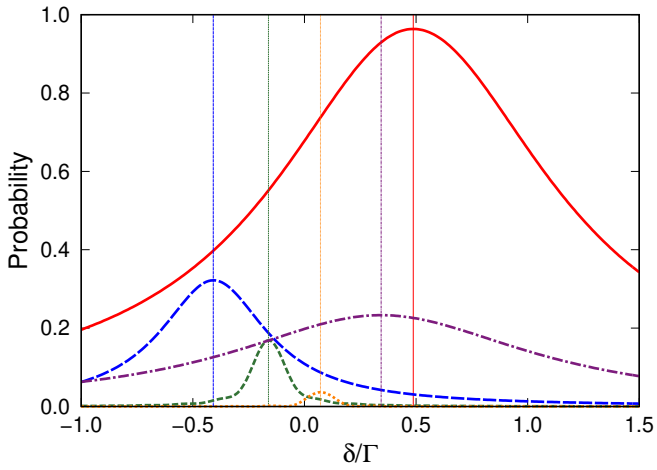

Figure 2.6. The decomposition of the state into its eigenmodes when excited by uniform light for a 5×5 array with $d = 0.4\lambda$ versus the detuning δ. The thick lines show the probability of each eigenmode in rescaled arbitrary units while varying the detuning. The thin vertical lines show the line shift Δ_α of the eigenmode with the corresponding color and dash-type. Only the 5 states that have a significant contribution are shown.

contributes to selecting the eigenstate. By using these factors, it is possible to influence which eigenstates contributes to the coupling of the atoms to the laser, to a certain extent. By using the orthogonality relations defined in Eq. (4.9), we can determine the contribution from each eigenstate as we vary the detuning. As seen from Fig. 2.6, the maximum contribution from a particular eigenstate is when the detuning matches with the shift associated with it.

2.3.5 Comparison to Trap Parameters

There are various mechanisms used in experiments for trapping atoms, including optical lattices, tweezers, ion traps, etc. But in general, we can assume that the trap is deep enough to be approximated as a harmonic oscillator potential. The vibrational state of the atom in a quantum harmonic potential with trap frequency ω_t can be denoted by n. If the atom is initially in the ground state, the relation between the recoil energy deposited and the final expectation value of the vibrational state is given by

$$\langle n \rangle = \frac{\Delta K}{\hbar \omega_t} \tag{2.21}$$

Typically, the trap frequencies used in experiments will be around 10 kHz in the out-of-plane direction and 100 kHz in the in-plane direction. For a Rubidium atom using the 780 nm resonance, a recoil of $4E_r$ due to the reflection of a single photon would bring the average vibrational state to $\langle n \rangle = 1.5$ and 0.15 for 10 kHz and 100 kHz respectively.

If subradiance doubles the recoil, the average vibrational state reached also doubles. This causes unnecessary heating or loss of coherence in the system. Even an $\langle n \rangle = 0.15$ could be an issue in quantum computing applications where the entanglement with the center of mass degrees of freedom must be less than 1%. In the case of the calculation in Section 2.3.2, the center atom receives $\sim 900E_r$ in the decay process. Even with a high trap frequency of 100 kHz, the center atom goes to the $\langle n \rangle = 35$ average vibrational state. The high vibrational state and the large spread over vibrational states would cause problems with decoherence in qubit implementations. The other atoms in the array would be in lower vibrational states and this uneven heating effect could lead to unforeseen issues.

2.4 Conclusion

We presented the calculations for the recoil energy and momentum deposited in an array of atoms interacting collectively with light. We studied the directional properties of the recoil and explored the effects of the eigenmodes of excitation in the system. The recoil energies added to each atom are proportional to the decay lifetimes of the eigenmodes and the more subradiant states experience more recoil than might be expected. This implies that recoil effects should be considered more carefully in experiments involving highly subradiant states. We note that when driving the array with uniform light, the excitation and recoil distribution in the array is not uniform but forms patterns that vary with the detuning. The patterns form due to the interference of the different eigenmodes coupling with the uniform light. These patterns also strongly contribute to the recoil of individual atoms. Calculations were done to determine the rate of energy deposition when the system reaches a steady state due to a constant influx of light.

We also calculated the recoil effects in cavities made of curved atomic arrays and found pronounced effects as the decay rate decreased. However, our calculations are not applicable

when the decay lifetimes become comparable to the timescale of the atomic vibration. Thus, our results for photon cavities (Sec. 2.3.2) can be taken only as a qualitative estimate. It is unclear how the momentum transfer occurs on such timescales. A fully quantum approach would require large amounts of computational resources but exploring this situation with a few simplifying assumptions would give a better answer to this question. Reference [74] explored the opposite regime where the internal state lifetimes are far larger than the motional timescale. It would be interesting to explore the physics at the interface of these two regimes.

2.A Appendix: Eigenstate decay analytical calculation

We derive an analytical method to calculate the kicks when the system starts off with a single excitation in any arbitrary excitation pattern. There is no driving from the laser interaction. We write the state in terms of the eigenmodes $\mathbf{V}_\alpha$ and $\mathbf{U}_\alpha$ which are the eigenvectors of $G_{ij} = g(\mathbf{r}_{ij})$ and $G''_{ij} = g(\mathbf{r}''_{ij})$ respectively.

$$\sum_{j'} G_{jj'}\mathbf{V}_{j'\alpha} = \mathcal{G}_\alpha \mathbf{V}_{j\alpha} \quad \sum_{j'} G''_{jj'}\mathbf{U}_{j'\alpha} = \mathcal{G}''_\alpha \mathbf{U}_{j\alpha} \tag{2.22}$$

Since G and G'' are non-Hermitian, their eigenvectors are not orthonormal and $\mathbf{V}_\alpha$ and $\mathbf{U}_\alpha$ have to be normalized to follow

$$\sum_{j} \mathbf{V}_{j\alpha}\mathbf{V}_{j\alpha'} = \delta_{\alpha\alpha'} \quad \sum_{j} \mathbf{U}_{j\alpha}\mathbf{U}_{j\alpha'} = \delta_{\alpha\alpha'} \tag{2.23}$$

Hence, we can write the $g(\mathbf{r}_{ij})$s as follows

$$\begin{aligned} g(\mathbf{r}_{ij}) &= \sum_\alpha \mathbf{V}_{i\alpha}\mathbf{V}_{j\alpha}\mathcal{G}_\alpha \\ g^*(\mathbf{r}''_{ij}) &= \sum_\alpha \mathbf{U}^*_{i\alpha}\mathbf{U}^*_{j\alpha}\mathcal{G}^*_\alpha \end{aligned} \tag{2.24}$$

In the case where there is no laser interaction, the terms $\rho_{\mathrm{e_j}g}$ and $\rho_{g\mathrm{e_j}}$ will vanish giving

$$\hat{\rho}(t) = \rho_{gg}(t)|g\rangle\langle g| + \sum_{\mathrm{jj'}} \rho_{\mathrm{e_j e_{j'}}}(t)\hat{\sigma}^{+}_{\mathrm{j}}|g\rangle\langle g|\hat{\sigma}^{-}_{\mathrm{j'}} \tag{2.25}$$

where the positional dependence has been suppressed for notational convenience. We can write the density matrix equation as

$$\frac{d\hat{\rho}}{dt} = \sum_{\mathrm{i,j}} \Big[-g(\mathbf{r}_{\mathrm{ij}})\hat{\sigma}^{+}_{\mathrm{i}}\hat{\sigma}^{-}_{\mathrm{j}}\hat{\rho} - g^{*}(\mathbf{r}''_{\mathrm{ij}})\hat{\rho}\hat{\sigma}^{+}_{\mathrm{i}}\hat{\sigma}^{-}_{\mathrm{j}} + 2R\mathrm{e}\{g(\mathbf{r}'_{\mathrm{ij}})\}\hat{\sigma}^{-}_{\mathrm{j}}\hat{\rho}\hat{\sigma}^{+}_{\mathrm{i}} \Big] \tag{2.26}$$

Solving this we get,

$$\frac{d\rho_{\mathrm{e_j e_{j'}}}(t)}{dt} = \sum_{k} \Big(-g(\mathbf{r}_{\mathrm{j}k})\rho_{\mathrm{e}_k\mathrm{e_{j'}}} - \rho_{\mathrm{e_j e}_k} g^{*}(\mathbf{r}''_{k\mathrm{j'}}) \Big) \tag{2.27}$$

Decomposing the $\rho_{\mathrm{e_j e_{j'}}}$ in terms of the eigenfunctions $\mathbf{V}_{\alpha}$ and $\mathbf{U}^{*}_{\alpha'}$

$$\rho_{\mathrm{e_j e_{j'}}} = \sum_{\alpha\alpha'} \mathbf{V}_{\mathrm{j}\alpha}\mathbf{U}^{*}_{\mathrm{j'}\alpha'}C_{\alpha\alpha'} \tag{2.28}$$

Using this, we get

$$\begin{aligned} \frac{dC_{\alpha\alpha'}}{dt} &= -(\mathcal{G}_{\alpha} + \mathcal{G}''^{*}_{\alpha'})C_{\alpha\alpha'} \\ \implies C_{\alpha\alpha'}(t) &= C_{\alpha\alpha'}(0)\mathrm{e}^{-(\mathcal{G}_{\alpha}+\mathcal{G}''^{*}_{\alpha'})t} \end{aligned} \tag{2.29}$$

Since the ρ_{gg} term only arises from the last term of Eq. (2.26), we get

$$\begin{aligned} \frac{d\rho_{gg}}{dt} &= \sum_{\mathrm{jj'}} 2R\mathrm{e}\{g(\mathbf{r}_{\mathrm{jj'}})\}\rho_{\mathrm{e_j e_{j'}}} \\ &= \sum_{\alpha\alpha'}\sum_{\mathrm{jj'}} 2R\mathrm{e}\{g(\mathbf{r}_{\mathrm{jj'}})\}\mathbf{V}_{\mathrm{j}\alpha}\mathbf{U}^{*}_{\mathrm{j'}\alpha'}C_{\alpha\alpha'}(t) \end{aligned} \tag{2.30}$$

Since $C_{\alpha\alpha'}(t)$ are exponentials,

$$\rho_{gg}(\infty) = \sum_{\alpha,\alpha'}\sum_{\mathrm{j,j'}} 2R\mathrm{e}\{g(r'_{\mathrm{jj'}})\}\mathbf{V}_{\mathrm{j}\alpha}\mathbf{U}^{*}_{\mathrm{j'}\alpha'}\frac{C_{\alpha,\alpha'}(0)}{\mathcal{G}_{\alpha} + \mathcal{G}''^{*}_{\alpha'}} \tag{2.31}$$

The expression for $C_{\alpha\alpha'}(0)$ can be obtained from Eq. (2.28) using the orthogonality relations (Eq. (2.23)) to be

$$C_{\alpha,\alpha'} = \sum_{\mathrm{jj'}} \mathbf{V}_{\mathrm{j}\alpha} \mathbf{U}^*_{\mathrm{j'}\alpha'} \rho_{\mathrm{e_j e_{j'}}} \tag{2.32}$$

If the system is initialized to one of its eigenstates β with $\rho(t=0) = \mathcal{N}_\beta |\mathbf{V}_\beta\rangle\langle\mathbf{V}_\beta|$, then

$$C_{\alpha,\alpha'}(t=0) = \mathcal{N}_\beta \delta_{\alpha\beta} \sum_{\mathrm{i}} \mathbf{V}^*_{\mathrm{i}\beta} \mathbf{U}^*_{\mathrm{i}\alpha'} \tag{2.33}$$

where $\mathcal{N}_\beta = (\sum_{\mathrm{i}} |\mathbf{V}_{\mathrm{i}\beta}|^2)^{-1}$ is the normalization factor.

2.A.1 Out-of-plane eigenstate recoil energy

When we analyze the kinetic energy kick imparted on the out-of-plane direction when the system is initialized to an eigenstate, we get a proportionality equation between the energy deposited and the state lifetimes. This can be derived by taking the second derivative from Eq. (2.12) only in the z-direction. When the system is initialized to an eigenstate β, the dominant terms in the summation of Eq. (2.31) will be the terms with $\alpha = \alpha' = \beta$. Hence the summation over the eigenstates will vanish giving

$$\rho_{gg}(\infty) = \sum_{\mathrm{j,j'}} 2Re\{g(r'_{\mathrm{jj'}})\} \mathbf{V}_{\mathrm{j}\beta} \mathbf{U}^*_{\mathrm{j'}\beta} \frac{C_{\beta,\beta}(0)}{\mathcal{G}_\beta + \mathcal{G}''^*_\beta} \tag{2.34}$$

To take derivatives in the z-direction, we shift the primed coordinates, $\mathbf{r}'_{\mathrm{j}} = \mathbf{r}_{\mathrm{j}} + \delta z$. This would result an insignificant change in $\mathcal{G}''_\beta = \mathcal{G}_\beta + 10^{-2} O(\delta z^3)$ and a second order change in the eigenvectors, $\mathbf{U}_{\mathrm{j}\beta} = \mathbf{V}_{\mathrm{j}\beta} + 10^{-2} O(\delta z^2)$. Hence when taking up to second derivatives, we can assume $\mathcal{G}''_\beta \approx \mathcal{G}_\beta$ and $\mathbf{U}_{\mathrm{j}\beta} \approx \mathbf{V}_{\mathrm{j}\beta}$. This implies that $\mathcal{G}_\beta + \mathcal{G}''^*_\beta = 2Re\{\mathcal{G}_\beta\} = \gamma_\beta$ and $\mathbf{V}_{\mathrm{j}\beta}\mathbf{U}^*_{\mathrm{j}\beta} = |\mathbf{V}_{\mathrm{j}\beta}|^2$. Using Eq. (2.33), $C_{\beta,\beta}(0)$ will also become $\mathcal{N}_\beta$. This gives

$$\rho_{gg}(\infty) = \sum_{\mathrm{j,j'}} 2Re\{g(r'_{\mathrm{jj'}})\} \mathbf{V}_{\mathrm{j}\beta} \mathbf{U}^*_{\mathrm{j'}\beta} \frac{\mathcal{N}_\beta}{\gamma_\beta} \tag{2.35}$$

When taking the second derivative for the atom k, only the term $\mathrm{j} = \mathrm{j'} = k$ will be non vanishing.

$$\rho_{gg}(\infty) = 2R\mathrm{e}\{g(r'_{kk})\}|\mathbf{V}_{k\beta}|^2\frac{\mathcal{N}_\beta}{\gamma_\beta} \tag{2.36}$$

At the limit of $\delta z \to 0$,

$$\lim_{\delta z\to 0}\frac{\partial^2 R\mathrm{e}\{g(\mathbf{r}'_{kk})\}}{\partial z^2} = -k^2\frac{\Gamma}{5} \tag{2.37}$$

Hence the kinetic energy deposited on atom k will be

$$\Delta K_z^{(k)} = \frac{\hbar^2k^2}{2m}\frac{2\Gamma}{5}|\mathbf{V}_{k\beta}|^2\frac{\mathcal{N}_\beta}{\gamma_\beta} \tag{2.38}$$

The total kinetic energy deposited on the whole array in the z-direction will be (using $\mathcal{N}_\beta = (\sum_{\mathrm{i}}|\mathbf{V}_{\mathrm{i}\beta}|^2)^{-1}$)

$$\frac{\Delta K_z}{E_r} = \frac{2}{5}\frac{\Gamma}{\gamma_\beta} \tag{2.39}$$

2.B Appendix: Steady state analytical calculation

In this appendix, we derive analytically a method to find the recoil at steady state by decomposing the state into its eigenstates. For simplicity in this derivation, $\rho_{\mathrm{e_j}g}$, $\rho_{g\mathrm{e_j}}$ and $\rho_{\mathrm{e_i}\mathrm{e_j}}$ will be represented as w_{j}, $\tilde{w}_{\mathrm{j}}$ and $\tilde{\rho}_{\mathrm{ij}}$ respectively and the positional dependence will not be explicitly shown. That is, Eq. (5.14) will be represented as

$$\begin{aligned}\hat{\rho} \quad &= \quad \rho_{gg}|g\rangle\langle g| + \sum_{\mathrm{i}} w_{\mathrm{i}}|\mathrm{e_i}\rangle\langle g| \\ &\quad + \sum_{\mathrm{j}}\tilde{w}_{\mathrm{j}}|g\rangle\langle \mathrm{e_j}| + \sum_{\mathrm{i,j}}\tilde{\rho}_{\mathrm{ij}}|\mathrm{e_i}\rangle\langle \mathrm{e_j}|\end{aligned} \tag{2.40}$$

A constant laser with detuning δ and Rabi frequency $\Omega(\mathbf{r}_{\mathrm{j}})$ is incident on the j^{th} atom of the array. By using Eq. (4.2), we can obtain the rate of change of the coefficients of the density matrix.

$$\dot{w}_{\mathrm{j}} = -\mathrm{i}\frac{\Omega(\mathbf{r}_{\mathrm{j}})}{2}\rho_{gg} + \mathrm{i}\delta w_{\mathrm{j}} - \sum_k g(\mathbf{r}_{\mathrm{j}k})w_k \tag{2.41a}$$

$$\dot{\tilde{w}}_{\mathrm{j}} = \mathrm{i}\frac{\Omega^*(\mathbf{r}'_{\mathrm{j}})}{2}\rho_{gg} - \mathrm{i}\delta\tilde{w}_{\mathrm{j}} - \sum_k g^*(\mathbf{r}''_{\mathrm{j}k})\tilde{w}_k \tag{2.41b}$$

$$\begin{aligned}\dot{\tilde{\rho}}_{\mathrm{ij}} = &-\mathrm{i}\frac{\Omega(\mathbf{r}_{\mathrm{i}})}{2}\tilde{w}_{\mathrm{j}} + \mathrm{i}\frac{\Omega^*(\mathbf{r}'_{\mathrm{j}})}{2}w_{\mathrm{i}} \\ &- \sum_k g(\mathbf{r}_{\mathrm{i}k})\tilde{\rho}_{k\mathrm{j}} - \sum_k g^*(\mathbf{r}''_{k\mathrm{j}})\tilde{\rho}_{\mathrm{i}k}\end{aligned} \tag{2.41c}$$

$$\begin{aligned}\dot{\rho}_{gg} = &\sum_{\mathrm{ij}} 2Re\{g(\mathbf{r}'_{\mathrm{ij}})\}\tilde{\rho}_{\mathrm{ij}} \\ &-\mathrm{i}\sum_{\mathrm{j}}\frac{\Omega^*(\mathbf{r}_{\mathrm{j}})}{2}w_{\mathrm{j}} + \mathrm{i}\sum_{\mathrm{j}}\frac{\Omega(\mathbf{r}'_{\mathrm{j}})}{2}\tilde{w}_{\mathrm{j}}\end{aligned} \tag{2.41d}$$

where $\Omega(\mathbf{r}_{\mathrm{j}})$ describes the spatial profile of the incoming laser as well as carrying a phase factor $\mathrm{e}^{-\mathrm{i}\mathbf{k_0}\cdot\mathbf{r}_{\mathrm{j}}}$. We can decompose the coefficients w_{j}, $\tilde{w}_{\mathrm{j}}$ and $\tilde{\rho}_{\mathrm{ij}}$ in terms of the eigenstates $\mathbf{V}_{\mathrm{j}\alpha}$ and $\mathbf{U}_{\mathrm{j}\alpha}$ (defined in Eq. (2.22)) to get w'_α, $\tilde{w}'_\alpha$ and $\tilde{\rho}'_{\alpha\alpha'}$ using

$$w'_\alpha = \sum_{\mathrm{j}} \mathbf{V}_{\mathrm{j}\alpha} w_{\mathrm{j}} \qquad w_{\mathrm{j}} = \sum_\alpha \mathbf{V}_{\mathrm{j}\alpha} w'_\alpha \tag{2.42a}$$

$$\tilde{w}'_\alpha = \sum_{\mathrm{j}} \mathbf{U}^*_{\mathrm{j}\alpha} \tilde{w}_{\mathrm{j}} \qquad \tilde{w}_{\mathrm{j}} = \sum_\alpha \mathbf{U}^*_{\mathrm{j}\alpha} \tilde{w}'_\alpha \tag{2.42b}$$

$$\tilde{\rho}'_{\alpha\alpha'} = \sum_{\mathrm{ij}} \mathbf{V}_{\mathrm{i}\alpha}\mathbf{U}^*_{\mathrm{j}\alpha}\tilde{\rho}_{\mathrm{ij}} \qquad \tilde{\rho}_{\mathrm{ij}} = \sum_{\alpha\alpha'} \mathbf{V}_{\mathrm{i}\alpha}\mathbf{U}^*_{\mathrm{j}\alpha}\tilde{\rho}'_{\alpha\alpha'} \tag{2.42c}$$

In the first order in time, the recoil will only build up on the ground state and the change in the other coefficients will be zero, i.e., $\dot{w}_{\mathrm{j}}$, $\dot{\tilde{w}}_{\mathrm{j}}$ and $\dot{\tilde{\rho}}_{\mathrm{ij}}$ will be zero. Therefore, we can solve for w'_α, $\tilde{w}'_\alpha$ and $\tilde{\rho}'_{\alpha\alpha'}$ using Eqs. (2.41a), (2.41b) and (2.41c), which gives

$$w'_\alpha = \frac{-\mathrm{i}\rho_{gg}}{2}\sum_{\mathrm{i}}\frac{\Omega(\mathbf{r}_{\mathrm{i}})\mathbf{V}_{\mathrm{i}\alpha}}{\mathcal{G}_\alpha - \mathrm{i}\delta} \tag{2.43a}$$

$$\tilde{w}'_\alpha = \frac{\mathrm{i}\rho_{gg}}{2}\sum_{\mathrm{i}}\frac{\Omega^*(\mathbf{r}'_{\mathrm{i}})\mathbf{U}^*_{\mathrm{i}\alpha}}{\mathcal{G}''^*_\alpha + \mathrm{i}\delta} \tag{2.43b}$$

$$\tilde{\rho}'_{\alpha\alpha'} = \frac{\rho_{gg}}{4} \sum_{\mathrm{i}} \frac{\Omega(\mathbf{r}_{\mathrm{i}})\mathbf{V}_{\mathrm{i}\alpha}}{\mathcal{G}_{\alpha} - \mathrm{i}\delta} \sum_{\mathrm{j}} \frac{\Omega^{*}(\mathbf{r}'_{\mathrm{j}})\mathbf{U}^{*}_{\mathrm{j}\alpha'}}{\mathcal{G}''^{*}_{\alpha'} + \mathrm{i}\delta} \tag{2.43c}$$

The term ρ_{gg} can be calculated using $Tr[\hat{\rho}] = 1$, but in the low intensity limit, it will be close to 1. These equations can be used in conjunction with Eqs. (2.41d) and (2.42) to calculate $\dot{\rho}_{gg}$ to find the recoil kinetic energy and momentum.

3. RECOIL USING QUANTIZED VIBRATIONAL STATES

The contents of this chapter were published as Deepak A. Suresh and F. Robicheaux (2022), Atom recoil in collectively interacting dipoles using quantized vibrational states, Phys. Rev. A 105, 033706 [87].

3.1 Introduction

The impulse model described in Ch. 2 was constructed under the slow oscillation, or equivalently, the sudden approximation, where the timescales of the atomic oscillations are much longer than the timescales of the internal state dynamics. This implies that the trap frequencies should be much smaller than the decay rate of the system. Typically, the trap frequencies used are 10 to 100 kHz while the decay rates of electronic excitations are often around 10s of MHz. While these trap frequency ranges would normally be within the sudden approximation, problems arise when the system becomes subradiant and the collective decay rates approach the trap frequencies.

The results from the impulse model also indicated that the recoil is typically proportional to the lifetime of the excitation in certain cases, leading to enormous recoils in highly subradiant systems. While the sudden approximation gives an intuitive understanding of how energy is added to the center of mass motion and how decoherence arises, the assumptions in the approximation are dubious for some of the more interesting atomic arrangements. The goal of this chapter is to clarify such ambiguous results and to extend the analysis beyond the approximations used in Ch. 2.

The quantum harmonic oscillator model described in this chapter calculates the recoil in collectively interacting systems but removes the assumptions in the sudden approximation. The N atoms are assumed to be trapped in harmonic potentials having quantized vibrational energy states. Using the density matrix formalism, we time evolve the combined-vibrational and internal state density matrix, to calculate the momentum and energy deposited in the system at a later time. This model does not have the limitation of the sudden approximation and can be used to simulate a wide range of trap frequencies and, thus, can serve as an important test of the sudden approximation. It will also provide insight into how the different

terms of the Hamiltonian and the Lindblad operator contribute to the recoil of the atoms. We focus on the transfer of energy in the system rather than the vibrational population as the population in the excited states trivially decreases as the frequency increases for the same energy transfer.

To simplify the calculations, we will work in the low intensity limit where there is only a single excitation in the system, i.e., only one atom can be electronically excited at a time. This will reduce the number of internal states from 2^N to $(N+1)$. We also investigate only cases where the spread of the atomic wavefunction is smaller than the distances of atom separation, to reduce the overlap of wavefunctions. This is expected in reasonable experimental arrangements because otherwise the atom grid is not well defined.

This chapter proceeds as follows. Section 3.2 discusses the model and equations used. Section 3.3.1 discusses the decay and laser interaction for a single atom to illustrate the role of recoil and Sec. 3.3.2 extends the analysis to N atoms. We discuss approximations to simulate a large number of atoms in Sec. 3.3.3 to calculate the recoil in arrays of atoms and subradiant cavities. Section 3.4 presents the conclusions and summarises the results and future outlook.

3.2 Methods

We shall consider N atoms, each trapped in a quantum harmonic potential with each atom having two internal electronic states. The center of each trap will form a spatial arrangement required by the experiment, for example, a square array. Since the atoms are in a harmonic trap potential, they will each have an infinite Hilbert space of vibrational levels. We can limit the number of vibrationally excited states for each atom to be states $n < N_{vib}$ for calculation purposes. When the spread of the atomic wavefunction is small, the effects on the harmonic oscillator wavefunctions are separable across the different directions. Hence, we can run the calculations by choosing one oscillation direction at a time. The N atoms together will have a combined vibrational Hilbert space of $V = (N_{vib})^N$ states. Since we are working in the low intensity limit and only one atom can be electronically excited at

any time, the total number of internal states is N + 1. Hence, the total number of states is $(N+1)(N_{vib})^N$.

The internal states will be represented by $|\mathrm{j}\rangle$, the collective vibrational states will be represented by $|m\rangle$ and the total state will be denoted by $|\mathrm{j}, m\rangle$. The internal state index goes from 0 to N, where j = 0 represent the electronic ground state (alternatively $|g\rangle$) with no atom excited and j = 1 to N represent only the jth atom being excited. The collective vibration state $|m\rangle$ is the tensor product of all possible vibrational states, i.e, $|m\rangle = |n_1\rangle \otimes |n_2\rangle \otimes \otimes |n_N\rangle$ where $|n_{\mathrm{i}}\rangle$ is the vibrational state of the ith atom. The index m goes from $m = 0$ to $(N_{vib})^N - 1$.

Hence, the density matrix will be represented by

$$\rho = \sum_{\mathrm{j},\mathrm{j}'} \sum_{m,m'} \rho_{\mathrm{j},\mathrm{j}'}^{m,m'} |\mathrm{j}, m\rangle\langle \mathrm{j}', m'| \tag{3.1}$$

The density matrix evolves according to the equation given by

$$\frac{d\hat{\rho}}{dt} = -\frac{\mathrm{i}}{\hbar}[\hat{H}, \hat{\rho}] + \mathcal{L}(\hat{\rho}) \tag{3.2}$$

where $\hat{\rho}$ is the density matrix of the system, $\hat{H}$ is the effective Hamiltonian and $\mathcal{L}(\hat{\rho})$ is the Lindblad super-operator. The effective Hamiltonian consists of three parts. (1) The trap potential of the atoms, which is a quantum harmonic oscillator Hamiltonian, (2) the laser Hamiltonian, and the (3) dipole-dipole resonant interaction.

The Hamiltonian of the trap potential will be given by

$$H_t = \sum_{\mathrm{j}} \hbar\omega_t (a_{\mathrm{j}}^\dagger a_{\mathrm{j}} + \frac{1}{2}) \tag{3.3}$$

where ω_t is the trap frequency of the harmonic oscillator and $a_{\mathrm{j}}^\dagger$ and a_{j} are the harmonic oscillator ladder operators for the $\mathrm{j}th$ atom in the chosen direction. The mean position of the wavefunction or the fixed point positions of the atoms will be given by $\mathbf{R}_{\mathrm{j}}$ and the spread of the atom or the position of the atom with respect to the mean will be given by $\mathbf{r}_{\mathrm{j}}$. The position operator along the chosen direction is given by $s_{\mathrm{j}} = \sqrt{\frac{\hbar}{2M\omega_t}}(a_{\mathrm{j}} + a_{\mathrm{j}}^\dagger)$. We define the

quantity $\kappa = k\sqrt{\frac{\hbar}{2M\omega_t}}$ where the length-scale for the atoms' motion and the spread of the atomic wavefunction is described by κ/k. Here, k is the wavenumber of the resonant light and M is the mass of a single atom.

When the laser interacts with the atoms, it imparts a momentum of $\hbar k$ which will manifest in the Hamiltonian through the position operators s_j The Hamiltonian due to the laser is

$$\hat{H}_L = \hbar \sum_\mathrm{j} \left[-\delta \hat{\sigma}_\mathrm{j}^+ \hat{\sigma}_\mathrm{j}^- + \left(\frac{\Omega}{2} \hat{\sigma}_\mathrm{j}^+ \mathrm{e}^{\mathbf{i}\mathbf{k}_0 \cdot (\mathbf{R}_\mathrm{j} + \hat{\mathbf{r}}_\mathrm{j})} + h.c. \right) \right] \tag{3.4}$$

where Ω is the Rabi frequency, δ is the detuning and $\mathbf{k}_0 = k\hat{\mathbf{z}}$ as the initial wavevector of the incoming photons. $\hat{\sigma}_\mathrm{j}^+$ and $\hat{\sigma}_\mathrm{j}^-$ are the raising and lowering operators of the electronic excitation of the jth atom. If the laser is propagating in the chosen direction of vibrational oscillation, the term $\mathbf{k}_0 \cdot \mathbf{r}_\mathrm{j}$ can be replaced by $\kappa(\hat{a}_\mathrm{j} + \hat{a}_\mathrm{j}^\dagger)$. Otherwise, the $\mathbf{k}_0 \cdot \mathbf{r}_\mathrm{j}$ term will be dropped and the laser will not cause any vibrational transitions.

In the following equations, the primed and unprimed coordinates are used to signify right and left multiplication of the density operator, respectively. To signify differences, we will use the following convention

$$\mathbf{r}_\mathrm{ij} \equiv \mathbf{r}_\mathrm{i} - \mathbf{r}_\mathrm{j}; \qquad \mathbf{r}'_\mathrm{ij} \equiv \mathbf{r}_\mathrm{i} - \mathbf{r}'_\mathrm{j}; \qquad \mathbf{r}''_\mathrm{ij} \equiv \mathbf{r}'_\mathrm{i} - \mathbf{r}'_\mathrm{j} \tag{3.5}$$

The resonant dipole-dipole interactions are given by the imaginary part of the Lindblad term and is given by

$$\hat{H}_{dd} = \hbar \sum_{\mathrm{i} \neq \mathrm{j}} Im\{g(\mathbf{R}_\mathrm{ij} + \mathbf{r}_\mathrm{ij})\} \hat{\sigma}_\mathrm{i}^+ \hat{\sigma}_\mathrm{j}^- \tag{3.6}$$

The real part of the Lindblad term describes the dynamics of the decay and is given by

$$\mathcal{L}(\hat{\rho}) = \sum_\mathrm{i,j} \left[2Re\{g(\mathbf{R}_\mathrm{ij} + \mathbf{r}'_\mathrm{ij})\} \hat{\sigma}_\mathrm{i}^- \hat{\rho} \hat{\sigma}_\mathrm{j}^+ - Re\{g(\mathbf{R}_\mathrm{ij} + \mathbf{r}_\mathrm{ij})\} \hat{\sigma}_\mathrm{i}^+ \hat{\sigma}_\mathrm{j}^- \hat{\rho} - \hat{\rho} \hat{\sigma}_\mathrm{i}^+ \hat{\sigma}_\mathrm{j}^- Re\{g^*(\mathbf{R}_\mathrm{ij} + \mathbf{r}''_\mathrm{ij})\} \right] \tag{3.7}$$

where the Green's function $g(\mathbf{R})$ is given by

$$g(\mathbf{R}) = \frac{\Gamma}{2} \left[h_0^{(1)}(kR) + \frac{3(\hat{R} \cdot \hat{q})(\hat{R} \cdot \hat{q}^*) - 1}{2} h_2^{(1)}(kR) \right] \tag{3.8}$$

where $\hat{q}$ is the dipole orientation, $R = |\mathbf{R}|$ is the norm of $\mathbf{R}$, $\hat{R} = \mathbf{R}/R$ is the unit vector along $\mathbf{R}$, Γ is the decay rate of a single atom and $h_l^{(1)}(x)$ are the outgoing spherical Hankel function of angular momentum l; $h_0^{(1)}(x) = \mathrm{e}^{\mathrm{i}x}/[\mathrm{i}x]$ and $h_2^{(1)}(x) = (-3\mathrm{i}/x^3 - 3/x^2 + \mathrm{i}/x)\mathrm{e}^{\mathrm{i}x}$.

When we calculate the Green's function, we take a Taylor expansion up to second order which is valid under the condition that the spread of the wavefunction (κ/k) is much less than the separation of atoms.

$$g(\mathbf{R}_{\mathrm{ij}} + \epsilon) = g(\mathbf{R}_{\mathrm{ij}}) + \Big(\frac{g'(\mathbf{R}_{\mathrm{ij}})}{k}\Big)k\epsilon + \Big(\frac{g''(\mathbf{R}_{\mathrm{ij}})}{k^2}\Big)\frac{k^2\epsilon^2}{2} + ... \tag{3.9}$$

where the derivatives are taken in the chosen oscillation direction. Since the Hankel functions in $g(R)$ are functions of kR, the k's in the denominator make the expansion term, $k\epsilon$, more explicit. The $\epsilon = s_{\mathrm{i}} - s_{\mathrm{j}}$ is expanded into the corresponding vibrational ladder operators. The zeroth order term does not depend on the spread of the atoms and does not cause any transitions in the vibrational state. The first and second order terms depend on the spread of the wavefunction and will induce single level and two level transitions in the vibrational states respectively.

Since the Green's function depends on both $\mathbf{r}_{\mathrm{j}}$ and $\mathbf{r}'_{\mathrm{j}}$, which correspond to the left or right operation on the density matrix, we have s_{j} and s'_{j} respectively. While the last two terms of the Lindblad expression only have left or right multiplication, the first term behaves differently. Upon expanding the Harmonic vibrational wavefunctions, we see that the first term acts on the combined density matrix as

$$\begin{aligned} R\mathrm{e}\{g(R_{\mathrm{ij}} + r'_{\mathrm{ij}})\}\hat{\sigma}_{\mathrm{i}}^-\hat{\rho}\hat{\sigma}_{\mathrm{j}}^+ =& R\mathrm{e}\{g(R_{\mathrm{ij}})\}\hat{\sigma}_{\mathrm{i}}^-\hat{\rho}\hat{\sigma}_{\mathrm{j}}^+ \\ &+R\mathrm{e}\{\frac{g'(R_{\mathrm{ij}})}{k}\}k(s_{\mathrm{i}}\hat{\sigma}_{\mathrm{i}}^-\hat{\rho}\hat{\sigma}_{\mathrm{j}}^+ - \hat{\sigma}_{\mathrm{i}}^-\hat{\rho}\hat{\sigma}_{\mathrm{j}}^+ s'_{\mathrm{j}}) \\ &+R\mathrm{e}\{\frac{g''(R_{\mathrm{ij}})}{k^2}\}\frac{k^2}{2}(s_{\mathrm{i}}^2\hat{\sigma}_{\mathrm{i}}^-\hat{\rho}\hat{\sigma}_{\mathrm{j}}^+ + \hat{\sigma}_{\mathrm{i}}^-\hat{\rho}\hat{\sigma}_{\mathrm{j}}^+ s_{\mathrm{j}}'^2 - 2s_{\mathrm{i}}\hat{\sigma}_{\mathrm{i}}^-\hat{\rho}\hat{\sigma}_{\mathrm{j}}^+ s'_{\mathrm{j}}) \end{aligned} \tag{3.10}$$

where the ks_{i}'s will be replaced by $\kappa(a_{\mathrm{i}} + a_{\mathrm{i}}^{\dagger})$ notation when solving the equations. The expectation values of the momentum and energy in the vibrational state of atom j can then be calculated from the density matrix,

$$p_{\mathrm{j}} = \frac{\mathrm{i}}{2\kappa} Tr\left[(a_{\mathrm{j}}^{\dagger} - a_{\mathrm{j}})\rho\right] \hbar k \tag{3.11}$$

$$E_{\mathrm{j}} = \frac{1}{2\kappa^2} Tr\left[(2a_{\mathrm{j}}^{\dagger} a_{\mathrm{j}} + 1)\rho\right] E_r \tag{3.12}$$

where $\hbar k$ and $E_r = \hbar^2 k^2/(2M)$ are the recoil momentum and energy deposited when one photon is absorbed or emitted by an atom. Since the expression for the energy is divided by κ^2, only the terms of the order κ^2 in the diagonal of the density matrix will primarily contribute to a change in energy. The contribution from the κ^4 terms and beyond will be negligible for small wavefunction spreads. The energy difference in the vibrational levels will be given by $1/\kappa^2$. That is, if $\kappa = 0.01$, the energy difference of consecutive vibrational levels will be $10^4 E_r$.

3.3 Results

The impulse model used in Ch. 2 calculates the kinetic energy and momentum kick imparted in a collective dipole interaction system interacting with a laser. Since the quantum oscillator model discussed in this chapter has a fundamental difference in the way the kinetic energy is imparted to the system, the two models can be compared and tested for validity. To account for the spread of the wavefunction, the impulse model can be spatially integrated over the wavefunction probability density using Gaussian quadrature integration for small number of atoms. At low frequencies, the sudden approximation is valid and both the models agree. The results match exactly at low wavefunction spreads and with a small difference for higher spreads. This difference can be shown to be due to stopping at the second order when expanding $g(R)$ in the Taylor's series, i.e., the error is mainly in the harmonic oscillator model for low trap frequencies.

The quantum oscillator model does not have any restrictions with respect to the trap frequency, and hence we can investigate the validity of the sudden approximation, beyond

the low frequency regime. We can also study the separate contributions from the different terms of the Hamiltonian and the Lindblad equations. We are more interested in the cases with higher trap frequencies where the vibrational energy spacing is much larger than E_r. Hence we do not need to include many vibrational levels. This also implies that the spread of the wavefunction will be small and we can limit the Taylor series expansion, Eq. (3.9), to second order terms.

3.3.1 Single atom decay

To begin, we analyze the simple decay process of a single atom trapped in a harmonic potential. The atom is initially excited and no laser interaction is present. The effective Hamiltonian becomes

$$H_t = \hbar\omega_t(a_1^\dagger a_1 + 1/2) \tag{3.13}$$

Since the H_t is purely diagonal with respect to the vibrational states, its contribution to the change in the density matrix,

$$\dot{\rho} = \frac{-\mathrm{i}}{\hbar}[H_t, \rho] \tag{3.14}$$

has zero diagonal elements and only interacts with the off-diagonal coherence terms of the density matrix. The Lindblad term for a single atom is

$$\mathcal{L}^{(1)}(\rho) = 2Re\{g(r'_{11})\}\sigma_1^-\rho\sigma_1^+ - Re\{g(r_{11})\}\sigma_1^-\sigma_1^+\rho - \rho\sigma_1^-\sigma_1^+Re\{g(r''_{11})\} \tag{3.15}$$

Since $r_{11} = r''_{11} = 0$, $Re\{g(r_{11})\} = Re\{g(r''_{11})\} = \Gamma/2$. The last two terms do not contribute to changes in the vibrational states. Expanding the first term using $r'_{11} = 0 + s_1 - s'_1$ up to the second order gives

$$Re\{g(r'_{11})\} = g(0) + \frac{g''(0)}{2}\kappa^2(s_1 - s'_1)^2 \tag{3.16}$$

since the first derivative $g'(0) = 0$. The next non-zero leading order term will be the fourth order, since the third derivative is again 0, but they will be of the order κ^4 and will not cause

significant contributions when calculating the energy. If we assume the atom is initially excited and in the vibrational ground state, the first term of Eq. (3.15) becomes

$$\begin{aligned}\mathcal{L}_1(\rho) = |g\rangle\langle g|\rho^{0,0}_{1,1}\Big(&\left(\Gamma + 2\kappa^2 g''(0)\right)|0\rangle\langle 0| - 2\kappa^2 g''(0)\ \ |1\rangle\langle 1| \\ &+ \kappa^2 g''(0)\sqrt{2}(|2\rangle\langle 0| + |0\rangle\langle 2|)\Big)\end{aligned} \tag{3.17}$$

We can analytically solve the above equation to obtain the change in the vibrational energy at infinite time when the decay is complete. The change in vibrational energy is given by

$$\Delta E = -2\frac{g''(0)}{\Gamma}E_r \tag{3.18}$$

This result remains valid when the initial density matrix is any incoherent combination of vibrational states. For an atom initially excited and polarized in the $\mathrm{e}_+ = -(\hat{\mathbf{x}} + \mathrm{i}\hat{\mathbf{y}})/\sqrt{2}$ direction, $\Delta E_z = 0.4E_r$ and $\Delta E_x = \Delta E_y = 0.3E_r$. The energy deposited due to the recoil from the emission of a single photon is independent of the frequency of the harmonic oscillator. This result is correct even if we go beyond the second order approximation in Eq. (3.16).

Laser interaction

When the atoms absorb a single photon from the laser, there is a momentum of $\hbar k$ added to the atoms. The contribution to the change in vibrational state comes as $\mathrm{e}^{\mathrm{i}ks_1}$ in Eq. (3.4). Since κ is small, a Taylor expansion gives

$$\begin{aligned}\mathrm{e}^{\mathrm{i}ks_1} &= 1 + \mathrm{i}ks_1 - \frac{k^2 s_1^2}{2} + ... \\ &= 1 + \mathrm{i}\kappa(a_1^\dagger + a_1) - \frac{\kappa^2}{2}(a_1^\dagger + a_1)^2 + ...\end{aligned} \tag{3.19}$$

Since the laser interacts with the density matrix through the coherence terms, the order of the transitions to the population from the first order and second order terms are κ^2 and κ^4 respectively. Hence, the energy deposited is primarily contributed by the first order term.

When there is a continuous laser incident on the atoms, the electronic internal states of the atoms reach a steady state. Instead of the total recoil energy and momentum deposited, we calculate the rate of recoil deposited in the atoms by time evolving the density matrix using Eq. (4.2). Figure 3.1 shows the energy deposited per incident photon in the direction of the incident laser on a single atom as we vary the trap frequency. It also shows the contribution of the kick due to the coherent laser interaction and the decoherent single atom decay term. To ignore long term effects like shifts in position due to radiation pressure, the expectation values are taken immediately after reaching electronic steady state. It is important to note that we are discussing the transfer of energy across different trap frequencies and not the population in the excited states. As the frequency goes up, the energy difference between the vibrational states will increase. If the energy transfer remains the same but the frequency goes up, there will necessarily be a lower population in excited vibrational states.

The atom absorbs a photon and randomly emits it in an arbitrary direction. At low trap frequencies, the absorption of the photon results in E_r recoil and the emission gives $0.4E_r$ in the laser direction. The recoil due to the emission agrees with the result of Eq. (3.18), and is independent of the trap frequency. But as we increase the frequency, the contribution for vibrational excitation from the laser becomes negligible. At low trap frequencies ($\omega_t \ll \Gamma$), the vibrational energy states are close enough that the linewidth spread of the excited state can allow vibrational transitions. On the other hand, at high trap frequencies ($\omega_t \gg \Gamma$), the vibrational energy states are far enough apart that there is no vibrational transitions due to the laser. Hence the kick from the laser reduces when the trap frequency is higher than the decay rate of the system. Effects such as side-band cooling can also be seen when the trap frequencies are higher than the decay rate.

Coherent and decoherent transfers

There are two types of vibrational population transfer occurring in the system. When the *population* transfers through the coherence terms (off-diagonal terms) of the density matrix it is called coherent transfer. This is a two-step process where the initial population terms couple to coherence terms which then couple to population terms in different vibrational

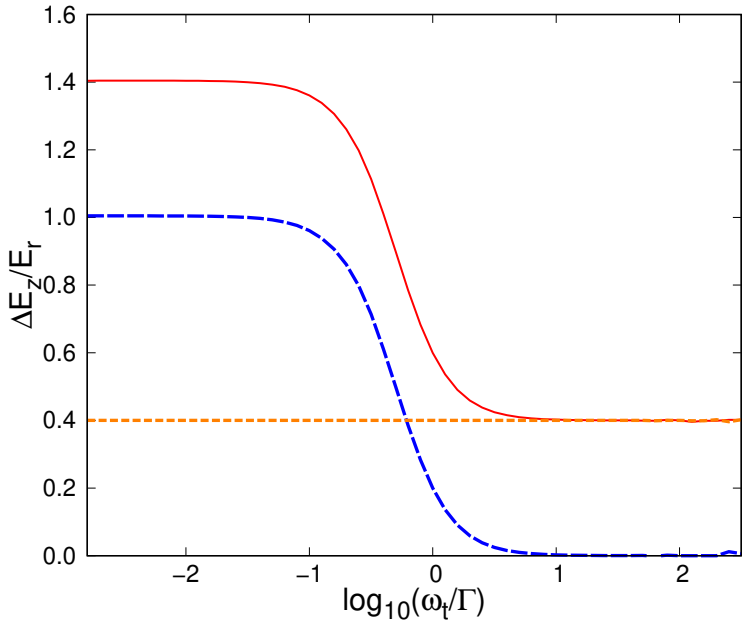

Figure 3.1. The vibrational energy deposited, per incoming photon, at steady state for a laser incident on a single atom. The red solid line shows the total energy deposited while the blue dashed and orange dashed lines show the contribution from the coherent laser transfer and the decoherent decay. The calculations were run using $N_{vib} = 5$.

states ultimately leading to a change in vibrational energy. Hence, any coherent transfers of the order κ^2 will lead to a population change of the order κ^4. The transfers due to the laser Hamiltonian are an example.

Decoherent transfers occur when the population directly transfers between the diagonal terms, without going through the coherence terms. This can be seen in the second line of Eq. (3.17), where there is a direct single level transition from the $|0\rangle\langle 0|$ to $|1\rangle\langle 1|$ vibrational state. Since the trap Hamiltonian acts on only the coherence terms, it does not affect the dynamics of the decoherent transfers. Hence, the decoherent *energy* transfers, such as the single atom decay term, are unaffected by the trap frequency.

3.3.2 Multi-atom decay

When there is more than one atom interacting, the H_{dd} Hamiltonian [Eq. (5.5)] and the two atom Lindblad terms [i.e, i $\neq$ j terms of Eq. (3.7)] come into effect. Since the vibrational raising and lowering operators in these terms act on different atoms, they cannot directly transfer the vibrational population. They go through the coherence terms and are coherent population transfers, see Sec. 3.3.1.

For simplicity, we can look at the case of two atoms. When there are two atoms very close to each other ($d \approx 0.02\lambda$), and one of the atoms is excited, the excitation rapidly hops between the two atoms while decaying, as seen from Fig. 3.2. This is the resonant dipole-dipole interaction arising from the Hamiltonian term from Eq. (5.5). Even though the excitation probability of the atom alternates, the recoil energy deposited on the atom increases continuously. All the recoil in this timescale comes from the near-field dipole dipole interactions, i.e., through the two atom dipole-dipole Hamiltonian [Eq. (5.5)].

When two atoms interact, the direction along the line connecting the atoms and the directions perpendicular have considerably different physics. Let the atoms be separated in the x-direction by a distance $d < \lambda$. In the directions along the separation, ie, in the x-direction, interatom forces arise due to the collective interactions. These forces act only along the line joining the two atoms. In the directions perpendicular to the separation, i.e.,

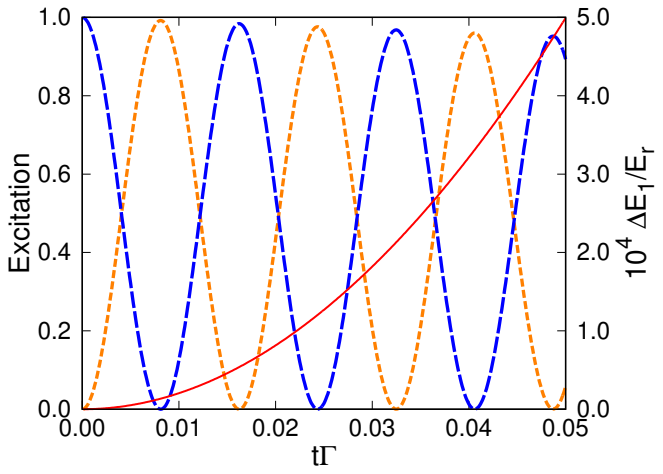

Figure 3.2. The excitation is exchanged between two atoms that are very close to each other ($d = 0.02\lambda$) when one atom is initially excited. Orange and blue dashed lines indicate the excitation probability of the two atoms. Red line shows the increase in the vibrational energy of the first atom. The calculation was done using $\kappa = 0.00001$ and $N_{vib} = 2$ using the full density matrix.

y and z-direction, there are no interatom forces and only the kick from the photon emitted contributes to the recoil.

In Figs. 3.3 and 3.4, κ is held constant while the trap frequency is altered. Since κ depends on M and ω_t, we assume that the mass also varies accordingly to compensate. While this is not a physical assumption, it is made in order to study and isolate the effects of the change in trap frequency while ignoring the more trivial effects of altering the spread of the wavefunction.

Transverse Oscillation

For two atoms, when the chosen direction of vibrational quantization is perpendicular to the separation of the atoms, there are no inter-atom forces. While taking the Taylor expansion, the first derivative of the Green's function $g'(\mathbf{R}_{ij})$ in the direction perpendicular to the separation is zero. This results in the equations being similar to the equations for the single atom case, where only zero and second order terms remain. But since the two atom Lindblad terms are coherent transfers, the second order term of κ^2 will contribute to only a κ^4 order of vibrational population transfer. Hence we see that in the perpendicular direction, only the contribution from the single atom Lindblad terms contribute to the change in vibrational energy to the lowest order in κ. The single atom terms being decoherent transfers also imply that the energy deposited in the perpendicular direction is independent of the trap frequency. Thus, the impulse model is valid even beyond the sudden approximation in the directions where there are no inter-atom interactions i.e., perpendicular to the atom array.

Figure 3.3 shows that the recoil in the perpendicular direction is independent of the frequency and agrees with the impulse model calculations. In Figs. 3.3 and 3.4, the atoms are initially excited to a singly excited state with the amplitude of the electronic excitation distributed uniformly or to an eigenstate of the complex Green's function matrix of the system. There is no laser interaction and the recoil is measured after the system is allowed to decay into the electronic ground state. Further details are included in Sec. III A of Ch. 2.

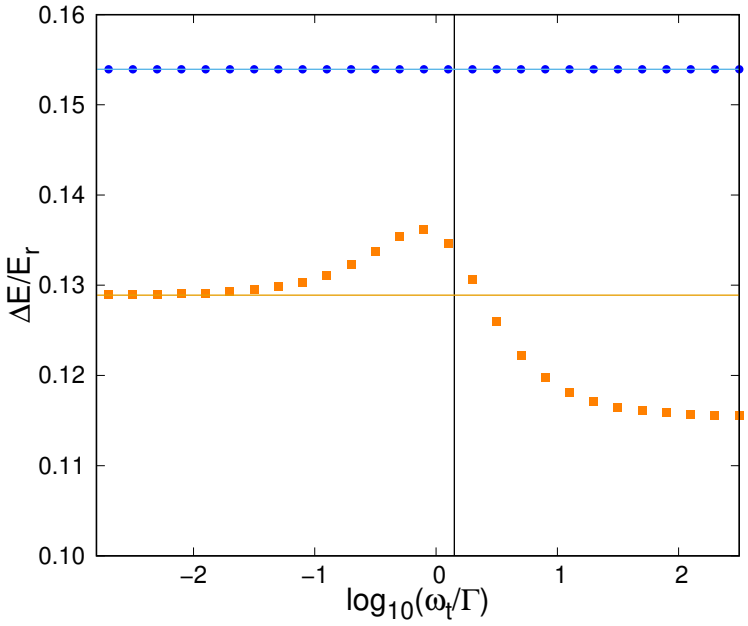

Figure 3.3. The energy deposited during the decay of two atoms uniformly excited, separated by $d = 0.4\lambda$ in the x-direction, versus the trap frequency. The blue circles and orange squares indicate the quantum harmonic oscillator model results in the z and x-direction respectively. The thin solid lines indicate the respective impulse model result. The black vertical line denotes the collective decay rate of the system. The calculations are done using full density matrix with $\kappa = 0.001$. To isolate the effects of the trap frequency, κ is kept constant and the mass M is varied to compensate for changing ω_t.

Another inference is that the rate of energy deposited into the system is only dependent on the single atom terms and is not directly dependent on the collective decay dynamics. The single atom term results in the rate of increase of the electronic ground state and, indirectly, the rate of accumulation of vibrational excitation being proportional to the excitation in the system. However, the collective decay dynamics is what determines the lifetime of the excitation. If we integrate the vibrational excitation accumulation over the entire decay process, the energy deposited in such a collective decay will be proportional to the lifetime of the collective excitation. This was also discussed in Sec. III A of Ch. 2.

Longitudinal Oscillation

In the case of the oscillations in the direction of the separation, the first derivative $g'(\mathbf{R}_{ij})$ in Eq. (3.9) is no longer zero. These first order coherent transfers contribute to a κ^2 order of population transfer. Hence there are two sources of vibrational excitation. Single atom decoherent transfers and first order two atom Lindblad coherent transfers. While the former is unaffected by the trap Hamiltonian, the latter interacts and develops a complicated dependence with the trap Hamiltonian. Figure 3.3 shows that the recoil in the direction of separation is dependent on the trap frequency and the impulse model is not valid beyond the sudden approximation.

Figure 3.4 shows an example of the energy deposited in the direction of separation varying with ω_t when the atoms are initially excited in different distributions. The contributions from the coherent and decoherent transfers are also shown. The decoherent transfers are independent of the trap frequency and only depends on the excitation probability of that atom and the decay rate of the system. The coherent transfers, on the other hand, change with the trap frequency and is highly dependent on the way the excitation is distributed among the atoms and can be either negative or positive. The threshold of what determines high trap frequency is set by the collective decay rate of the system and not the individual decay rate of the atom (Γ).

Another distinguishing feature of the coherent and decoherent transfers is the directionality. The coherent transfers are facilitated by the near field dipole-dipole interaction between the two atoms and the recoil in this process is strictly in the direction of separation. The laser interaction is also coherent and has a strict directionality with respect to the direction of the incident light. On the other hand, the decoherent transfer is from spontaneous decay where the direction of photon emission is random and the probability distribution of the direction is governed by the dipole orientation.

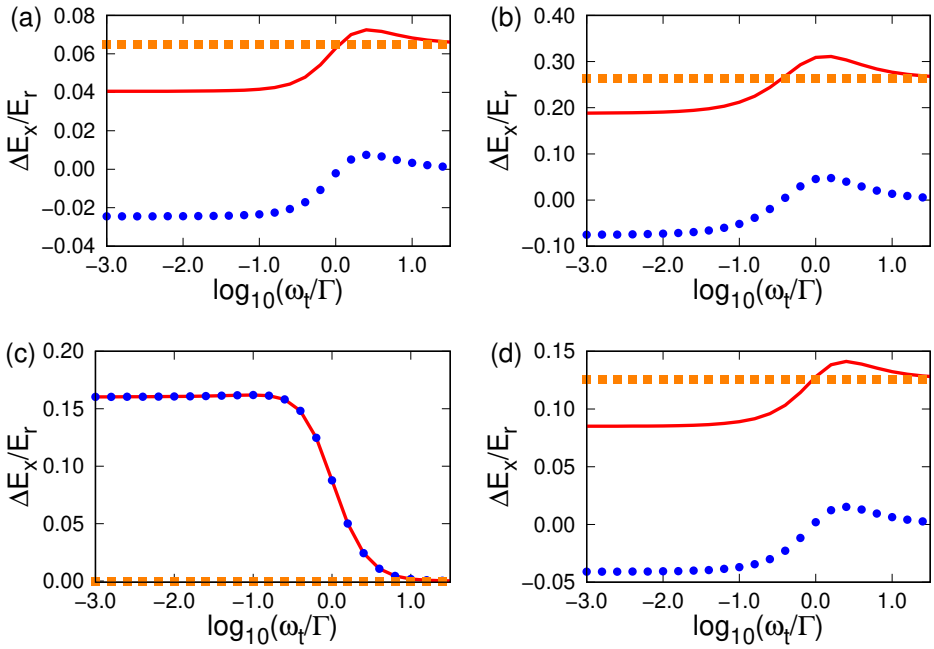

Figure 3.4. The vibrational energy deposited during the decay of the excitation. We look at the energy deposited in the x-direction on the center atom when there are three atoms in a line in x-direction separated by $d = 0.4\lambda$. The red solid line shows the total energy deposited while the blue circles and orange squares show the contribution from the coherent and decoherent transfers respectively. The initial excitation is different for the 4 cases. (a) has uniform excitation, (b)-(d) have the 3 eigenstates as excitation. The increase or decrease in energy is dependent on the excitation pattern in the higher ω_t region. (c) has zero decoherent transfers because the center atom has zero excitation probability in this particular eigenstate. The calculations are done using full density matrix with $\kappa = 0.001$. To isolate the effects of the trap frequency, κ is kept constant and the mass M is varied to compensate for changing ω_t.

3.3.3 Large ensemble of atoms

From Sec. 3.2, the number of states required for calculations increases exponentially with increasing number of atoms. All the atoms having N_{vib} vibrational states would result in all the possible permutation of vibrational state ensembles, i.e., $(N_{vib})^N$ states.

While the internal state dynamics of absorption, decay, and exchange in excitation are the driving factors of the dynamics of the vibrational states, in the approximation that the spread of the wavefunction is much smaller than the distance separating the atoms, we see that the vibrational state dynamics have little to no effect on the internal state dynamics. Hence we can approximate the calculation so that only one atom is allowed to have quantized vibrational states while the rest are fixed in space. This reduces the total available vibrational states to just N_{vib}. We calculated the vibrational energy acquired when four atoms in a square are initially excited and decay into the ground state. The error when using this approximation is only 0.2% when the wavefunction spread is as high as 25% of the separation.

We also see from Sec. 3.3.2 that the second order transfers in the vibrational state are of the order of κ^4. When taking the expectation of energy, they hardly contribute when κ is small. The same reasoning applies to the lasers (as seen in Sec. 3.3.1). Hence we can limit N_{vib} to two without losing generality in this case. For small enough $\kappa = 0.01$, the maximum vibrational energy in the atom can reach up to $10^4 E_r$ which will be within the expected recoil limits. To verify this, the results were tested for convergence using different N_{vib} in a small number of atoms.

With these two approximations, we can limit the number of states to $N_{vib} \times (N+1)$ that is, $2(N+1)$ which brings it within the realm of computation for up to 250 atoms.

Arrays of atoms

If there is a constant laser incident perpendicular to an array of closely packed atoms, the recoil in the two different directions have different behavior. Since the laser Hamiltonian does not have two atom interactions, the recoil of the atoms in the direction perpendicular to the array is similar to the single atom laser interaction seen in Sec. 3.3.1. The recoil

within the plane of the array is due to the in-plane collective decay effects as seen in Sec. 3.3.2 and is dependent on the distribution of the excitation. Figure 3.5 shows the trend of the recoil in the different directions as a function of the trap frequency. The calculations from the impulse model are also included as a solid line.

Typically, the trap frequencies in the in-plane (x and y) directions are higher and are about 100kHz, while the perpendicular trap frequencies are often an order of magnitude lower at about 10kHz. These trap frequencies will give a spread of $\kappa/k = 0.08\lambda$ and 0.25λ respectively for a Cs atom. When in steady state, such frequency ranges will be within the slow oscillation approximation and the results from the impulse model can be reproduced with the current model.

When there is a perfect reflection of a photon from an atom array, there is a momentum of $2\hbar k$ imparted on the atoms. Hence, the momentum change of the atoms describe the reflectivity of the atom array. This can also be used to study the effects of higher vibrational excited states on the reflectivity. At 10 kHz frequency in the z-direction, the momentum imparted on the central atom of an array reduces by approximately 8% when the atom is in the first vibrational excite state instead of in the ground state. However, at 100 kHz frequency in the z-direction, there is only a decrease of 0.6%. This reinforces that atomic mirror experiments would need to have high trap frequencies to have a reflection probabilities close to 1.

Cavity

In Ref. [86], we calculated the kinetic energy kick on a cavity when it decays from a highly subradiant eigenmode. This follows the design of the cavity used in Ref. [13] to perform quantum information processing. Under the slow oscillation approximation, the central atom experienced a kick of up to $926E_r$ in the duration of the decay in the direction perpendicular to the plane. The results were thought to be purely qualitative because of the large lifetimes violating the slow oscillation approximation.

The results from the Sec. 3.3.2 imply that those calculations were more accurate than suggested in Ch. 2 for the direction perpendicular to the array. In the perpendicular di-

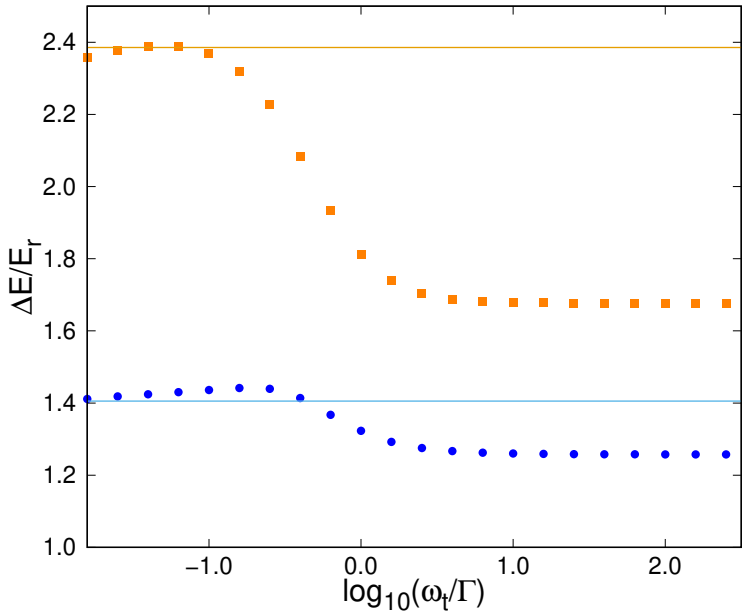

Figure 3.5. The vibrational energy deposited in the center atom of a 11×11 atom array with $d = 0.8\lambda$ separation when in steady state with an incident laser in the z-direction. The orange squares represent the recoil energy in the z-direction, while the blue circles denote the recoil energy in the x-direction, per photon incident on the center atom. The orange and blue thin lines denote the comparison with the impulse model. This data is calculated using the approximations discussed in Sec 3.3.3.

rection, since there are no or negligible inter-atom forces, the trap frequency does not play a significant role in determining the vibrational energy deposited. The recoil due to the decoherent transfers accumulates over an extended duration due to the subradiant decay resulting in large recoil energies deposited. Another way to interpret this is the large quality factor causing there to be multiple reflections of the photon on the array faces.

Calculations for the same cavity as that in Ch. 2, using the harmonic oscillator model resulted in the center atom experiencing similar vibrational energy deposited, approximately $922E_r$ in the direction perpendicular to the array. This recoil was unaffected when the trap frequencies were increased beyond the decay rate of the system. On the other hand, the energy deposited in the in-plane direction at high frequencies decreased to $15.0E_r$ as compared to $16.6E_r$ at low frequencies. These results show that the recoil of the atoms due to collective decay, especially in highly subradiant systems, should not be ignored.

3.4 Conclusion

We presented a model to describe and calculate the recoil in light-matter collective interaction using quantum harmonic oscillator trap potentials. We compared our results with the results of the impulse model used in Ch. 2 under the slow oscillation approximation and explored the regime beyond. We studied the contribution to recoil from the different terms of the Hamiltonian and Lindblad equation. In essence, the single-atom Lindblad term causes a recoil in a random direction and the energy deposited is independent of the trap frequency used. The laser Hamiltonian causes a recoil in the direction of the laser propagation and recoil energy deposited falls off to zero when the trap frequency goes beyond the collective decay rate of the system. The two-atom Lindblad terms induce a recoil in the direction of the separation between the atoms and it is dependent on both the trap frequency and the distribution of the excitation in the system.

In atom arrays, in the directions where there are no inter-atom forces or lasers, the recoil is independent of trap frequency and the impulse model can be used even beyond the slow oscillation approximation. If the atoms are excited by a laser or for those directions in

the plane of the atom array, the impulse model is no longer valid when the trap frequency approaches or is higher than the decay rate of the system.

This model was used to verify the extremely high recoil calculated in a cavity with high subradiance. This shows that recoil effects have to be considered seriously when working with highly subradiant systems. The effects of vibrational excitation in the reflectivity of arrays were also studied.

References [74], [88] worked on the opposite regime of the sudden approximation, where the focus is on the slow center of mass motion rather than the fast internal state dynamics. Studying this regime, especially the collective modes of vibration of the atoms using the quantum harmonic oscillator model could lead to a better understanding and control of atom arrays.

4. PHOTON STATISTICS OF EMITTED LIGHT IN COLLECTIVELY INTERACTING ATOM ARRAYS

4.1 Introduction

Making photons interact has been a longstanding goal in optics. The regime of non-linear effects at low intensities, where individual photons interact strongly with one another can be called 'Quantum nonlinear optics' [36]. It holds great potential for applications in optical transistors, non-linear optical switches [37], quantum information and communication [38], and metrology using non-classical fields [39], [40]. The scattering of two photons with the help of interaction with other systems has been explored in Refs. [41]–[45]

On a single photon level, collective interactions in free space have had many applications in coherent control [1]–[13], [15], [17], [20]–[24]. The interaction with emitters has been harnessed to make individual photons interact with each other, especially in the more controllable case of emitters coupled to waveguides [46]–[57].

In the case of atom-light interactions with high intensities, many of the atoms are simultaneously excited, sometimes even reaching full inversion. Superradiance and subradiance can be seen in the emission of photons. Ref. [89], [90] have studied the correlations in the photons emitted in such systems. They showed that bunching is a characteristic of the emission in superradiant systems in this regime of near-total inversion. Alternatively, will these associations be valid in the opposite regime where the intensity is low enough that there are only one or two excitations on average? The process of building coherences for the enhanced/suppressed emission is quite different in the two cases.

The correlations will be investigated when the system is excited by a constant drive and reaches steady state. There are two contributions from where correlations might arise. The first is due to the interference of the incoming driving light and the emitted light, which is analogous to the $g^{(2)}$ in the forward direction in most systems like atom arrays. In the low-intensity limit, this effect primarily comes from the single excitation terms of the ensemble, which has a population proportional to the intensity ($\propto \Omega^2$). The terms from the two excitations will be proportional to the square of intensity ($\propto \Omega^4$) and will not have a significant contribution.

On the other hand, in the backward direction, the correlations arise only due to the light emitted by the ensemble. The correlations arise purely due to the interactions between the atoms in the ensemble. The second-order correlation between two emitted photons no longer depends only on the single excitation states but also on the doubly excited states. Hence, we will include and focus on how the doubly excited states evolve, and contribute to the dynamics of the second-order correlation of the photon emission. In this chapter, we will study the correlations only in the emitted light, without including the incoming laser field, which is analogous to studying the backward scattering of light.

More generally, we study the properties of the emitted light when the intensity of the incoming light is weak. We particularly emphasize investigating the early time correlation function $g^{(2)}(0)$ to determine the emission statistics. It describes the probability of two photons being emitted together, normalized by their independent emission. Uncorrelated emission will have $g^{(2)}(0) = 1$. If the atoms are more prone to be emitted together, it is called bunched emission and will have a $g^{(2)}(0) > 1$. The opposite is called anti-bunching and will have a $g^{(2)}(0) < 1$.

We study these dynamics using density matrix formalism using both the single and double excitation states of the ensemble. We study how the early time $g^{(2)}(0)$, which pertains to the emission of two photons together, depends quantitatively on the decay rates of both the single and double excitation eigenmodes. Reference [44] has also studied the effects of the double excitation manifold in the context of two-photon scattering in waveguide QED systems. Reference [91] has also explored single and double excitation eigenmodes but in the case of atom rings and orbital angular momentum. Our study will focus on the double-excited states as a consequence of working beyond the edge of the low-intensity/single excitation regime.

We also observed that the interference of two coherent beams can allow better control of the correlations in the photon emission. By being able to selectively detect light emitted by a single mode, we can control the $g^{(2)}(\tau = 0)$ to go from antibunched to bunched behavior by changing the relative phase of the two beams. If the beams are eigenmodes of the system, their orthogonality will also ensure that the relative phase does not alter the intensity of the light that we are detecting. A source that can have its correlation properties changed

in real-time without changing the intensity can be used as an interesting building block for novel applications.

The formalism used for calculations is detailed in Sec. 5.2. Section 4.3.1 investigates the properties of the double excitation states and how they connect to the single excitation manifold. Section 4.3.2 investigates the initial time correlation, $g^{(2)}(0)$, of the emitted light when the atoms are excited by a single eigenmode. The effects of interference of two different modes is explored in Sec. 4.3.3

4.2 Methods

We consider N atoms and assume each to be a two-level system. The atoms are arranged in 1D or 2D arrays with separation (d) less than the wavelength of the resonant light (λ). The dynamics of the system is calculated using the density matrix formalism.

The Low-intensity limit is often assumed when performing calculations for collective interaction dynamics. There can only be a single excitation in the system at any time, which means that only the single excitation states have to be considered in the density matrix. The $g^{(2)}$ correlations, which describe the correlation between the emission of two photons, also requires the doubly excited states to be considered. This increases the total number of states (of the order N^2) which considerably reduces the total number of atoms that can be accurately simulated.

The raising and lowering operators of the j^{th} atom are represented by $\hat{\sigma}_{\mathrm{j}}^{+}$ and $\hat{\sigma}_{\mathrm{j}}^{-}$ respectively. The state where all the atoms are in the ground state is represented by $|g\rangle$ and the states where only the atom $'\mathrm{j}'$ is excited will be represented by $|\mathrm{e_j}\rangle = \hat{\sigma}_{\mathrm{j}}^{+}|g\rangle$. The doubly excited state will be represented by $|\mathrm{ee}_\mu\rangle = \hat{\sigma}_{m_1}^{+}\hat{\sigma}_{m_2}^{+}|g\rangle$ and the index $\mu = (m_1, m_2)$ represents

atom m_1 and m_2 being excited. Since $m_1 \neq m_2$, the index μ goes from 0 to $N(N-1)/2-1$. Hence the density matrix will be represented by

$$\begin{aligned}\rho = a_0|g\rangle\langle g| + \sum_{\mathrm{j}} v_{\mathrm{j}}^*|g\rangle\langle \mathrm{e_j}| + \sum_{\mu} w_{\mu}^*|g\rangle\langle \mathrm{ee}_{\mu}| \\ + \sum_{\mathrm{j}} v_{\mathrm{j}}|\mathrm{e_j}\rangle\langle g| + \sum_{\mathrm{i,j}} \tilde{\rho}_{\mathrm{ij}}|\mathrm{e_i}\rangle\langle \mathrm{e_j}| + \sum_{\mathrm{j},\mu} s_{\mathrm{j}\mu}^*|\mathrm{e_j}\rangle\langle \mathrm{ee}_{\mu}| \\ + \sum_{\mu} w_{\mu}|\mathrm{ee}_{\mu}\rangle\langle g| + \sum_{\mathrm{j},\mu} s_{\mathrm{j}\mu}|\mathrm{ee}_{\mu}\rangle\langle \mathrm{e_j}| + \sum_{\mu,\nu} \tilde{\tilde{\rho}}_{\mu\nu}|\mathrm{ee}_{\mu}\rangle\langle \mathrm{ee}_{\nu}|\end{aligned} \tag{4.1}$$

The dynamics of the system will be calculated by using the Hamiltonian and the Lindblad superoperator

$$\frac{d\hat{\rho}}{dt} = -\frac{\mathrm{i}}{\hbar}[\hat{H}, \hat{\rho}] + \mathcal{L}(\hat{\rho}) \tag{4.2}$$

The laser interaction is described by the Laser Hamiltonian in the rotating wave approximation given by

$$\hat{H}_L = \hbar \sum_{\mathrm{j}} \left[-\delta \hat{\sigma}_{\mathrm{j}}^+ \hat{\sigma}_{\mathrm{j}}^- + \frac{\Omega_{\mathrm{j}}}{2} \hat{\sigma}_{\mathrm{j}}^+ + \frac{\Omega_{\mathrm{j}}^*}{2} \hat{\sigma}_{\mathrm{j}}^- \right] \tag{4.3}$$

where $\Omega_{\mathrm{j}} = \Omega_0 \mathrm{e}^{\mathrm{i}\mathbf{k}_0 \cdot \mathbf{r}_{\mathrm{j}}}$ is the Rabi frequency of atom j, which governs the intensity of the driving laser and δ is the detuning. $\mathbf{r_j}$ gives the position of the jth atom. The laser Hamiltonian can induce transitions from the ground state to the first excited state and also from the first excited state to the second excited state.

Since this study is restricted to the low-intensity limit, the Rabi frequency should be small: $\Omega \ll \Gamma$, which is the decay rate of a single atom. Even beyond that, the Rabi frequency should be smaller than the eigenmode decay rates: $\Omega \ll \gamma_\alpha$ to ensure there are only one or two photons in the case of long-lived eigenmodes. The probability of excitation in the first excited state is proportional to Ω^2, while the probability of excitation in the second excited state is of order Ω^4.

The collective interaction and spontaneous emission are modeled by the dipole-dipole exchange Hamiltonian and the non-Hermitian Lindblad super-operator. The former is given by

$$\hat{H}_{dd} = \hbar \sum_{\mathrm{i}\neq\mathrm{j}} Im\{g(\mathbf{r}_{\mathrm{ij}})\}\hat{\sigma}_{\mathrm{i}}^{+}\hat{\sigma}_{\mathrm{j}}^{-} \tag{4.4}$$

which governs the exchange of excitation among the atoms and contributes to energy shifts in the system. The $\mathbf{r}_{\mathrm{ij}} = \mathbf{r}_{\mathrm{i}} - \mathbf{r}_{\mathrm{j}}$ denotes the distance between atoms i and j, and the $g(\mathbf{r}_{\mathrm{ij}})$ is the free space dyadic Green's function given by Eq. (5.11). This will also contribute to the effective Hamiltonian $\hat{H}$ in Eq. (4.2).

The Lindblad operator is given by

$$\mathcal{L}(\hat{\rho}) = \sum_{\mathrm{i,j}} \left[2Re\{g(\mathbf{r}_{\mathrm{ij}})\}\hat{\sigma}_{\mathrm{i}}^{-}\hat{\rho}\hat{\sigma}_{\mathrm{j}}^{+} - Re\{g(\mathbf{r}_{\mathrm{ij}})\}\hat{\sigma}_{\mathrm{i}}^{+}\hat{\sigma}_{\mathrm{j}}^{-}\hat{\rho} - Re\{g^{*}(\mathbf{r}_{\mathrm{ij}})\}\hat{\rho}\hat{\sigma}_{\mathrm{i}}^{+}\hat{\sigma}_{\mathrm{j}}^{-}\right] \tag{4.5}$$

where the i = j terms describe the single atom spontaneous emission and the i $\neq$ j terms describe the collective interaction. The Green's function $g(\mathbf{r}_{\mathrm{ij}})$ is given by

$$g(\mathbf{r}_{\mathrm{ij}}) = \frac{\Gamma}{2}\left[\frac{3(\hat{r}_{\mathrm{ij}}\cdot\hat{q}_{\mathrm{i}})(\hat{r}_{\mathrm{ij}}\cdot\hat{q}_{\mathrm{j}}^{*}) - (\hat{q}_{\mathrm{i}}\cdot\hat{q}_{\mathrm{j}}^{*})}{2}h_{2}^{(1)}(kr_{\mathrm{ij}}) + (\hat{q}_{\mathrm{i}}\cdot\hat{q}_{\mathrm{j}}{}^{*})h_{0}^{(1)}(kr_{\mathrm{ij}})\right] \tag{4.6}$$

where $\hat{q}_{\mathrm{i}}$ is the dipole orientation of the i^{th} atom, $r_{\mathrm{ij}} = |\mathbf{r}_{\mathrm{ij}}|$ is the norm of $\mathbf{r}_{\mathrm{ij}}$, $\hat{r}_{\mathrm{ij}} = \mathbf{r}_{\mathrm{ij}}/r_{\mathrm{ij}}$ is the unit vector along $\mathbf{r}_{\mathrm{ij}}$, Γ is the decay rate of a single atom and $h_{l}^{(1)}$ are the outgoing spherical Hankel function of angular momentum l. When i = j, that is when $\mathbf{r}_{\mathrm{ij}} = 0$, the imaginary part of the function becomes undefined, while the real part is defined. Hence, we redefine $g(\mathbf{r}_{\mathrm{ij}})$ to be

$$\begin{aligned} g(\mathbf{r}_{\mathrm{ij}}) &= g(\mathbf{r}_{\mathrm{ij}}) \qquad for \quad \mathrm{i}\neq\mathrm{j} \\ &= Re\{g(\mathbf{r}_{\mathrm{ij}})\} \quad for \quad \mathrm{i}=\mathrm{j} \end{aligned} \tag{4.7}$$

4.2.1 Eigenmodes

The Green's function of the interaction between the atoms can be used to construct a matrix $G_{\mathrm{ij}} = g(\mathbf{r}_{\mathrm{ij}})$ which when diagonalized will give the natural single excitation eigenmodes of the system. Each eigenvector $\mathbf{V}_{\alpha}$ corresponds to a mode of the system with a particular

decay rate given by the real part of the eigenvalue γ_α and energy shift given by the imaginary part Δ_α.

$$\sum_{\mathrm{j}} G_{\mathrm{ij}} \mathbf{V}_{\mathrm{j}\alpha} = \mathcal{G}_\alpha \mathbf{V}_{\mathrm{i}\alpha} = (\frac{\gamma_\alpha}{2} + \mathrm{i}\Delta_\alpha)\mathbf{V}_{\mathrm{i}\alpha} \tag{4.8}$$

The index α will be used in general to denote the single excitation eigenmodes Since the G_{ij} matrix is not Hermitian, the orthogonality conditions are different. The eigenmodes have to be normalized to follow

$$\sum_{\mathrm{i}} \mathbf{V}_{\mathrm{i}\alpha} \mathbf{V}_{\mathrm{i}\alpha'} = \delta_{\alpha,\alpha'} \tag{4.9}$$

For the two excitation states, a similar matrix can be defined using the Green's function. It connects the two excitation states that have a single common atom excited, i.e., the state can change from one ($|\mathrm{ee}_\mu\rangle$) to the other ($|\mathrm{ee}_\nu\rangle$) using a single photon jump operator ($\hat{\sigma}^+_{m_1}\hat{\sigma}^-_{n_1}$). Since the two excitation states are twice more likely to decay, the diagonal terms will be $2 \times R\mathrm{e}\{g(0)\} = \Gamma$.

$$\begin{aligned}
\tilde{G}_{\mu\nu} &= g(\mathbf{r}_{m_1 n_1}) \quad for \quad m_2 = n_2, m_1 \neq n_1 \\
&= g(\mathbf{r}_{m_2 n_2}) \quad for \quad m_1 = n_1, m_2 \neq n_2 \\
&= \Gamma \quad for \quad m_1 = n_1, m_2 = n_2 \\
&= 0 \quad for \quad m_1 \neq n_1, m_2 \neq n_2
\end{aligned} \tag{4.10}$$

This can be diagonalized to obtain the eigenmodes that correspond to the doubly excited states. The index β will be used to generally denote two excitation eigenmodes. These eigenvectors $\mathbf{W}_{\mu\beta}$ also follow a similar situation where the real part of the eigenvalue denotes the decay rate of a single photon being emitted and the atom descending into the single excitation states.

$$\sum_{\nu} \tilde{G}_{\mu\nu} \mathbf{W}_{\nu\beta} = \mathcal{G}^{(2)}_\beta \mathbf{W}_{\mu\beta} = (\frac{\gamma^{(2)}_\beta}{2} + \mathrm{i}\Delta^{(2)}_\beta)\mathbf{W}_{\mu\beta} \tag{4.11}$$

It is important to note that the γ_β describes the rate at which the first photon is emitted. Each such state will then connect to a mix of single excitation states after the emission.

4.2.2 Calculation of $g^{(2)}$ correlation

To calculate the $g^{(2)}$, the system is driven with a laser until it reaches steady state up to time t. Then the density matrix is projected into a state where the system has emitted a photon.

$$\frac{\hat{\sigma}^{-}\hat{\rho}(t)\hat{\sigma}^{+}}{\langle\hat{\sigma}^{+}\hat{\sigma}^{-}\rangle(t)} \rightarrow \hat{\rho}'(t) \tag{4.12}$$

where $\hat{\sigma}^{-}$ defines the emission of a photon in a particular direction $\mathbf{k}$ or from a particular eigenmode α,

$$\hat{\sigma}^{-} = \sum_{\mathrm{j}} \mathrm{e}^{-\mathbf{i}\mathbf{k}.\mathbf{r}_{\mathrm{j}}}\hat{\sigma}_{\mathrm{j}}^{-} \quad OR \quad \hat{\sigma}^{-} = \sum_{\mathrm{j}} V_{\mathrm{j}\alpha}\hat{\sigma}_{\mathrm{j}}^{-} \tag{4.13}$$

This projected density matrix is then evolved again in time using Eq. (4.2) up to time $t+\tau$. Then the probability of another photon being emitted is calculated and normalized with the intensity

$$g^{(2)}(\tau) = \frac{Tr[\hat{\sigma}^{-}\hat{\rho}'(t+\tau)\hat{\sigma}^{+}]}{\langle\hat{\sigma}^{+}\hat{\sigma}^{-}\rangle(t)} \tag{4.14}$$

which can also be written as

$$g^{(2)}(\tau) = \frac{Tr[\hat{\sigma}^{-}(t+\tau)\hat{\sigma}^{-}(t)\hat{\rho}\hat{\sigma}^{+}(t)\hat{\sigma}^{+}(t+\tau)]}{[\langle\hat{\sigma}^{+}\hat{\sigma}^{-}\rangle(t)]^{2}} \tag{4.15}$$

In many cases, we focus on the $g^{(2)}$ when $\tau = 0$, that is without any time delay, or the instantaneous two-photon correlation. That simplifies Eq. (4.15) as

$$g^{(2)}(\tau = 0) = \frac{Tr[\hat{\sigma}^{-}\hat{\sigma}^{-}\hat{\rho}\hat{\sigma}^{+}\hat{\sigma}^{+}]}{\langle\hat{\sigma}^{+}\hat{\sigma}^{-}\rangle^{2}} \tag{4.16}$$

If the system is excited to a particular eigenmode α using the operator $\hat{\sigma}_{\alpha}^{+} = \sum_{\mathrm{j}} V_{\mathrm{j}\alpha}\hat{\sigma}_{\mathrm{j}}^{+}$, we cannot use the same set of $\hat{\sigma}_{\alpha}^{+}$, $\hat{\sigma}_{\alpha}^{-}$ for the detection of light emitted in that mode. Due to the unusual orthogonality relation defined in Eq. (4.9), the raising and lowering operators used for the detection have to be redefined as $\hat{\sigma}_{\alpha}'^{+} = \sum_{\mathrm{j}} V_{\mathrm{j}\alpha}^{*}\hat{\sigma}_{\mathrm{j}}^{+}$, $\hat{\sigma}_{\alpha}'^{-} = (\hat{\sigma}_{\alpha}'^{+})^{*}$ to give $\hat{\sigma}_{\alpha'}'^{-}\hat{\sigma}_{\alpha}^{+}|g\rangle = \delta_{\alpha,\alpha'}|g\rangle$.

4.3 Results

Using the formalism described in Sec. 5.2, the density matrix can be evolved to study the dynamics of both the single and the double excitation states. This chapter will focus exclusively on correlations in the emitted light, and the correlations with the driving light fields will be ignored.

To keep the data shown consistent, the configuration of the atoms will be kept the same in this section. The atoms are in a square lattice in the XZ plane with lattice separation d ranging from 0.3λ to 1.0λ. The atoms are polarized along the Z-axis. While the data shown is only for a two-dimensional array, the results are consistent across 1D, 2D, 3D, and low-density Gaussian clouds.

4.3.1 Double excitation eigenmodes

In this section, we will provide some basic descriptions of the second excitation eigenmodes. We will also explore the connection between the single and doubly excited states. A detailed investigation of the characteristics of the double excitation eigenmodes has been done in [44]. Even though their description is for Waveguide-qubit systems, many of the properties are similar to atoms in free space.

The most subradiant double excitation state decays faster than the most subradiant single excitation state in a single configuration of atoms in space. When two atoms are being excited, each excitation can only hop to the other N-2 atoms that are not excited, which is analogous to the second excited atom being invisible to the first excited atom. This 'hole' interferes with the perfect destructive interference necessary to get to the most subradiant state. The alternate is true for the superradiant state where the most superradiant second excitation state decays faster than the most superradiant single excitation state.

The manifold of the two excitation states is of $N(N-1)/2$ dimensions and the corresponding eigenmodes can be renormalized to form a complete ortho-normal subspace with the new definition of the inner product as in Eq. (4.9). On the other hand, there are $N^2/2$ vectors that can be made when any two single excitation eigenmodes are used to excite the ground state procedurally. This discrepancy in the number of states of the second excitation

eigenmodes and two single excitations comes about because there cannot be two excitations on a single atom, i.e., $\hat{\sigma}_{\mathrm{i}}^{+}\hat{\sigma}_{\mathrm{i}}^{+}|g\rangle = 0$.

The real part of the eigenmode γ_β gives the rate of decay of the double excitation eigenmode. Once the first photon is emitted into free space, the system is brought into a combination of single excitation states. This combination of single excitation states will then result in a corresponding average decay rate for the second photon. This decay rate of the second photon will be represented by ζ_β has been plotted in Fig. 4.1 and is defined by,

$$\zeta_\beta = \frac{4}{\gamma_\beta} Tr[\sum_{\mathrm{iji'j'}} Re\{g(\mathbf{r}_{\mathrm{i'j'}})\} Re\{g(\mathbf{r}_{\mathrm{ij}})\} \hat{\sigma}_{\mathrm{i'}}^{-} \hat{\sigma}_{\mathrm{i}}^{-} \rho_\beta \hat{\sigma}_{\mathrm{j}}^{+} \hat{\sigma}_{\mathrm{j'}}^{+}] \tag{4.17}$$

where ρ_β is the density matrix initialized to contain only the second excitation eigenmode β. In most cases, the ζ_β is approximately close to $\gamma_\beta/2$, especially for higher atom separations. There are exceptions to this when the atom separations get smaller. Specifically, for states that have very small γ_β, the ζ_β's are not as suppressed and tend to go above the line that depicts $\zeta_\beta = \gamma_\beta/2$. This becomes more relevant in Sec. 4.3.2.

The single and double excitation eigenmodes are vectors with different sizes and normalization schemes which makes it hard to draw conclusions on how they correlate with each other. To understand this, we can define a quantity that describes the overlap of the double excitation eigenmode β with two single excitation eigenmodes α_1 and α_2. This can also be understood as the tendency of mode β to emit two photons, each in mode α_1 and α_2.

$$L_{\alpha_1\alpha_2\beta} = \sum_{\mu} (V_{m_1\alpha_1} V_{m_2\alpha_2} + V_{m_1\alpha_2} V_{m_2\alpha_1}) W_{\mu\beta} \tag{4.18}$$

When $\alpha_1 = \alpha_2$, it can be redefined as $X_{\alpha\beta}$ which is analogous to a projection of $(V_{\mathrm{i}\alpha})^2$ over $W_{\mu\beta}$. This describes the geometric overlap of the double excitation eigenmode with the state where both photons are in the same single excitation eigenmode. This quantity will become more relevant in Sec. 4.3.2.

$$X_{\alpha\beta} = \sum_{\mu} (2 V_{m_1\alpha} V_{m_2\alpha}) W_{\mu\beta} \tag{4.19}$$

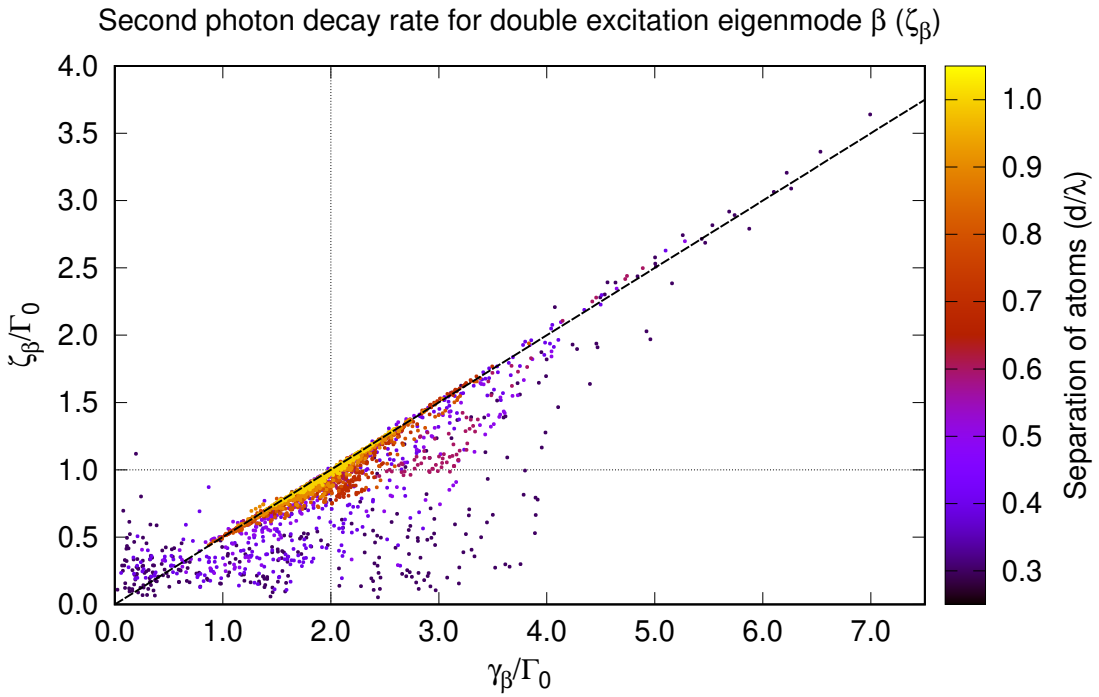

Figure 4.1. The decay rate of the second photon (ζ_β) versus the decay rate of the first photon (γ_β) from a double excitation eigenmode β. The separation has been varied from 0.3 to 1.0 λ. The color shows the separation d of the atoms in the array. The dashed line corresponds to $\zeta_\beta = \gamma_\beta/2$.

Fig. 4.2 shows the $|X_{\alpha\beta}|$ and $|L_{\alpha_1\alpha_2\beta}|$ ($\alpha_1 \neq \alpha_2$) for a square array with 25 atoms with separations of 0.3 and 0.8 λ. The points correspond to the N- single excitation eigenmodes α and $N(N-1)/2$ double excitation eigenmodes β.

Although $|X_{\alpha\beta}|$ and $|L_{\alpha_1\alpha_2\beta}|$ only depend on the spatial profile of the eigenmodes, they are inherently still connected to the decay rates of the eigenmodes. In both plots, the overlap is maximized when the sum of the single excitation decay rates matches the double excitation decay rates. In the case of$|X_{\alpha\beta}|$, the overlap is maximum when $\gamma_\beta = 2\gamma_\alpha$.

The spread of the points along the x-axis (difference in decay rate) depends on the separation of the atoms d. For large separations, most of the points are clustered around a difference of 0. On the other hand, for small separations, there is a larger spread, and states that have a considerable difference still have non-negligible contributions.

4.3.2 Single mode excitation

In experiments, it is usually possible to detect/input light from only a single mode (a common example is a Gaussian light mode). But using the geometry of the atom ensemble, it can be made to excite eigenmodes with different decay rates. For example, when using Gaussian light to excite and detect light from a finite array of atoms, having the separation between the atoms to be less than half a wavelength will result in the superradiant modes being predominantly excited. The opposite is true for separations in the range of half to one wavelength where the subradiant modes are excited. Hence we first consider a situation where we are exciting and detecting the same mode of light, but each mode will be an eigenmode of the atomic ensemble. While most of the eigenmodes in atomic systems will be difficult to directly excite in experiments, we are studying this to isolate the effect of only the decay rate on the correlations in the light. There are also certain systems, like Transmon waveguide QED, where exact eigenmodes can be directly driven without using light.

In the calculations, hypothetical lasers that can exactly address a particular single excitation eigenmode of the system can be used. The corresponding spatial profile and detuning of the eigenmode can be imprinted on the driving laser. After emitting a photon, the time

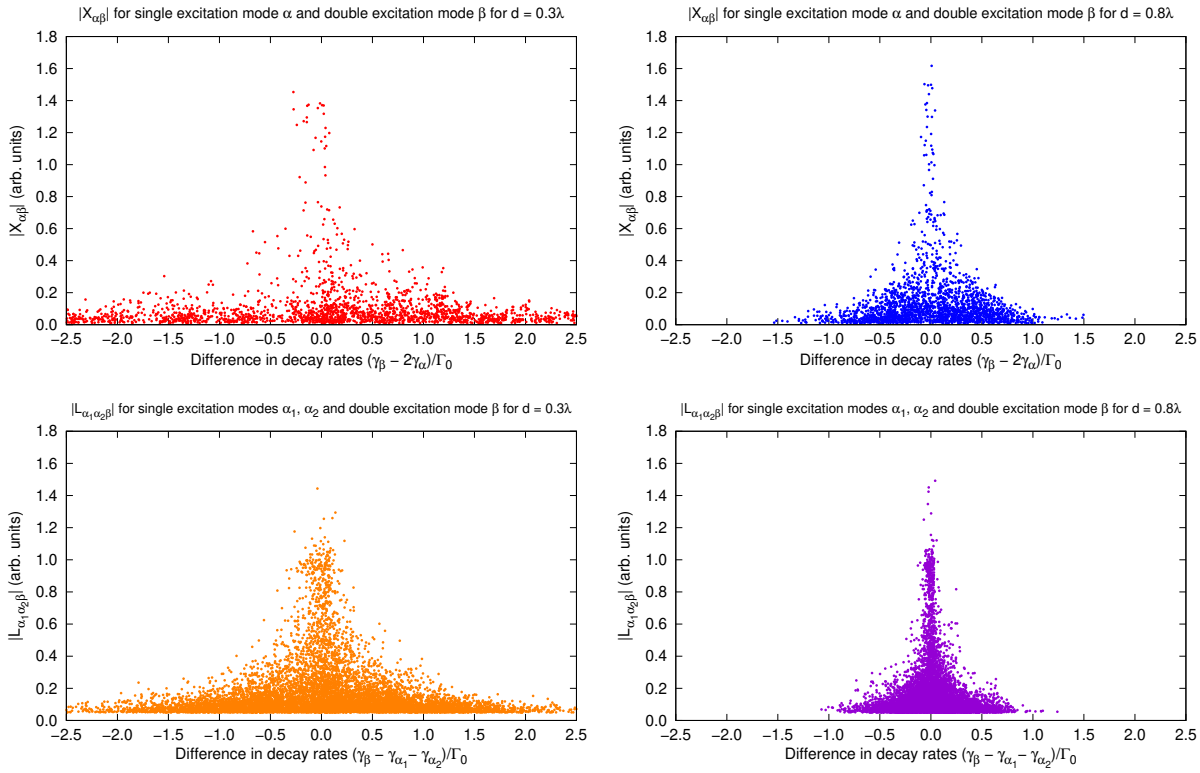

Figure 4.2. (a),(b) The $|X_{\alpha\beta}|$ versus the difference in decay rate of the single and double excitation eigenmodes $(\gamma_\beta - 2\gamma_\alpha)/\Gamma_0$ for $d = 0.3\lambda$ (red) and 0.8λ (blue). (c),(d) The $|L_{\alpha_1\alpha_2\beta}|$ versus the difference in decay rate of the single and double excitation eigenmodes $(\gamma_\beta - \gamma_{\alpha_1} - \gamma_{\alpha_2})/\Gamma_0$, where $\alpha_1 \neq \alpha_2$ for $d = 0.3\lambda$ (orange) and 0.8λ (purple). The data is calculated for a square array of 25 atoms. The smaller separations seem to have a larger spread in the points.

the system takes to recover back to steady state is usually determined by the eigenmode's decay rate.

On the other hand, the early-time photon correlation $g^{(2)}(0)$ does not trivially depend on this decay rate. Since $g^{(2)}(0)$ describes how likely it is to emit two photons together, the decay rates of the double excitation eigenmodes will also contribute. Therefore, we numerically and analytically study and understand the dependence of the early-time second-order photon correlation on the decay rates of the single and double excitation eigenmodes.

Detection in the same Eigenmode α

In this section, the $g^{(2)}(0)$ will be calculated when the light is emitted into the same single excitation eigenmode with which it is excited. This represents how two photons each in a single excitation eigenmode $V_{i\alpha}$ connects with the double excitation modes $W_{\mu\beta}$, which was described by $X_{\alpha\beta}$ as discussed in Sec. 4.3.1 and in Fig. 4.2(a) and 4.2(b).

While the $g^{(2)}(0)$ can be calculated numerically by time evolving the density matrix to steady state and taking projections, we can simplify the calculation by using eigenmode decomposition. An analytical expression can be derived for the steady state and $g^{(2)}(0)$ when exciting using a single eigenmode. The derivation is detailed in the Appendix 4.A.

The $g^{(2)}(0)$ when driven and detected using the single excitation eigenmode α with decay rate γ_α and a detuning corresponding its line shift $\delta = \Delta_\alpha$ is given by,

$$g^{(2)}(0) = Re\{\gamma_\alpha\}^2 \left| \sum_\beta \frac{X_{\alpha\beta}^2}{\gamma_\beta^{(2)} + 2i(\Delta_\beta^{(2)} - 2\Delta_\alpha)} \right|^2 \tag{4.20}$$

where the sum over β goes over all the double excitation eigenmodes.

The $g^{(2)}(0)$ can be understood as the ratio between the decay rates of the single excitation eigenmodes over the decay rates of the double excitation eigenmodes weighted over the coupling coefficient $X_{\alpha\beta}$. The detuning also plays a role in decreasing how well the double excitation eigenmode is excited. As seen in Fig. 4.2(a), the coupling coefficient $X_{\alpha\beta}$ only has a significant contribution when $\gamma_\alpha \approx \gamma_\beta^{(2)}/2$ resulting in the $g^{(2)}(0)$ almost always being less than 1.

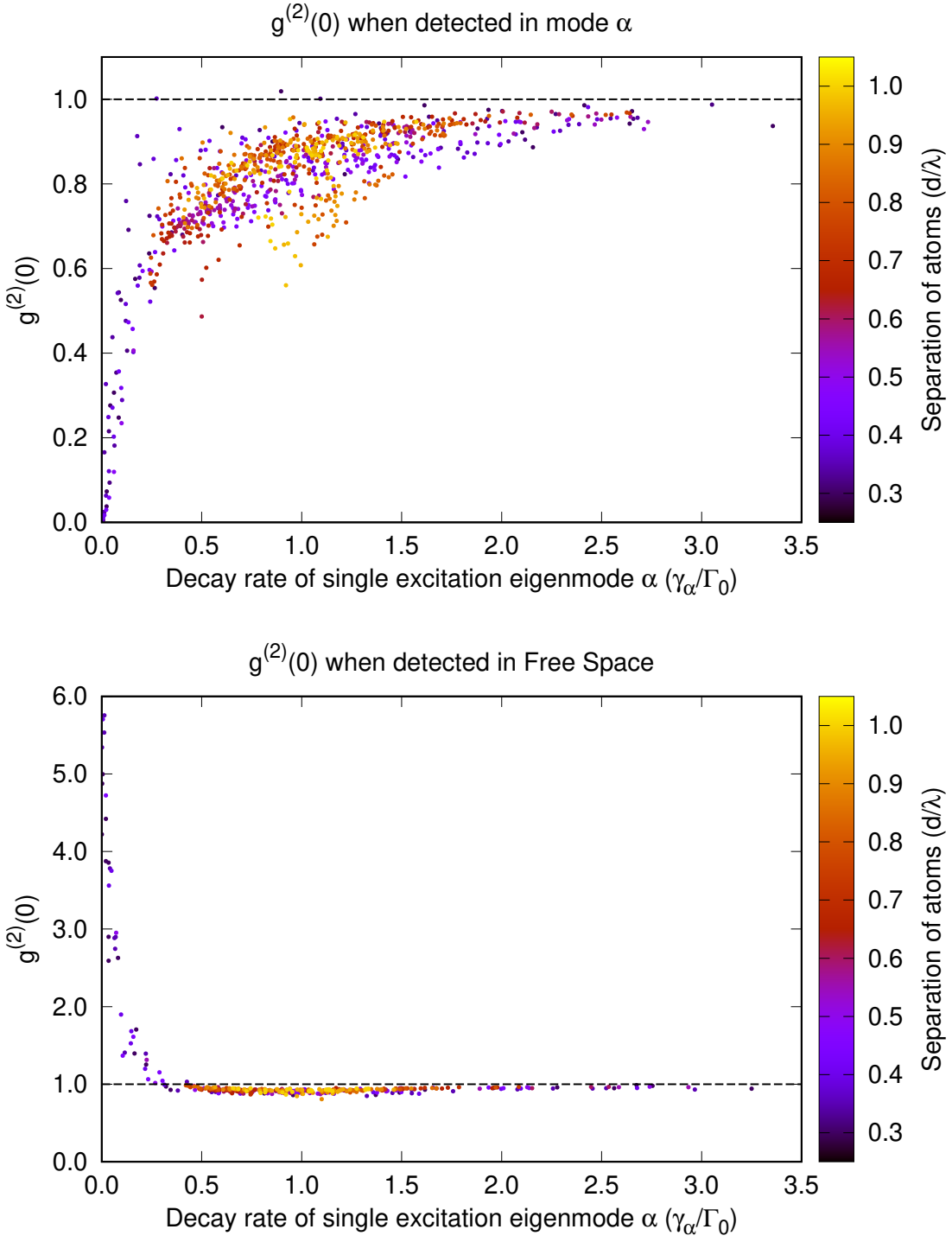

Figure 4.3. The $g^{(2)}(0)$ when excited using a single eigenmode α for an ensemble of 25 atoms arranged in a square array, versus the decay rate of the eigenmode (γ_α). (a) depicts the situation when the detection is also in mode α, while (b) corresponds to detection over all of free space. The separation has been varied from 0.3 to 1.0 λ. The color shows the separation d of the atoms in the array.

Another way to interpret this is as a ratio of the population of the doubly excited states over the single excitation states. In the low-intensity limit, the population of a state is generally proportional to $1/\Gamma^2$ at steady state. This means that we are summing over all the populations of the two excitation eigenmodes and normalizing it with the population in the single excitation states.

For highly subradiant states, the $g^{(2)}(0)$ is very low and is almost proportional to the decay rate. This shows a clear correlation between antibunching and low-intensity subradiance. But once the decay rate reaches 0.5Γ, the $g^{(2)}(0)$ starts to saturate and approaches 1. Even for highly superradiant states, the $g^{(2)}(0)$ is only around or less than 1. This means that, unlike in the high-intensity situation where superradiance implies bunching, superradiance in the low-intensity limit only makes the photon emission uncorrelated.

When the separation is less than 0.3λ, the line shifts of the single excitation states start increasing drastically and the effects due to the mismatch of detuning with the second excitation eigenmodes start playing a greater role. As the denominator in Eq. (4.20) increases, the $g^{(2)}(0)$ gets smaller and starts approaching zero. There will also be some rare eigenmodes with $g^{(2)}(0)$ a little higher than 1.

Detection in all of Free space

So far, we described the photons being detected in the same mode they were excited in. In this section, the detection scheme covers the light emitted into all of free space. This type of detection is more relevant in some experimental implementations, especially in Waveguide QED where all the light being emitted can be easily detected from the two ends of the waveguide. Since light can be emitted into all possible modes, it will include the possibility of the two photons being emitted into a combination of modes α_1 and α_2. This also consists of both photons being emitted into the same mode, which overlaps with the situation in Sec. 4.3.2.

The intensity of light can be calculated from the surrounding term of the Lindblad Operator $2R\mathrm{e}\{g(\mathbf{r}_{ij})\}\hat{\sigma}_i^- \hat{\rho}\hat{\sigma}_j^+$ that represents the emission of light and lowering of the excitation in the system. Since the eigenmodes of $g(\mathbf{r}_{ij})$ discussed so far, will no longer be eigenmodes

of this decay operator $2Re\{g(\mathbf{r}_{ij})\}$, we cannot derive a simple relation like Eq. (4.20). Nevertheless, it can be directly calculated and we can draw simple conclusions.

The results have been plotted in Fig. 4.3(b) for a similar configuration. Contrary to the Fig. 4.3(a), the $g^{(2)}(0)$ in this case starts as bunched emission for subradiant states and approaches 1 again for superradiant states. The initial time emission correlation $g^{(2)}(0)$ describes the possibility of the second photon being emitted immediately after the first photon is emitted. As seen in Fig. 4.1, for a double excitation eigenmode β, the second photon decay rate ζ_β follows the line $\zeta_\beta = \gamma_\beta/2$ for large γ_β, but fails to keep up as it reaches very small decay rates. When excited using subradiant states, even though the decay rate of the first photon is small, the second photon rate is comparatively larger, leading to the larger $g^{(2)}(0)$ and bunched emission.

In conclusion, when exciting the system using a single characteristic eigenmode α, the trend of the $g^{(2)}(0)$ versus the decay rate γ_α depends on the type of detection of the photons. For subradiant states, detecting in the same eigenmode α displayed anti-bunched emission, while detecting in all of free space results in bunched emission. On the other hand, superradiant states tend to converge on $g^{(2)}(0) = 1$ irrespective of the detection scheme.

4.3.3 Two interfering modes

In this section, we will discuss how two different single excitation eigenmodes interfere and interact with the double excitation eigenmodes. We let the two eigenmodes, α_1 and α_2, have a relative phase and observe the effects on $g^{(2)}(0)$ while varying this phase. The Rabi frequency for each atom will be given by,

$$\Omega_j = \Omega_0(a_1\mathbf{V}_{j\alpha_1} + a_2 e^{i\phi}\mathbf{V}_{j\alpha_2}) \tag{4.21}$$

where ϕ is the relative phase, and a_1,a_2 are relative amplitudes of the two modes.

When the two eigenmodes interfere, the orthogonality ensures that the populations in the single excitation eigenmodes do not vary with the relative phase. But for the case of the double excitation eigenmodes, the correlations are emphasized and affect their population. Since the $g^{(2)}(0)$ is effectively the ratio of population in two excitations, with the square of

the population in the single excitation, we can see a change in $g^{(2)}(0)$ without a change in intensity.

For a system with 16 atoms in a square array with separation $d = 0.4\lambda$, we can have the $g^{(2)}(0)$ oscillate between 0.002 and 4 using the most subradiant and most superradiant eigenstates as the two interfering modes. Although the amplitudes a_1 and a_2 have been set as equal in this situation, varying their ratio allows for control in the range of accessible $g^{(2)}(0)$. The recovery time of the $g^{(2)}(\tau)$ will simply be the decay rate of the mode that is being detected. This essentially means that with the relative phase as a knob, the $g^{(2)}(0)$ of the emitted light can be controlled. This can also be thought of as a controllable non-linearity.

To get an intuition behind this, we can study the simple case with two atoms. The eigenmodes of the system are $|+\rangle = (|eg\rangle + |ge\rangle)/\sqrt{2}$ and $|-\rangle = (|eg\rangle - |ge\rangle)/\sqrt{2}$. By interfering two modes with an arbitrary relative phase, the minima of $\langle ee\rangle$ occurs when the modes cancel out on one atom and only the other atom interacts with the incident light. This means that the phase controls whether the incident light interacts with one or two atoms. While this seems simple, the situation becomes non-trivial when many atoms are involved and the level of non-linearity can be changed on a much larger scale.

When there are many atoms, the caveat is that having a beam that can address or detect individual eigenmodes becomes difficult. In some cases, the variation in the spatial part of the eigenmode becomes so fast that it becomes dark and cannot be simply accessed with optical beams. Therefore, we need systems that are similar, yet have a greater degree of control than free space atoms.

One such system with a higher degree of control is the Transmon Waveguide QED systems. These are artificial atom-like systems made using superconducting circuits that can interact with each other through microwave waveguides. These transmons can also be directly driven using the electronics, in addition to the usual optical driving through the waveguide. This facilitates individual addressing of the qubits which can be used to access any arbitrary eigenmode of the system. This can then be the knob that can be used to control the $g^{(2)}$ emission of the optical mode. The chirality in such systems can also be utilized to make the different modes emit in a different direction

4.4 Conclusion

We studied the photon statistics of the emitted light in collectively interacting dipole systems using the double excitation states. We described the emission properties of the double excitation eigenmodes and explored how they couple to the single excitation eigenmodes. Since the Green's function between dipoles is not hermitian but complex symmetric, we need to redefine the orthogonality relation to get ortho-normal eigenmodes.

When the system is excited by a single excitation eigenmode, we study the $g^{(2)}(0)$ of the emission when the photons are detected in (i) the same excitation eigenmode or (ii) free space. For superradiant states, irrespective of the detection type, the emission is mostly uncorrelated, and the $g^{(2)}(0)$ tended towards 1. On the other hand for subradiant states, the emission is either (i) antibunched or (ii) bunched depending on the type of detection. This is contrary to the many-photon situation where superradiance induces bunching and subradiance causes anti-bunching.

When the system is excited by two distinct single excitation eigenmodes, the interference between the two can cause interesting dependencies on the photon statistics. By changing the phase between the two incident excitations, the non-linearity of the system can be controlled to an extent resulting in being able to arbitrarily control the $g^{(2)}(0)$ of the emitted light.

Most of the effects observed can be attributed to the coupling between the different sets of eigenmodes. This formalism can be easily extended to other types of atom-atom interactions once the corresponding eigenmodes and orthogonality relations can be established.

4.A Appendix: Single mode emission analytical calculation

The density matrix can be evolved in time using Eq. (4.2) until it reaches steady state. However, this method becomes tedious to calculate when N increases or when dealing with highly subradiant modes. Hence we can use the low-intensity approximation and directly calculate the steady state using eigenstate decomposition. Each of the types of terms in the

density matrix represented in Eq. (5.14) can be transformed into the correspond eigenmode basis.

$$\begin{aligned} \tilde{v}_\alpha &= \sum_{\mathrm{j}} v_{\mathrm{j}} \mathbf{V}_{\mathrm{j}\alpha} \qquad v_{\mathrm{j}} = \sum_{\alpha} \tilde{v}_\alpha \mathbf{V}_{\mathrm{j}\alpha} \\ \tilde{w}_\beta &= \sum_{\mu} w_\mu \mathbf{W}_{\mu\beta} \qquad w_\mu = \sum_{\beta} \tilde{w}_\beta \mathbf{W}_{\mu\beta} \end{aligned} \tag{4.22}$$

and similar relations can be shown for the other terms.

In the low-intensity limit, the Rabi frequency is much smaller than the decay timescales. As a consequence, each term in Eq. (5.14), to the right or below is one order higher with respect to Ω, i.e., $a_0 \propto \Omega^0$, $v_{\mathrm{j}} \propto \Omega^1$, $w_\mu, \tilde{\rho}_{\mathrm{ij}} \propto \Omega^2$, $s_{\mathrm{j}\mu} \propto \Omega^3$ and $\tilde{\tilde{\rho}}_{\mu\nu} \propto \Omega^4$. It can be shown that by ignoring the higher order Ω terms in the rate equations, the terms in Eq. (5.14) become

$$\tilde{\rho}_{\mathrm{ij}} = \frac{v_{\mathrm{i}} v_{\mathrm{j}}^*}{a_0} \quad s_{\mathrm{j}\mu} = \frac{w_\mu v_{\mathrm{j}}^*}{a_0} \quad \tilde{\tilde{\rho}}_{\mu\nu} = \frac{w_\mu w_\nu^*}{a_0} \tag{4.23}$$

where a_0 is the population in the ground state, which can be calculated from $Tr[\rho] = 1$.

Using these Eqs. (4.2), (4.22), and (4.23), the steady state value can be directly calculated from Ω_{j}

$$\begin{aligned} \tilde{v}_\alpha &= \frac{\mathrm{i}a_0}{2} \frac{\sum_{\mathrm{j}} \Omega_{\mathrm{j}} \mathbf{V}_{\mathrm{j}\alpha}}{(\mathcal{G}_\alpha - \mathrm{i}\delta)} \\ \tilde{w}_\beta &= \frac{\mathrm{i}a_0}{2} \frac{\sum_{\mu} (\Omega_{m_1} v_{m_2} + \Omega_{m_2} v_{m_1}) \mathbf{W}_{\mu\beta}}{(\mathcal{G}^{(2)}_\beta - 2\mathrm{i}\delta)} \end{aligned} \tag{4.24}$$

When the system is excited using a particular single excitation eigenmode $\tilde{\alpha}$, $\Omega_{\mathrm{j}} = \Omega_0 \mathbf{V}_{\mathrm{j}\tilde{\alpha}}$ and $\delta = \Delta_{\tilde{\alpha}}$ will give

$$\begin{aligned} \tilde{v}_\alpha &= \frac{\mathrm{i}a_0 \Omega_0}{2\gamma_{\tilde{\alpha}}} \delta_{\alpha,\tilde{\alpha}} \\ \tilde{w}_\beta &= \frac{a_0 \Omega_0^2}{4\gamma_{\tilde{\alpha}}} \frac{X_{\tilde{\alpha}\beta}}{(\mathcal{G}^{(2)}_\beta - 2\mathrm{i}\Delta_{\tilde{\alpha}})} \end{aligned} \tag{4.25}$$

For detecting the light emitted into the same eigenmode $\tilde{\alpha}$, we use $\hat{\sigma}^-_{\tilde{\alpha}} = \sum_{\mathrm{j}} V_{\mathrm{j}\tilde{\alpha}} \hat{\sigma}^-_{\mathrm{j}}$ to arrive at Eq. (4.20)

$$
\begin{aligned}
g^{(2)}(0) =& \frac{Tr\{\hat{\sigma}_{\tilde{\alpha}}^{-}\hat{\sigma}_{\tilde{\alpha}}^{-}\rho\hat{\sigma}_{\tilde{\alpha}}^{+}\hat{\sigma}_{\tilde{\alpha}}^{+}\}}{Tr\{\hat{\sigma}_{\tilde{\alpha}}^{-}\rho\hat{\sigma}_{\tilde{\alpha}}^{+}\}^2} \\
=& Re\{\gamma_{\tilde{\alpha}}\}^2 \left| \sum_{\beta} \frac{X_{\tilde{\alpha}\beta}^2}{\gamma_{\beta}^{(2)} + 2\mathrm{i}(\Delta_{\beta}^{(2)} - 2\Delta_{\tilde{\alpha}})} \right|^2
\end{aligned}
\tag{4.26}
$$

5. COLLECTIVE INTERACTIONS IN ATOMS NEAR A MICRORING RESONATOR

5.1 Introduction

The study of collective effects due to dipole interactions has been a major topic of interest since Dicke described the concept of superradiance in his seminal paper in 1954 [1]. There has been abundant research following this on the different aspects of collective dipole interactions like superradiance, subradiance, and collective Lamb shifts [2]–[12]. These effects have been utilized for applications in quantum control, photon storage, and quantum information [18], [19], [33], [34].

Great progress has been achieved in engineering nanophotonic interfaces for versatile control over light-matter interaction. The interaction between atoms has been experimentally implemented using nanofibers [14], [58]–[64], photonic crystals [65], [66], and slot waveguides [67], [68]. Since the atoms are usually trapped close to dielectric surfaces, the complexities of modeling the interactions have been explored in Refs. [35], [69]–[71].

Recently, cold atoms have been trapped adjacent to a nanophotonic micro-ring resonator [92], [93] to be used as a versatile light-matter interaction platform. The ring-resonator can act as a whispering gallery mode cavity and facilitate chiral atom-atom interactions.

This platform has several unique advantages over other light-matter interfaces. The atoms can interact with each other through two different channels, through free space and through the resonator, each with a different characteristic k-vector. The interaction strength with the resonator channel can also be varied by adjusting the position of the atoms.

One of the potentials of this unique light-matter interface is the concept of "selective radiance" as was first described in Ref. [35]. These selectively radiant states have been described as simultaneously superradiant in a desired mode and subradiant in undesired or error-inducing channels. Due to the nature of the coupling with the ring resonator cavity, the atoms will superradiantly couple with the cavity and the decay rate will scale with the atom number [93]. If the decay into free space can be reduced due to the collective interactions, the interface becomes more robust towards error from spontaneous emission into the vacuum.

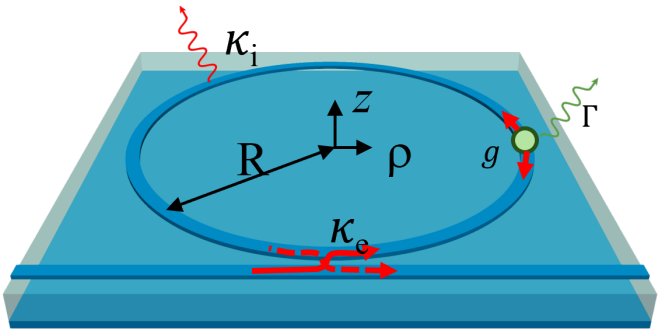

Figure 5.1. Representative image of the micro-ring resonator is coupled to a waveguide

This light-matter platform could have potential applications involving quantum memories [94], quantum simulation [95]–[98], quantum networks [99], and applications in quantum computing [100]–[102]. It also holds the potential for implementing photon interactions [41], [47], [50], non-Markovian [103], and topological models [104].

In this chapter, we theoretically and computationally model the atom and ring resonator system to understand the physics underlying the interactions and explore further possibilities. We give particular emphasis on how the collective interactions of the atoms in free space can affect the interaction with the micro-ring resonator. We describe the system and the numerical methods used in Sec. 5.2. We simulate the current status of the experiment, which involves trapping a cloud of atoms above the ring resonator in Sec. 5.3.2. In Sec. 5.3.3, we explore the potential of trapping atoms in arrays near the ring resonator and consider disorders that arise in the experiments.

5.2 Methods

The experimental system consists of a micro-ring resonator coupled to a waveguide, as represented in Fig. 5.1. The waveguide near-critically couples with the resonator and acts as the input-output channel. This rate of coupling (κ_e) is comparable to the intrinsic loss rate of the resonator cavity (κ_i). The micro-ring resonator acts as a whispering gallery mode cavity that can sustain light circulating in the two directions.

The experiment uses the TM mode, where the +1 circularly polarized light can only travel in one direction and the -1 polarization will couple with the other. Once excited

by a +1 polarized light, to a large extent, the atom only re-emits into the same mode. This configuration results in the atom-atom interaction through the waveguide being chiral. Modes traveling in only one direction will be supported. Since the back-scattering rate from the atoms is also very small, light traveling in the other direction can be ignored.

Cold atoms are cooled and trapped above the micro-ring resonator with a density of around $10^{13} cm^{-3}$ in an almost cigar-shaped configuration. The number of atoms in the cloud can be varied from a few to up to 60 atoms. These atoms are coupled to the evanescent field of the circulating light in the resonator. Since the evanescent field drops off exponentially above the ring, each atom has a different interaction strength with the cavity. This interaction strength can also be controlled by moving the atom cloud closer or farther away from the resonator.

We shall consider N atoms interacting with the micro-ring resonator. The +1 circularly polarized mode will be considered as a cavity. Since we are restricted to the low-intensity limit, there can only be one excitation in the system at any time. Hence the Hilbert space of the atom excitations can be simplified to $N + 1$ states. The raising and lowering operators of the j^{th} atom are represented by $\hat{\sigma}_{\mathrm{j}}^{+}$ and $\hat{\sigma}_{\mathrm{j}}^{-}$ respectively. The state where all the atoms are in the ground state is represented by $|g\rangle$ and the states where only the atom $'\mathrm{j}'$ is excited will be represented by $|\mathrm{e_j}\rangle = \hat{\sigma}_{\mathrm{j}}^{+}|g\rangle$. The single-atom decay rate of the atoms will be denoted by Γ_0 and will serve to set the timescale of the system.

The cavity can be modeled as a harmonic oscillator with raising (lowering) operators, $\hat{a}, \hat{a}^{\dagger}$. The Hamiltonian of the atom-cavity interaction can be represented as

$$H_I = \sum_{\mathrm{j}} g_{\mathrm{j}} \mathrm{e}^{\mathrm{i}\phi_{\mathrm{j}}} (\hat{a}\hat{\sigma}_{\mathrm{j}}^{+} + \hat{a}^{\dagger}\hat{\sigma}_{\mathrm{j}}^{-}) - \sum_{\mathrm{j}} \Delta_A \hat{\sigma}_{\mathrm{j}}^{+}\hat{\sigma}_{\mathrm{j}}^{-} \tag{5.1}$$

where g_{j} depends on the evanescent electric field at the position of atom j, and $\phi_{\mathrm{j}} = n_{eff}\mathbf{k}_0 \cdot \mathbf{r}_{\mathrm{j}}$. $\Delta_A = \omega - \omega_A$ is the detuning of the atom resonance with the input light. n_{eff} is the effective refractive index of the ring-resonator waveguide and $\mathbf{k}_0$ is the wavevector associated with the resonant wavelength of light.

In the experiment, the single-atom cooperativity plays a more relevant role in describing the strength of the atom-cavity interaction. The single atom cooperativity of the jth atom will be given by,

$$C_{\mathrm{j}} = \frac{4g_{\mathrm{j}}^2}{(\kappa_{\mathrm{i}} + \kappa_{\mathrm{e}})\Gamma_0} \tag{5.2}$$

This single atom cooperativity decays exponentially with distance from the resonator with a decay length of $42nm$. The average single-atom cooperativity will be denoted as C_1. In general, the total cooperativity of the waveguide interaction scales as NC_1.

The cavity decay will be defined by the Lindblad operator for the resonator cavity,

$$\mathcal{L}_R(\rho) = (\kappa_{\mathrm{i}} + \kappa_{\mathrm{e}})[\hat{a}\rho\hat{a}^\dagger - \frac{1}{2}\hat{a}^\dagger\hat{a}\rho - \frac{1}{2}\rho\hat{a}^\dagger\hat{a}] \tag{5.3}$$

The incoming and outgoing waves in the external waveguide can be represented by the corresponding input and output cavity operator, $\hat{s}_{\mathrm{in}}, \hat{s}_{\mathrm{in}}^\dagger; \hat{s}_{out}, \hat{s}_{out}^\dagger$. Hence the Hamiltonian coupling the input mode of the waveguide and the cavity is given by

$$H_{\mathrm{e}} = -\sqrt{\kappa_{\mathrm{e}}}(\hat{s}_{in}^\dagger\hat{a} + \hat{s}_{\mathrm{in}}\hat{a}^\dagger) - \Delta_C\hat{a}^\dagger\hat{a} \tag{5.4}$$

where $\Delta_C = \omega - \omega_C$ gives the detuning between the input light in the waveguide and the cavity resonance. Since the separations between adjacent atoms are small and comparable to the wavelength of the light, there will be collective dipole-dipole interactions. This can be modeled using the free space dyadic Green's function, and the corresponding Lindblad operator and dipole-dipole exchange Hamiltonian.

The resonant dipole-dipole interaction is described by the imaginary part of the Green's function and is given by

$$\hat{H}_{dd} = \hbar\sum_{\mathrm{i}\neq\mathrm{j}} Im\{G_{\mathrm{ij}}^{FS}\}\hat{\sigma}_{\mathrm{i}}^+\hat{\sigma}_{\mathrm{j}}^- \tag{5.5}$$

The Lindblad term describes the dynamics of the decay and is given by

$$\mathcal{L}_{FS}(\hat{\rho}) = \sum_{\mathrm{i,j}}\left[2Re\{G_{\mathrm{ij}}^{FS}\}\hat{\sigma}_{\mathrm{i}}^-\hat{\rho}\hat{\sigma}_{\mathrm{j}}^+ - Re\{G_{\mathrm{ij}}^{FS}\}\hat{\sigma}_{\mathrm{i}}^+\hat{\sigma}_{\mathrm{j}}^-\hat{\rho} - Re\{G_{\mathrm{ij}}^{FS}\}\hat{\rho}\hat{\sigma}_{\mathrm{i}}^+\hat{\sigma}_{\mathrm{j}}^-\right] \tag{5.6}$$

where the Green's function $g(\mathbf{R})$ is given by

$$G_{\mathrm{ij}}^{FS} = \frac{\Gamma}{2}\left[h_0^{(1)}(kr_{\mathrm{ij}}) + \frac{3(\hat{r_{\mathrm{ij}}}\cdot\hat{q})(\hat{r_{\mathrm{ij}}}\cdot\hat{q}^*)-1}{2}h_2^{(1)}(kr_{\mathrm{ij}})\right] \tag{5.7}$$

where $\hat{q}_{\mathrm{i}}$ is the dipole orientation of the i^{th} atom, $r_{\mathrm{ij}} = |\mathbf{r}_{\mathrm{ij}}|$ is the norm of $\mathbf{r}_{\mathrm{ij}}$, $\hat{r}_{\mathrm{ij}} = \mathbf{r}_{\mathrm{ij}}/r_{\mathrm{ij}}$ is the unit vector along $\mathbf{r}_{\mathrm{ij}}$, Γ is the decay rate of a single atom and $h_l^{(1)}$ are the outgoing spherical Hankel function of angular momentum l. $h_0^{(1)}(x) = \mathrm{e}^{\mathrm{i}x}/(\mathrm{i}x)$ and $h_2^{(1)}(x) = \mathrm{e}^{\mathrm{i}x}(-3\mathrm{i}/x^3 - 3/x^2 + \mathrm{i}/x)$.

Since the cavity dynamics happen at a much faster rate than the internal state dynamics, $(\kappa_{\mathrm{e}}, \kappa_{\mathrm{i}} \approx 100\Gamma)$, the cavity field can be adiabatically eliminated to better capture the dynamics of the internal excitations of the atoms. This will also drastically decrease the computational requirements. By enforcing that the cavity reaches a steady state at every time-step of the internal dynamic evolution, we can arrive at an expression for the $\langle\hat{a}\rangle$ depending on the atomic excitations.

$$\hat{a} = \frac{2\mathrm{i}\sqrt{\kappa_{\mathrm{e}}}}{\kappa}\hat{s}_{in} - \frac{2\mathrm{i}}{\kappa}\sum_{\mathrm{j}} g_{\mathrm{j}}\mathrm{e}^{\mathrm{i}\phi_{\mathrm{j}}}\hat{\sigma}_{\mathrm{j}}^{-} \tag{5.8}$$

By replacing $\hat{a}$ in Eq. 5.1 and Eq. 5.3, we can re-write the master equation in the form,

$$\frac{d\hat{\rho}}{dt} = -\frac{\mathrm{i}}{\hbar}[\hat{H},\hat{\rho}] + \mathcal{L}_{FS}(\hat{\rho}) + \mathcal{L}_C(\hat{\rho}) \tag{5.9}$$

where $\hat{\rho}$ is the density matrix of the system, $\hat{H}$ is the effective Hamiltonian and $\mathcal{L}_{FS}(\hat{\rho})$ is the Lindblad super-operator for the interaction through free space as defined in Eq. (5.6). The interaction of the atoms through the ring resonator cavity is now included from the Lindblad operator $\mathcal{L}_C(\hat{\rho})$ which will be defined as,

$$\mathcal{L}_C(\hat{\rho}) = \sum_{\mathrm{i,j}}\left[2G_{\mathrm{ij}}^C\hat{\sigma}_{\mathrm{i}}^{-}\hat{\rho}\hat{\sigma}_{\mathrm{j}}^{+} - G_{\mathrm{ij}}^C\hat{\sigma}_{\mathrm{i}}^{+}\hat{\sigma}_{\mathrm{j}}^{-}\hat{\rho} - (G_{\mathrm{ij}}^C)^*\hat{\rho}\hat{\sigma}_{\mathrm{i}}^{+}\hat{\sigma}_{\mathrm{j}}^{-}\right] \tag{5.10}$$

The atom-cavity interaction also contains a Hamiltonian part that describes the resonant hopping, similar to Eq. (5.5), and has been absorbed into the Lindblad term for simplicity. The G^C_{ij} is the Green's function of the interaction through the cavity and is given by,

$$G^C_{\mathrm{ij}} = \frac{g_{\mathrm{i}} g^*_{\mathrm{j}}}{\tilde{\kappa}} \mathrm{e}^{\mathrm{i}\mathbf{k}\cdot(\mathbf{r}_{\mathrm{i}}-\mathbf{r}_{\mathrm{j}})n_{eff}} \tag{5.11}$$

where $\tilde{\kappa} = (\kappa_{\mathrm{i}} + \kappa_{\mathrm{e}})/2 - \mathrm{i}\Delta_C$ and g_{j} is the evanescent coupling of the atom with the micro-ring resonator mode, Eq. (5.2), which has an exponential dependence on the z-position. The Hamiltonian defined in Eq. (5.1) and Eq. (5.4) will be redefined in a form similar to the rotating wave laser Hamiltonian

$$\hat{H}_L = \hbar \sum_{\mathrm{j}} \left[-\Delta_A \hat{\sigma}^+_{\mathrm{j}} \hat{\sigma}^-_{\mathrm{j}} + \frac{\Omega_{\mathrm{j}}}{2} \hat{\sigma}^+_{\mathrm{j}} + \frac{\Omega^*_{\mathrm{j}}}{2} \hat{\sigma}^-_{\mathrm{j}} \right] \tag{5.12}$$

where $\Omega_{\mathrm{j}} = \Omega_0 g_{\mathrm{j}} \mathrm{e}^{\mathrm{i}(\mathbf{k}\cdot\mathbf{r}_{\mathrm{j}})n_{eff}}$ is the coupling with each atom is excited due to the evanescent mode of the micro-ring. The Ω_0 can be connected with the waveguide input-output operator in Eq. (5.4) as

$$\Omega_0 = \frac{\mathrm{i}\sqrt{\kappa_{\mathrm{e}}}}{\tilde{\kappa}} |\hat{s_{in}}| \tag{5.13}$$

After adiabatically eliminating the cavity mode, the reduced density matrix, which only describes the atom's internal states will be represented as,

$$\begin{aligned} \rho = a_0 |g\rangle\langle g| + \sum_{\mathrm{j}} v^*_{\mathrm{j}} |g\rangle\langle \mathrm{e_j}| \\ + \sum_{\mathrm{j}} v_{\mathrm{j}} |\mathrm{e_j}\rangle\langle g| + \sum_{\mathrm{i,j}} \tilde{\rho}_{\mathrm{ij}} |\mathrm{e_i}\rangle\langle \mathrm{e_j}| \end{aligned} \tag{5.14}$$

The cavity model and the adiabatically eliminated Lindblad model have both been numerically compared and verified in the weak field limit. An important limitation to adiabatic elimination is that the cavity cannot be in the strong-coupling regime.

An important approximation is that the atoms are stationary within the timescale of the internal excitation decay. This is reasonable since the atoms in the cloud have a mean

velocity of 3 cm/s which corresponds to a couple of nanometers of movement in one excitation lifetime. Hence, to capture the dynamics of the ensemble, we can use Monte Carlo to take the average of many different possible positions for the atoms. In each iteration, the positions of the atoms are randomly assigned according to the configuration of the atom cloud.

The density matrix can then be time-evolved using the master equation shown in Eq. 5.9 with Runge-Kutta methods. Once the system reaches steady state, the transmission ratio can be calculated using the expectation values of the $\langle\hat{\sigma}_{\mathrm{j}}^{-}\rangle$ operator of the atoms using Eq. 5.8.

$$\mathcal{T} = \left|1 - \frac{2\kappa_{\mathrm{e}}}{\kappa} + \frac{2\sqrt{\kappa_{\mathrm{e}}}}{\kappa}\sum_{\mathrm{j}} g_{\mathrm{j}} \mathrm{e}^{\mathrm{i}\phi_{\mathrm{j}}} \langle\hat{\sigma}_{\mathrm{j}}^{-}\rangle\right|^2 \tag{5.15}$$

Time evolving the master equation in this particular scenario can give rise to a few complications in the calculations. Since the atom cloud is considerably dense, the atoms in the random positions could end up being very close to another atom. This will cause the free space Green's function to blow up and go beyond the energy scale of the calculation. Additionally, since these systems tend to have some states with subradiant character, the time to reach steady states is much longer than the timescale of typical excitation decay. These issues make it challenging to reach convergence when using more than a few atoms. Hence, we utilize the low-intensity limit and can derive a procedure to directly calculate the steady state using eigenmode decomposition.

5.2.1 Eigenmodes of the excitation

To understand the characteristics of the system, we can study the eigenmodes of the Green's function of the two different interaction channels. Apart from having a mismatched k-vector, the nature of the Green's function matrices are different.

The Green's function of the atom-cavity interaction is Hermitian because of the chirality of the resonator. If $G_{\mathrm{ij}}^{C} = |G_{\mathrm{ij}}^{C}|\mathrm{e}^{\mathrm{i}\phi}$, then due to the standing wave nature of the resonator mode, $G_{\mathrm{ji}}^{C} = |G_{\mathrm{ij}}^{C}|\mathrm{e}^{\mathrm{i}(2\pi n-\phi)} = |G_{\mathrm{ij}}^{C}|\mathrm{e}^{-\mathrm{i}\phi}$. This results in purely real eigenvalues, meaning none of the eigenmodes of the atom-cavity interaction have any energy shift associated with them. There is only one non-zero eigenmode with decay rate NC_1 and $N-1$ completely

dark subradiant states. These eigenmodes also follow the familiar orthogonality relation $\mathbf{U} \cdot \mathbf{V} = \mathbf{U}^{\dagger}\mathbf{V}$.

On the other hand, the Green's function of the Free space decay is complex-symmetric. This means that $G^{FS}_{\mathrm{ij}} = G^{FS}_{\mathrm{ji}}$. This results in the eigenmodes having a different orthogonality relation $\langle \mathbf{U}, \mathbf{V} \rangle = \mathbf{U}\mathbf{V}$.

The combined Green's function will be neither Hermitian nor Complex-symmetric. This will result in having different left (L) and right eigenvectors (R) and a different orthogonality relation.

$$\begin{aligned} G\mathbf{R}_{\alpha} &= \mathcal{G}_{\alpha}\mathbf{R}_{\alpha} \\ \mathbf{L}^{\dagger}_{\alpha}G &= \mathcal{G}_{\alpha}\mathbf{L}^{\dagger}_{\alpha} \end{aligned} \tag{5.16}$$

where $\mathcal{G}_{\alpha}$ are the eigenvalues of eigenmode α of the full Green's function. The Left and Right eigenvectors $\mathbf{L}_{\alpha}$ and $\mathbf{R}_{\alpha}$ can then be normalized to follow

$$\sum_{\mathrm{j}} \mathbf{L}^{\dagger}_{\mathrm{j}\alpha}\mathbf{R}_{\mathrm{j}\alpha'} = \delta_{\alpha,\alpha'} \tag{5.17}$$

Using this orthogonality relation and solving the master equation Eq. (5.9) for steady state in the low-intensity limit (ignoring terms of order Ω^3), we get

$$v_{\mathrm{i}} = \frac{-\mathrm{i}a_0}{2} \frac{\sum_{\mathrm{j}\alpha} \Omega_{\mathrm{j}}\mathbf{L}^{\dagger}_{\mathrm{j}\alpha}\mathbf{R}_{\mathrm{i}\alpha}}{(\mathcal{G}_{\alpha} - \mathrm{i}\Delta_A)} \tag{5.18}$$

and $\tilde{\rho}_{\mathrm{ij}} = v_{\mathrm{i}}v^{*}_{\mathrm{j}}/a_0$, and the ground state population a_0 can be calculated using $Tr[\rho] = 1$. Using this result to directly calculate the final steady state instead of time propagating the density matrix will provide an exponential speed in the time required to run computations. In the case of pulsed excitation, the state can be directly initialized into a Timed Dicke State with a small population since the pulse time will be too short to cause mixing into any other states.

5.2.2 Rates into the cavity and free space

The rate of photons being emitted into the two channels can be calculated using the quantum jump operator ($\sigma^-\rho\sigma^+$).

$$R_C = \sum_{\mathrm{i,j}} 2G^C_{\mathrm{ij}}\hat{\sigma}^-_{\mathrm{i}}\rho\hat{\sigma}^+_{\mathrm{j}} \tag{5.19}$$

$$R_F = \sum_{\mathrm{i,j}} 2R\mathrm{e}\{G^{FS}_{\mathrm{ij}}\}\hat{\sigma}^-_{\mathrm{i}}\rho\hat{\sigma}^+_{\mathrm{j}} \tag{5.20}$$

Although each eigenstate evolves as an exponential, the rates are a sum of interference of all the eigenmodes. Hence the rates, as well as the total excitation probability do not decay exponentially. The decay rate of the light emitted into the two channels varies over time. In this chapter, the focus will be on the instantaneous decay rate, right after the moment when the drive is turned off in order to study the initial time behaviors of the system. The decay rates into the free space and resonator cavity channels have been defined as

$$\Gamma_F = \frac{R_F}{\langle \mathrm{e} \rangle} \qquad \Gamma_C = \frac{R_C}{\langle \mathrm{e} \rangle} \tag{5.21}$$

where $\langle \mathrm{e} \rangle$ is the total excitation probability in the system.

It is interesting to note that the decay rate into free space is independent of the single atom cooperativity C_1. This is because, at low intensities, the decay rate into free space is solely dependent on the relative phase and the relative amplitude of the excitation on the atoms. Moving the atoms in the z-axis and changing the atom-cavity interaction strength changes neither of the two.

5.3 Results

We consider two main configurations, atoms in a randomly distributed cloud and an array of atoms. The focus of this study will be on the decay characteristics due to emission into free space and into the resonator cavity.

In the experiment, the most reliable measurement that can be made is the rate of photons being emitted into the cavity mode, which can be measured as a change in transmission rate

from the output waveguide. These measurements can be utilized to verify the theoretical calculations, and further calculations can be performed to expand the scope and understanding of the experiment.

The atoms can be excited using either a Gaussian short-timed pulse or can be driven up to steady state. The physics behind both of these situations are considerably different. In the case of the short pulse, the state that the atoms get excited into will be a Timed Dicke State (TDS) with a k-vector corresponding to the resonator mode. Since the pulse time is short, the detuning will also play a negligible role. This will be a superradiant state of the atom-cavity interaction. For decay into free space, the state will have a higher k-vector than k_0, and are typically associated with subradiance.

The system can also be driven until steady state (SS) by using a significantly longer pulse duration. Since there is constant driving, the system is usually pumped into subradiant modes. The detuning will also play an important role in determining which modes are excited.

5.3.1 Evanescent coupling

The atoms couple with the resonator mode through an evanescent coupling. The coupling decreases exponentially with distance from the resonator. The atom's average position along the z-axis depends on the trapping potential, allowing control of the single atom cooperativity C_1. This provides an opportunity for studying the scaling of different parameters as a function of the atom-cavity interaction strength.

With the current capabilities of the experiment, the average position of the atoms can be as close as $400nm$ away from the surface which corresponds to $C_1 \approx 0.05$. In the proposed plan to implement an atom array, the trapping methodology can afford the atoms to be much closer to the resonator waveguide, leading to much higher average cooperativities ($C_1 \sim 10$).

Although the position-dependent coupling can provide an opportunity for controlling the interaction strength, it can also cause issues when it comes to the randomized position of atoms in the cloud. The spread of the atoms in the z-direction due to the trapping potential

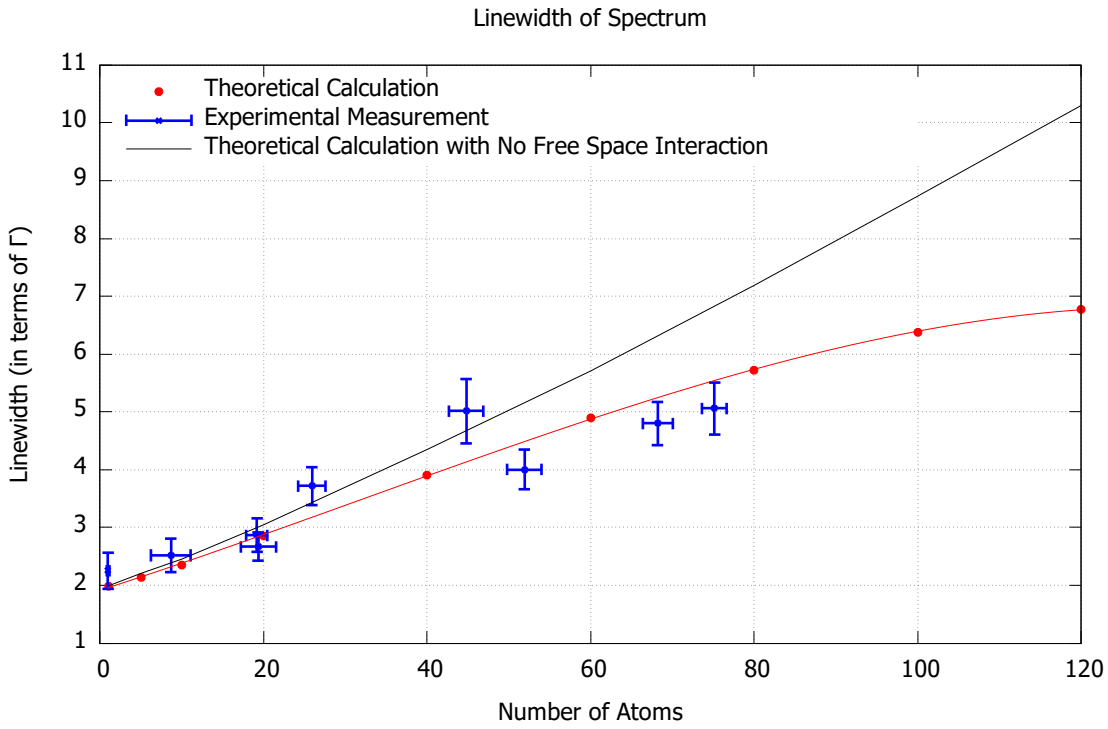

Figure 5.2. The measured and calculated linewidth of the spectrum as a function of number of atoms. Blue points with error bars denote experimental data. Red circles with lines show theoretical calculations. The black line shows the theoretical calculation of the hypothetical situation where there is no free space collective interaction.

will cause a spread in the single-atom cooperativity of the atoms. This is further explored in the context of atom arrays in Sec. 5.3.3

5.3.2 Atom Cloud

In the current state of the experiment, a cloud of atoms is trapped and cooled near the micro-ring resonator. The cloud is shaped almost like a cigar with a lengthwise spread of around $2\mu m$ along the waveguide. In the transverse direction, the cloud is tightly trapped to a spread of around $100nm$. Although the position dependence on the z-direction above the resonator is not Gaussian, it has an approximate spread of $200nm$.

When the atom cloud is excited into a Timed Dicke State (TDS) using a fast pulse of light, it is excited into a state similar to a spin-wave excitation with the k-vector as $\sim 1.7k_0$.

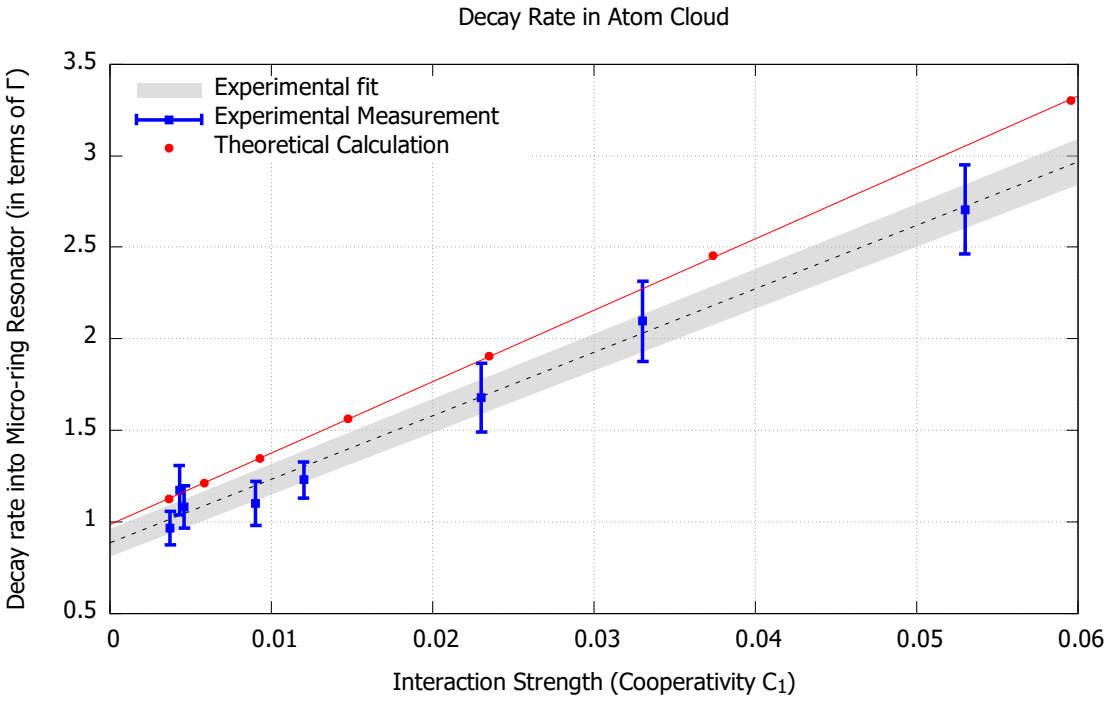

Figure 5.3. Measured and calculated decay rate of R_C as a function of the average single atom cooperativity C_1. Blue squares with error bars denote experimental measurements. Gray shaded area denotes the experimental fit. Red circles with lines denote theoretical calculations.

While one might expect this state to be subradiant to free space, Ref. [105] has shown that for an atom cloud, the smallest decay rate for such high-k states in atom clouds is Γ_0.

The TDS state will be perfectly superradiant to the cavity with a decay rate of $NC_1\Gamma_0$, while having a decay rate of Γ_0 into free space. Therefore, the TDS will excite a state with a total decay rate $(1 + NC_1)\Gamma_0$.

When the atom cloud is excited to Steady State (SS), even though the excitation is with a high k-vector, the state is pumped towards subradiant states. The free space interaction facilitates the mixing between the superradiant state and the completely dark subradiant states of the atom-cavity interaction. The cavity decay rate dips below the superradiant rate of $NC_1\Gamma_0$, but remains larger than the single atom cooperativity of $C_1\Gamma_0$. Although there is a reduction in the superradiance, it is not subradiant with respect to emission into the cavity.

Without the free space interaction, the state will only be excited to the superradiant mode of the atom-cavity interaction and the decay rate will scale as $(1 + NC_1)\Gamma_0$. This is depicted in Fig. 5.2 where the measured and calculated line-width of the spectrum of transmission is shown.

The eigenmodes of the atom-cavity Green's function are purely dissipative and will not contribute to line-shifts. On the other hand, the interaction through free space will contribute to a shift depending on the density of the atoms. Therefore, a shift in the spectrum due to the free-space interaction can be expected. Contrary to expectations, the shifts observed experimentally were an order of magnitude higher than the calculations. Several effects like AC Stark shift, vicinity to a dielectric surface, and motion of the atoms were explored but were unable to explain the discrepancy. Much larger shifts are expected in the case of atom arrays, and clearer answers are expected once they are implemented in the next stage of the experiment.

Although the rate of the photon emission into the output waveguide is the only robust experimental measure, the early time decay rate of the photon rate can also be computed. This is equivalent to calculating the $\langle \dot{R}_c/R_c \rangle$. Fig. 5.3 shows the measurement and calculation of this quantity as a function of the single atom cooperativity C_1.

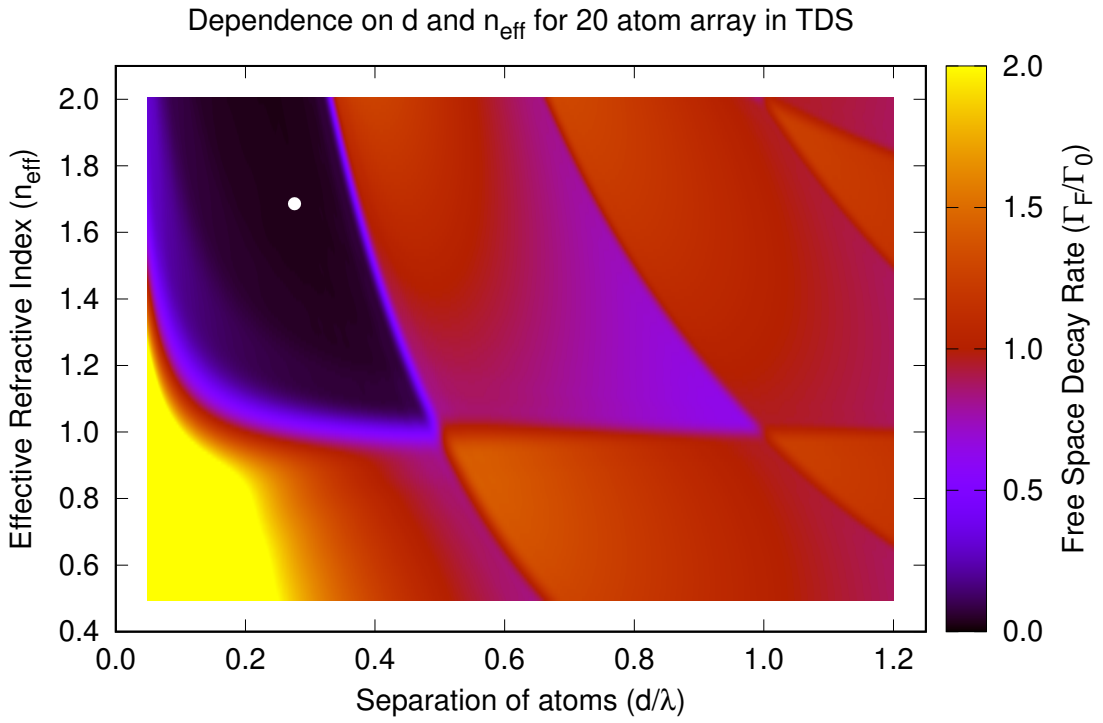

Figure 5.4. The decay rate into free space when a perfect atom array is excited to the TDS through the resonator, as the separation d and effective refractive index n_{eff} are varied. The white point denotes the proposed parameters of the experiment.

In a system with non-exponential decay, the measurement of the rate of decay of the photon rate is not analogous to the measurement of the decay rate. It remains a challenge in experiments to reliably measure the rate of decay in a system. In this particular platform where the interaction strength can be varied and non-exponential decay is present, the discrepancy is much more apparent.

5.3.3 Atom Arrays

Although the system can become subradiant to free space through a steady state excitation in atom clouds, the degree of superradiant interaction with the cavity will also decrease. Timed Dicke States will be more useful in utilizing the full superradiance benefit of this platform. In this section, we explore the potential of atom arrays in reaching subradiance in free space through the simple Timed Dicke State excitation.

The next stage of the experiment involves the implementation of an array of atoms trapped above the ring resonator. The atoms will be trapped using an evanescent field trap, resulting in the atoms being separated by about 0.3λ. This is close to half the wavelength of the high-k excitation mode of the ring resonator. When the atoms are excited through the resonator, it can facilitate almost perfectly subradiant states into free space due to the alternating phases in adjacent atoms.

The higher effective refractive index n_{eff} of the resonator plays a major role in contributing to accessing highly subradiant states in the case of atom arrays. The decay rate into free space as a function of the effective refractive index of the resonator, and the separation of the atom d has been depicted in Fig. 5.4. Although very good subradiance ($\Gamma_F < 0.1$) can only be achieved in the regime of high n_{eff} and separations $d < 0.5\lambda$, there are still other regions where nominal subradiance ($\Gamma_F < 0.5$) can be achieved. As mentioned at the end of Sec. 5.2.2, in the low-intensity limit, Γ_F is only dependent on the relative phase between the atomic excitation and is therefore independent of the single atom cooperativity C_1.

The white dot depicts the proposed parameters of the upcoming experiment. For a perfect array with separation of $d = 0.3\lambda$ and effective refractive index $n_{eff} = 1.69$, the free space decay rate $\Gamma_F = 0.035\Gamma_0$.

Effects of Disorder

Although atom arrays show great promise in achieving subradiance in free space, inevitable defects due to experimental implementations can be limiting. We study how two common sources of imperfection can disturb the perfect coherences that go into making an ideal subradiant state.

The coupling of the cavity mode with the atoms has an exponential dependence on the z-position due to the nature of the evanescent coupling. Thus, the spread in the z-position due to trapping will cause a spread in C_1 of each atom. The randomness in the single atom cooperativity C_1 contributes to another source of decoherence.

In Fig. 5.5(a), the decay rate into free space is plotted as a function of the spread in the z-position of the atoms. In this case, the spread in the other two directions is assumed

to be negligible to isolate the effect of the z-spread. The red squares denote the case when all the atoms have a uniform C_1 and the red squares denote the situation where the C_1 is z-position dependent. Just the spread in position alone can cause decoherence and reduce the degree of subradiance, but the randomness in C_1 causes a much larger effect At $50nm$ spread, the reduction in subradiance into free space due to randomness in C_1 is 8 times larger than the reduction due to randomness in z-position alone. This emphasizes the importance of confining the atom tightly in the z-direction in the case of a system with evanescent coupling.

In Fig. 5.5(b), the effect of the filling fraction of the array is depicted. The atoms are filled in each site with a probability depending on the filling fraction until there are 20 or 40 atoms in the system. This is done to maintain the scaling of the waveguide interaction with the number of atoms. The trend is almost linear, connecting the points from Γ_0 at 0% filling fraction to the minimum possible decay rate at 100% filling fraction. This emphasizes the importance of implementing arrays with a high filling fraction to achieve good subradiance in free space. Even if the state is completely dark for a perfect array, 50% filling fraction can only allow a minimum of $\Gamma_F = 0.5\Gamma_0$.

Circular Array

For the linear array that we have been discussing so far, most of the emission into free space occurs at the ends of the array. Reference [35] has shown an exponential increase in subradiance when using rings. The structure of the micro-ring resonator naturally lends itself to the potential of having a ring of atoms trapped all along the resonator. The evanescent field trap runs throughout the resonator and the atoms can be guided around the ring. Since the atoms are still interacting with the chiral mode, the orientation of the dipole will be along the radial direction.

Figure 5.6 shows the comparison between a linear array and a ring array trapped along the micro-ring resonator. It depicts the decay rate into free space that is achievable using a TDS excitation through the waveguide as a function of the number of atoms in the array.

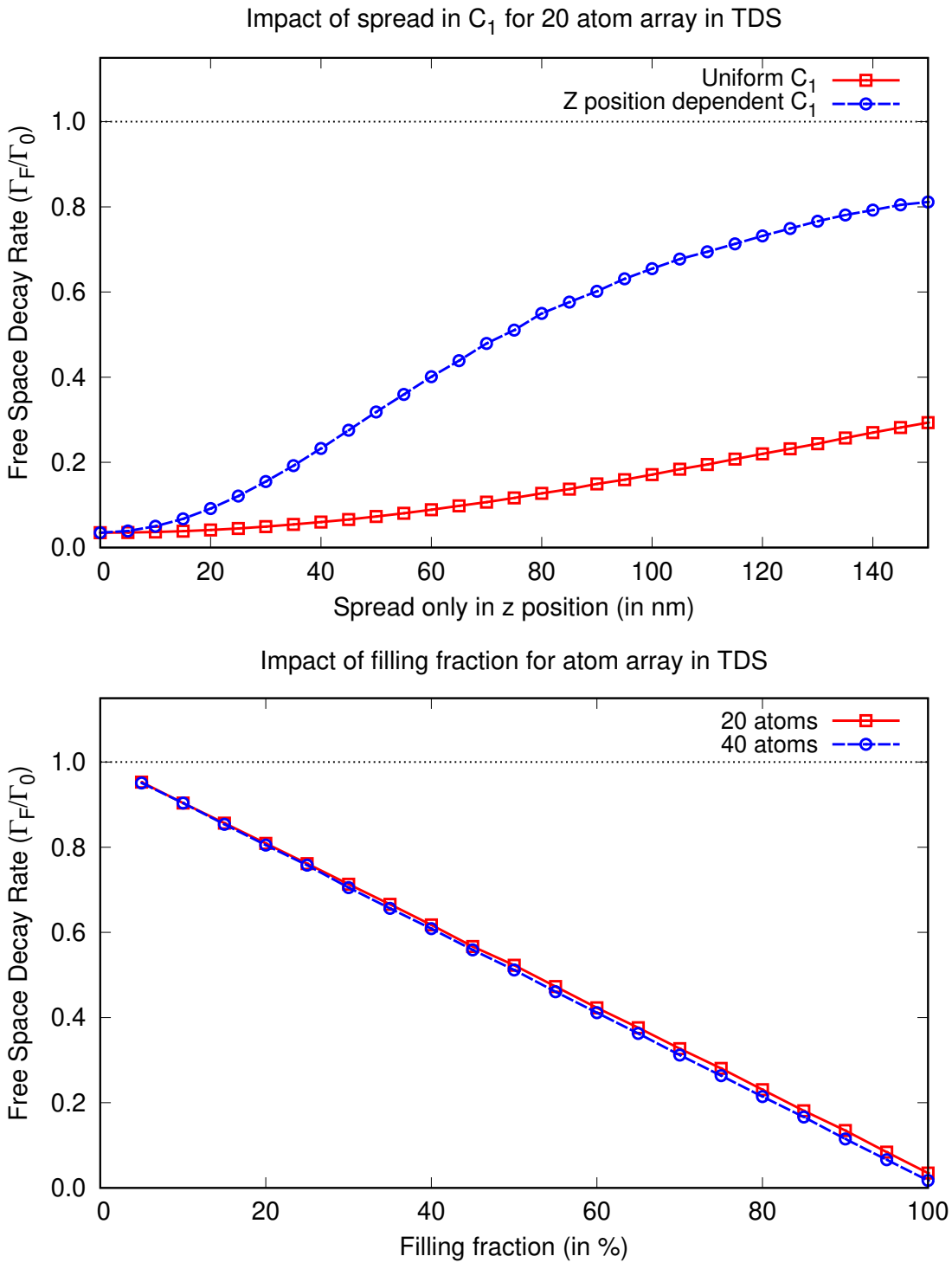

Figure 5.5. Effects of disorder in atom arrays with Times Dicke States. The decay rate into free space has been plotted versus (a) the spread in z-position and (b) the filling fraction.

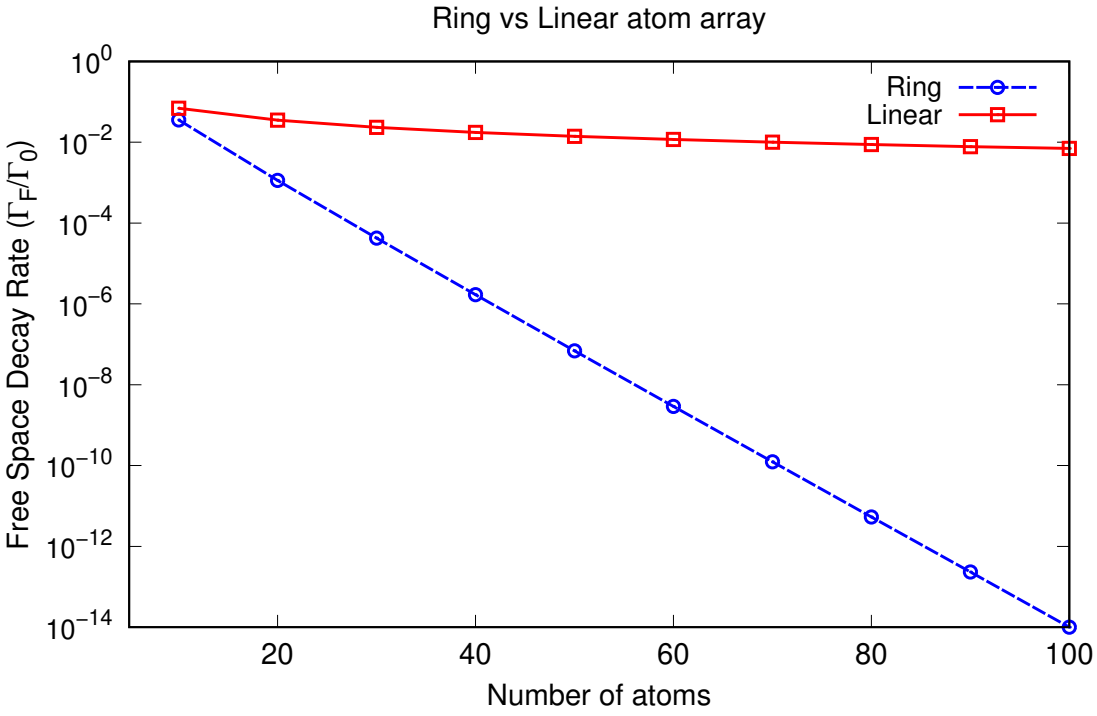

Figure 5.6. The decay rate when excited with a Timed Dicke state for an atom and a ring versus the number of atoms in the array. Red squares denote a linear array and blue circles denote a ring array.

This is similar to Fig 7 in Ref. [35] since we can almost reach the perfect subradiant state with the ring resonator setup and evanescent field traps which use the same high k-vectors.

The ring of atoms can form another whispering gallery mode resulting in minimal loss of photons into free space. The interactions between this mode and the whispering gallery mode of the resonator hold great potential for applications in quantum control and photon storage.

Although there is great promise with a ring due to the exponential scaling, the effects of disorder described in Se. 5.3.3 will play a similar role in limiting the effectiveness of the system.

5.4 Conclusion

We have studied the effects of collective dipole interactions in a system of atoms trapped in the vicinity of a nanophotonic micro-ring resonator. We simulated the current experimental setup to understand the dynamics and to inform potential future research directions. The atoms can interact with each other through two channels, free space and the chiral resonator cavity. The different properties and the mismatched k-vector of the two channels lead to interesting dynamics.

We studied the spectrum and decay rates of a cloud of atoms trapped near the resonator. The atom-cavity interaction has a single superradiant mode with all the other modes being completely dark. When driven to a steady state, the free space interactions can cause mixing between these states and pump the whole system towards subradiance.

We explored the potential of trapping atoms in sub-wavelength arrays along the resonator. We studied the effects of the interplay between the effective refractive index of the waveguide and the separation of the atoms in the array. We explored the effects of potential factors of disorder in experimental implementations. This platform can also be used to form a ring of atoms around the ring resonator to achieve much better scaling on subradiance when compared to linear arrays of atoms.

This versatile light-matter interaction platform holds great potential with its many degrees of control and tunable parameters. Implementing atom arrays will open up the possibil-

ity of ”selective radiance”. Expanding the study to three-level atoms opens new application possibilities, such as EIT and photon storage.

6. SUMMARY AND OUTLOOK

In this thesis, we discussed two published and two to-be-submitted manuscripts that describe the effects of collective dipole interactions in various contexts. In Chap. 2 and Chap. 3, we studied the impact of the recoil in atom arrays when interacting collectively with incident light in various scenarios. The eigenstates of the excitations of an atomic array and its effects on the recoil are studied. The recoil, in certain cases, was found to be proportional to the lifetime of the excitation in the process of collective spontaneous decay. The recoil energy deposited by a single photon emission in a highly subradiant decay was about a thousand times higher than expected. This suggests significant challenges in utilizing subradiant states of atoms for quantum information processing, as it could lead to atoms being expelled from the trap. Further, the effects of the trap frequency and the contributions to the recoil from the different terms of the Lindblad superoperator and the Hamiltonian are studied. In Chap. 4, we study the photon statistics of the emitted light from collectively interacting dipole systems in the low-intensity limit using the double excitation states. We study the properties of the double excitation eigenmodes and how they connect with the single excitation eigenmodes. We explore how the lifetimes of the eigenmodes can impact the initial time correlation $g^{(2)}(0)$ of the emission. In Chap. 5 we explore the experimental system of atoms trapped near a nanophotonic micro-ring resonator and the potential for being used as a versatile light-matter interaction platform. The atoms can interact with each other through two channels, free space and the chiral resonator cavity. We simulate the current experiment involving randomized atom clouds and further explore the potential of ordered atomic arrays.

Collective interactions have increasingly become an important tool for coherent control and quantum manipulation applications. Dense atom arrays have been shown to have exciting applications like coherent control of light, topological states, and quantum information processing. But most of these demand very small inter-atom separations and high trapping frequencies, which can be very hard to achieve with atoms trapped with light. An alternative approach could be exploring other systems like impurities in solid state or quantum dots to overcome these issues. There have been recent engineering advances in creating dense arrays in such systems [106]. While this approach may introduce new challenges, like inhomoge-

neous broadening, the advantage of being able to overcome the issues with atoms trapped in free space, makes it a promising avenue worth investigating.

Although nanophotonic systems are experimentally difficult to work with, there has been considerable progress toward various implementations that can facilitate interactions between atoms. These systems offer stronger interaction between the atoms when compared to just free space. The study of the nanophotonic system discussed has only barely scratched the surface and further work remains for exploring other potential applications.

REFERENCES

[1] R. H. Dicke, "Coherence in spontaneous radiation processes," *Phys. Rev.*, vol. 93, pp. 99–110, 1 Jan. 1954. DOI: 10.1103/PhysRev.93.99. [Online]. Available: https://link.aps.org/doi/10.1103/PhysRev.93.99.

[2] R. J. Bettles, S. A. Gardiner, and C. S. Adams, "Cooperative ordering in lattices of interacting two-level dipoles," *Phys. Rev. A*, vol. 92, p. 063 822, 6 Dec. 2015. DOI: 10.1103/PhysRevA.92.063822. [Online]. Available: https://link.aps.org/doi/10.1103/PhysRevA.92.063822.

[3] N. E. Rehler and J. H. Eberly, "Superradiance," *Phys. Rev. A*, vol. 3, pp. 1735–1751, 5 May 1971. DOI: 10.1103/PhysRevA.3.1735. [Online]. Available: https://link.aps.org/doi/10.1103/PhysRevA.3.1735.

[4] R. Friedberg, S. Hartmann, and J. Manassah, "Frequency shifts in emission and absorption by resonant systems ot two-level atoms," *Physics Reports*, vol. 7, no. 3, pp. 101–179, 1973, ISSN: 0370-1573. DOI: https://doi.org/10.1016/0370-1573(73)90001-X. [Online]. Available: http://www.sciencedirect.com/science/article/pii/037015737390001X.

[5] M. Gross, C. Fabre, P. Pillet, and S. Haroche, "Observation of near-infrared dicke superradiance on cascading transitions in atomic sodium," *Phys. Rev. Lett.*, vol. 36, pp. 1035–1038, 17 Apr. 1976. DOI: 10.1103/PhysRevLett.36.1035. [Online]. Available: https://link.aps.org/doi/10.1103/PhysRevLett.36.1035.

[6] M. O. Scully, "Collective lamb shift in single photon dicke superradiance," *Phys. Rev. Lett.*, vol. 102, p. 143 601, 14 Apr. 2009. DOI: 10.1103/PhysRevLett.102.143601. [Online]. Available: https://link.aps.org/doi/10.1103/PhysRevLett.102.143601.

[7] Z. Meir, O. Schwartz, E. Shahmoon, D. Oron, and R. Ozeri, "Cooperative lamb shift in a mesoscopic atomic array," *Phys. Rev. Lett.*, vol. 113, p. 193 002, 19 Nov. 2014. DOI: 10.1103/PhysRevLett.113.193002. [Online]. Available: https://link.aps.org/doi/10.1103/PhysRevLett.113.193002.

[8] J. Pellegrino, R. Bourgain, S. Jennewein, *et al.*, "Observation of suppression of light scattering induced by dipole-dipole interactions in a cold-atom ensemble," *Phys. Rev. Lett.*, vol. 113, p. 133 602, 13 Sep. 2014. DOI: 10.1103/PhysRevLett.113.133602. [Online]. Available: https://link.aps.org/doi/10.1103/PhysRevLett.113.133602.

[9] A. Browaeys, D. Barredo, and T. Lahaye, "Experimental investigations of dipole–dipole interactions between a few Rydberg atoms," *Journal of Physics B: Atomic, Molecular and Optical Physics*, vol. 49, no. 15, p. 152 001, Jun. 2016. DOI: 10.1088/0953-4075/49/15/152001. [Online]. Available: https://doi.org/10.1088/0953-4075/49/15/152001.

[10] S. L. Bromley, B. Zhu, M. Bishof, *et al.*, "Collective atomic scattering and motional effects in a dense coherent medium," *Nature Communications*, vol. 7, no. 1, p. 11 039, Mar. 2016, ISSN: 2041-1723. DOI: 10.1038/ncomms11039. [Online]. Available: https://doi.org/10.1038/ncomms11039.

[11] D. Plankensteiner, C. Sommer, H. Ritsch, and C. Genes, "Cavity antiresonance spectroscopy of dipole coupled subradiant arrays," *Phys. Rev. Lett.*, vol. 119, p. 093 601, 9 Aug. 2017. DOI: 10.1103/PhysRevLett.119.093601. [Online]. Available: https://link.aps.org/doi/10.1103/PhysRevLett.119.093601.

[12] S. Jennewein, L. Brossard, Y. R. P. Sortais, *et al.*, "Coherent scattering of near-resonant light by a dense, microscopic cloud of cold two-level atoms: Experiment versus theory," *Phys. Rev. A*, vol. 97, p. 053 816, 5 May 2018. DOI: 10.1103/PhysRevA.97.053816. [Online]. Available: https://link.aps.org/doi/10.1103/PhysRevA.97.053816.

[13] P.-O. Guimond, A. Grankin, D. V. Vasilyev, B. Vermersch, and P. Zoller, "Subradiant bell states in distant atomic arrays," *Phys. Rev. Lett.*, vol. 122, p. 093 601, 9 Mar. 2019. DOI: 10.1103/PhysRevLett.122.093601. [Online]. Available: https://link.aps.org/doi/10.1103/PhysRevLett.122.093601.

[14] P. Solano, P. Barberis-Blostein, F. K. Fatemi, L. A. Orozco, and S. L. Rolston, "Superradiance reveals infinite-range dipole interactions through a nanofiber," *Nature Communications*, vol. 8, no. 1, p. 1857, Nov. 2017, ISSN: 2041-1723. DOI: 10.1038/s41467-017-01994-3. [Online]. Available: https://doi.org/10.1038/s41467-017-01994-3.

[15] A. Grankin, P. O. Guimond, D. V. Vasilyev, B. Vermersch, and P. Zoller, "Free-space photonic quantum link and chiral quantum optics," *Phys. Rev. A*, vol. 98, p. 043 825, 4 Oct. 2018. DOI: 10.1103/PhysRevA.98.043825. [Online]. Available: https://link.aps.org/doi/10.1103/PhysRevA.98.043825.

[16] L. F. Buchmann, K. Mølmer, and D. Petrosyan, "Creation and transfer of nonclassical states of motion using rydberg dressing of atoms in a lattice," *Phys. Rev. A*, vol. 95, p. 013 403, 1 Jan. 2017. DOI: 10.1103/PhysRevA.95.013403. [Online]. Available: https://link.aps.org/doi/10.1103/PhysRevA.95.013403.

[17] Y. Wang, X. Zhang, T. A. Corcovilos, A. Kumar, and D. S. Weiss, "Coherent addressing of individual neutral atoms in a 3d optical lattice," *Phys. Rev. Lett.*, vol. 115, p. 043 003, 4 Jul. 2015. DOI: 10.1103/PhysRevLett.115.043003. [Online]. Available: https://link.aps.org/doi/10.1103/PhysRevLett.115.043003.

[18] R. J. Bettles, S. A. Gardiner, and C. S. Adams, "Enhanced optical cross section via collective coupling of atomic dipoles in a 2d array," *Phys. Rev. Lett.*, vol. 116, p. 103 602, 10 Mar. 2016. DOI: 10.1103/PhysRevLett.116.103602. [Online]. Available: https://link.aps.org/doi/10.1103/PhysRevLett.116.103602.

[19] E. Shahmoon, D. S. Wild, M. D. Lukin, and S. F. Yelin, "Cooperative resonances in light scattering from two-dimensional atomic arrays," *Phys. Rev. Lett.*, vol. 118, p. 113 601, 11 Mar. 2017. DOI: 10.1103/PhysRevLett.118.113601. [Online]. Available: https://link.aps.org/doi/10.1103/PhysRevLett.118.113601.

[20] J. P. Clemens, L. Horvath, B. C. Sanders, and H. J. Carmichael, "Collective spontaneous emission from a line of atoms," *Phys. Rev. A*, vol. 68, p. 023 809, 2 Aug. 2003. DOI: 10.1103/PhysRevA.68.023809. [Online]. Available: https://link.aps.org/doi/10.1103/PhysRevA.68.023809.

[21] B. Yan, S. A. Moses, B. Gadway, *et al.*, "Observation of dipolar spin-exchange interactions with lattice-confined polar molecules," *Nature*, vol. 501, no. 7468, pp. 521–525, Sep. 2013, ISSN: 1476-4687. DOI: 10.1038/nature12483. [Online]. Available: https://doi.org/10.1038/nature12483.

[22] V. Mkhitaryan, L. Meng, A. Marini, and F. J. G. de Abajo, "Lasing and amplification from two-dimensional atom arrays," *Phys. Rev. Lett.*, vol. 121, p. 163 602, 16 Oct. 2018. DOI: 10.1103/PhysRevLett.121.163602. [Online]. Available: https://link.aps.org/doi/10.1103/PhysRevLett.121.163602.

[23] S. D. Jenkins, J. Ruostekoski, N. Papasimakis, S. Savo, and N. I. Zheludev, "Many-body subradiant excitations in metamaterial arrays: Experiment and theory," *Phys. Rev. Lett.*, vol. 119, p. 053 901, 5 Aug. 2017. DOI: 10.1103/PhysRevLett.119.053901. [Online]. Available: https://link.aps.org/doi/10.1103/PhysRevLett.119.053901.

[24] R. Bekenstein, I. Pikovski, H. Pichler, E. Shahmoon, S. F. Yelin, and M. D. Lukin, "Quantum metasurfaces with atom arrays," *Nature Physics*, vol. 16, no. 6, pp. 676–681, Jun. 2020, ISSN: 1745-2481. DOI: 10.1038/s41567-020-0845-5. [Online]. Available: https://doi.org/10.1038/s41567-020-0845-5.

[25] D. Barredo, S. de Léséleuc, V. Lienhard, T. Lahaye, and A. Browaeys, "An atom-by-atom assembler of defect-free arbitrary two-dimensional atomic arrays," *Science*, vol. 354, no. 6315, pp. 1021–1023, 2016, ISSN: 0036-8075. DOI: 10.1126/science.aah3778. eprint: https://science.sciencemag.org/content/354/6315/1021.full.pdf. [Online]. Available: https://science.sciencemag.org/content/354/6315/1021.

[26] M. Endres, H. Bernien, A. Keesling, *et al.*, "Atom-by-atom assembly of defect-free one-dimensional cold atom arrays," *Science*, vol. 354, no. 6315, pp. 1024–1027, 2016, ISSN: 0036-8075. DOI: 10.1126/science.aah3752. eprint: https://science.sciencemag.org/content/354/6315/1024.full.pdf. [Online]. Available: https://science.sciencemag.org/content/354/6315/1024.

[27] B. J. Lester, N. Luick, A. M. Kaufman, C. M. Reynolds, and C. A. Regal, "Rapid production of uniformly filled arrays of neutral atoms," *Phys. Rev. Lett.*, vol. 115, p. 073 003, 7 Aug. 2015. DOI: 10.1103/PhysRevLett.115.073003. [Online]. Available: https://link.aps.org/doi/10.1103/PhysRevLett.115.073003.

[28] T. Xia, M. Lichtman, K. Maller, *et al.*, "Randomized benchmarking of single-qubit gates in a 2d array of neutral-atom qubits," *Phys. Rev. Lett.*, vol. 114, p. 100 503, 10 Mar. 2015. DOI: 10.1103/PhysRevLett.114.100503. [Online]. Available: https://link.aps.org/doi/10.1103/PhysRevLett.114.100503.

[29] F. Nogrette, H. Labuhn, S. Ravets, *et al.*, "Single-atom trapping in holographic 2d arrays of microtraps with arbitrary geometries," *Phys. Rev. X*, vol. 4, p. 021 034, 2 May 2014. DOI: 10.1103/PhysRevX.4.021034. [Online]. Available: https://link.aps.org/doi/10.1103/PhysRevX.4.021034.

[30] A. González-Tudela, C.-L. Hung, D. E. Chang, J. I. Cirac, and H. J. Kimble, "Subwavelength vacuum lattices and atom–atom interactions in two-dimensional photonic crystals," *Nature Photonics*, vol. 9, no. 5, pp. 320–325, May 2015, ISSN: 1749-4893. DOI: 10.1038/nphoton.2015.54. [Online]. Available: https://doi.org/10.1038/nphoton.2015.54.

[31] J. Rui, D. Wei, A. Rubio-Abadal, *et al.*, "A subradiant optical mirror formed by a single structured atomic layer," *Nature*, vol. 583, no. 7816, pp. 369–374, Jul. 2020, ISSN: 1476-4687. DOI: 10.1038/s41586-020-2463-x. [Online]. Available: https://doi.org/10.1038/s41586-020-2463-x.

[32] K. E. Ballantine and J. Ruostekoski, "Cooperative optical wavefront engineering with atomic arrays," *Nanophotonics*, vol. 10, no. 7, pp. 1901–1909, 2021. DOI: doi:10.1515/nanoph-2021-0059. [Online]. Available: https://doi.org/10.1515/nanoph-2021-0059.

[33] G. Facchinetti, S. D. Jenkins, and J. Ruostekoski, "Storing light with subradiant correlations in arrays of atoms," *Phys. Rev. Lett.*, vol. 117, p. 243 601, 24 Dec. 2016. DOI: 10.1103/PhysRevLett.117.243601. [Online]. Available: https://link.aps.org/doi/10.1103/PhysRevLett.117.243601.

[34] M. T. Manzoni, M. Moreno-Cardoner, A. Asenjo-Garcia, J. V. Porto, A. V. Gorshkov, and D. E. Chang, "Optimization of photon storage fidelity in ordered atomic arrays," *New Journal of Physics*, vol. 20, no. 8, p. 083 048, Aug. 2018. DOI: 10.1088/1367-2630/aadb74. [Online]. Available: https://doi.org/10.1088/1367-2630/aadb74.

[35] A. Asenjo-Garcia, M. Moreno-Cardoner, A. Albrecht, H. J. Kimble, and D. E. Chang, "Exponential improvement in photon storage fidelities using subradiance and "selective radiance" in atomic arrays," *Phys. Rev. X*, vol. 7, p. 031 024, 3 Aug. 2017. DOI: 10.1103/PhysRevX.7.031024. [Online]. Available: https://link.aps.org/doi/10.1103/PhysRevX.7.031024.

[36] D. E. Chang, V. Vuletić, and M. D. Lukin, "Quantum nonlinear optics — photon by photon," *Nature Photonics*, vol. 8, no. 9, pp. 685–694, Sep. 2014, ISSN: 1749-4893. DOI: 10.1038/nphoton.2014.192. [Online]. Available: https://doi.org/10.1038/nphoton.2014.192.

[37] D. A. B. Miller, "Are optical transistors the logical next step?" *Nature Photonics*, vol. 4, no. 1, pp. 3–5, Jan. 2010, ISSN: 1749-4893. DOI: 10.1038/nphoton.2009.240. [Online]. Available: https://doi.org/10.1038/nphoton.2009.240.

[38] H. J. Kimble, "The quantum internet," *Nature*, vol. 453, no. 7198, pp. 1023–1030, Jun. 2008, ISSN: 1476-4687. DOI: 10.1038/nature07127. [Online]. Available: https://doi.org/10.1038/nature07127.

[39] A. Muthukrishnan, M. O. Scully, and M. S. Zubairy, "Quantum microscopy using photon correlations," *Journal of Optics B: Quantum and Semiclassical Optics*, vol. 6, no. 6, S575, 2004.

[40] V. Giovannetti, S. Lloyd, and L. Maccone, "Advances in quantum metrology," *Nature Photonics*, vol. 5, no. 4, pp. 222–229, Apr. 2011, ISSN: 1749-4893. DOI: 10.1038/nphoton.2011.35. [Online]. Available: https://doi.org/10.1038/nphoton.2011.35.

[41] D. Roy, C. M. Wilson, and O. Firstenberg, "Colloquium: Strongly interacting photons in one-dimensional continuum," *Rev. Mod. Phys.*, vol. 89, p. 021 001, 2 May 2017. DOI: 10.1103/RevModPhys.89.021001. [Online]. Available: https://link.aps.org/doi/10.1103/RevModPhys.89.021001.

[42] Y. Liang and A. Czarnecki, "Photon–photon scattering: A tutorial," *Canadian Journal of Physics*, vol. 90, no. 1, pp. 11–16, 2012. DOI: 10.1139/p11-144. eprint: https://doi.org/10.1139/p11-144. [Online]. Available: https://doi.org/10.1139/p11-144.

[43] V. I. Yudson and P. Reineker, "Multiphoton scattering in a one-dimensional waveguide with resonant atoms," *Phys. Rev. A*, vol. 78, p. 052 713, 5 Nov. 2008. DOI: 10.1103/PhysRevA.78.052713. [Online]. Available: https://link.aps.org/doi/10.1103/PhysRevA.78.052713.

[44] Y. Ke, A. V. Poshakinskiy, C. Lee, Y. S. Kivshar, and A. N. Poddubny, "Inelastic scattering of photon pairs in qubit arrays with subradiant states," *Phys. Rev. Lett.*, vol. 123, p. 253 601, 25 Dec. 2019. DOI: 10.1103/PhysRevLett.123.253601. [Online]. Available: https://link.aps.org/doi/10.1103/PhysRevLett.123.253601.

[45] J.-T. Shen and S. Fan, "Strongly correlated two-photon transport in a one-dimensional waveguide coupled to a two-level system," *Phys. Rev. Lett.*, vol. 98, p. 153 003, 15 Apr. 2007. DOI: 10.1103/PhysRevLett.98.153003. [Online]. Available: https://link.aps.org/doi/10.1103/PhysRevLett.98.153003.

[46] A. S. Prasad, J. Hinney, S. Mahmoodian, *et al.*, "Correlating photons using the collective nonlinear response of atoms weakly coupled to an optical mode," *Nature Photonics*, vol. 14, no. 12, pp. 719–722, Dec. 2020, ISSN: 1749-4893. DOI: 10.1038/s41566-020-0692-z. [Online]. Available: https://doi.org/10.1038/s41566-020-0692-z.

[47] A. S. Sheremet, M. I. Petrov, I. V. Iorsh, A. V. Poshakinskiy, and A. N. Poddubny, "Waveguide quantum electrodynamics: Collective radiance and photon-photon correlations," *Rev. Mod. Phys.*, vol. 95, p. 015 002, 1 Mar. 2023. DOI: 10.1103/RevModPhys.95.015002. [Online]. Available: https://link.aps.org/doi/10.1103/RevModPhys.95.015002.

[48] H. Zheng and H. U. Baranger, "Persistent quantum beats and long-distance entanglement from waveguide-mediated interactions," *Phys. Rev. Lett.*, vol. 110, p. 113 601, 11 Mar. 2013. DOI: 10.1103/PhysRevLett.110.113601. [Online]. Available: https://link.aps.org/doi/10.1103/PhysRevLett.110.113601.

[49] A. Albrecht, L. Henriet, A. Asenjo-Garcia, P. B. Dieterle, O. Painter, and D. E. Chang, "Subradiant states of quantum bits coupled to a one-dimensional waveguide," *New Journal of Physics*, vol. 21, no. 2, p. 025 003, 2019.

[50] Y.-X. Zhang and K. Mølmer, "Theory of subradiant states of a one-dimensional two-level atom chain," *Phys. Rev. Lett.*, vol. 122, p. 203 605, 20 May 2019. DOI: 10.1103/PhysRevLett.122.203605. [Online]. Available: https://link.aps.org/doi/10.1103/PhysRevLett.122.203605.

[51] J. Zhong, N. A. Olekhno, Y. Ke, *et al.*, "Photon-mediated localization in two-level qubit arrays," *Phys. Rev. Lett.*, vol. 124, p. 093 604, 9 Mar. 2020. DOI: 10.1103/PhysRevLett.124.093604. [Online]. Available: https://link.aps.org/doi/10.1103/PhysRevLett.124.093604.

[52] Y.-X. Zhang, C. Yu, and K. Mølmer, "Subradiant bound dimer excited states of emitter chains coupled to a one dimensional waveguide," *Phys. Rev. Res.*, vol. 2, p. 013 173, 1 Feb. 2020. DOI: 10.1103/PhysRevResearch.2.013173. [Online]. Available: https://link.aps.org/doi/10.1103/PhysRevResearch.2.013173.

[53] A. N. Poddubny, "Quasiflat band enabling subradiant two-photon bound states," *Phys. Rev. A*, vol. 101, p. 043 845, 4 Apr. 2020. DOI: 10.1103/PhysRevA.101.043845. [Online]. Available: https://link.aps.org/doi/10.1103/PhysRevA.101.043845.

[54] Y. Marques, I. A. Shelykh, and I. V. Iorsh, "Bound photonic pairs in 2d waveguide quantum electrodynamics," *Phys. Rev. Lett.*, vol. 127, p. 273 602, 27 Dec. 2021. DOI: 10.1103/PhysRevLett.127.273602. [Online]. Available: https://link.aps.org/doi/10.1103/PhysRevLett.127.273602.

[55] A. V. Poshakinskiy and A. N. Poddubny, "Bound state of distant photons in waveguide quantum electrodynamics," *Phys. Rev. A*, vol. 108, p. 023 707, 2 Aug. 2023. DOI: 10.1103/PhysRevA.108.023707. [Online]. Available: https://link.aps.org/doi/10.1103/PhysRevA.108.023707.

[56] N. Fayard, I. Ferrier-Barbut, A. Browaeys, and J.-J. Greffet, "Optical control of collective states in one-dimensional ordered atomic chains beyond the linear regime," *Phys. Rev. A*, vol. 108, p. 023 116, 2 Aug. 2023. DOI: 10.1103/PhysRevA.108.023116. [Online]. Available: https://link.aps.org/doi/10.1103/PhysRevA.108.023116.

[57] A. Juan-Delgado, R. Esteban, Á. Nodar, J.-B. Trebbia, B. Lounis, and J. Aizpurua, "Tailoring the statistics of light emitted from two interacting quantum emitters," *Phys. Rev. Res.*, vol. 6, p. 023 207, 2 May 2024. DOI: 10.1103/PhysRevResearch.6.023207. [Online]. Available: https://link.aps.org/doi/10.1103/PhysRevResearch.6.023207.

[58] F. Le Kien and A. Rauschenbeutel, "Nanofiber-mediated chiral radiative coupling between two atoms," *Phys. Rev. A*, vol. 95, p. 023 838, 2 Feb. 2017. DOI: 10.1103/PhysRevA.95.023838. [Online]. Available: https://link.aps.org/doi/10.1103/PhysRevA.95.023838.

[59] R. Pennetta, M. Blaha, A. Johnson, *et al.*, "Collective radiative dynamics of an ensemble of cold atoms coupled to an optical waveguide," *Phys. Rev. Lett.*, vol. 128, p. 073 601, 7 Feb. 2022. DOI: 10.1103/PhysRevLett.128.073601. [Online]. Available: https://link.aps.org/doi/10.1103/PhysRevLett.128.073601.

[60] R. Pennetta, D. Lechner, M. Blaha, A. Rauschenbeutel, P. Schneeweiss, and J. Volz, "Observation of coherent coupling between super- and subradiant states of an ensemble of cold atoms collectively coupled to a single propagating optical mode," *Phys. Rev. Lett.*, vol. 128, p. 203 601, 20 May 2022. DOI: 10.1103/PhysRevLett.128.203601. [Online]. Available: https://link.aps.org/doi/10.1103/PhysRevLett.128.203601.

[61] C. Liedl, S. Pucher, F. Tebbenjohanns, P. Schneeweiss, and A. Rauschenbeutel, "Collective radiation of a cascaded quantum system: From timed dicke states to inverted ensembles," *Phys. Rev. Lett.*, vol. 130, p. 163 602, 16 Apr. 2023. DOI: 10.1103/PhysRevLett.130.163602. [Online]. Available: https://link.aps.org/doi/10.1103/PhysRevLett.130.163602.

[62] C. Liedl, F. Tebbenjohanns, C. Bach, S. Pucher, A. Rauschenbeutel, and P. Schneeweiss, "Observation of superradiant bursts in a cascaded quantum system," *Phys. Rev. X*, vol. 14, p. 011 020, 1 Feb. 2024. DOI: 10.1103/PhysRevX.14.011020. [Online]. Available: https://link.aps.org/doi/10.1103/PhysRevX.14.011020.

[63] C. Bach, F. Tebbenjohanns, C. Liedl, P. Schneeweiss, and A. Rauschenbeutel, *Emergence of second-order coherence in superfluorescence*, 2024. arXiv: 2407.12549 [quant-ph]. [Online]. Available: https://arxiv.org/abs/2407.12549.

[64] D. Su, Y. Jiang, S. Cardenas-Lopez, *et al.*, "Dynamical beats of short pulses in waveguide qed," *Phys. Rev. Res.*, vol. 5, p. L042041, 4 Dec. 2023. DOI: 10.1103/PhysRevResearch.5.L042041. [Online]. Available: https://link.aps.org/doi/10.1103/PhysRevResearch.5.L042041.

[65] A. Goban, C.-L. Hung, J. D. Hood, *et al.*, "Superradiance for atoms trapped along a photonic crystal waveguide," *Phys. Rev. Lett.*, vol. 115, p. 063 601, 6 Aug. 2015. DOI: 10.1103/PhysRevLett.115.063601. [Online]. Available: https://link.aps.org/doi/10.1103/PhysRevLett.115.063601.

[66] J. D. Hood, A. Goban, A. Asenjo-Garcia, *et al.*, "Atom–atom interactions around the band edge of a photonic crystal waveguide," *Proceedings of the National Academy of Sciences*, vol. 113, no. 38, pp. 10 507–10 512, 2016. DOI: 10.1073/pnas.1603788113. eprint: https://www.pnas.org/doi/pdf/10.1073/pnas.1603788113. [Online]. Available: https://www.pnas.org/doi/abs/10.1073/pnas.1603788113.

[67] R. Ritter, N. Gruhler, H. Dobbertin, *et al.*, "Coupling thermal atomic vapor to slot waveguides," *Phys. Rev. X*, vol. 8, p. 021 032, 2 May 2018. DOI: 10.1103/PhysRevX.8.021032. [Online]. Available: https://link.aps.org/doi/10.1103/PhysRevX.8.021032.

[68] H. Alaeian, A. Skljarow, S. Scheel, T. Pfau, and R. Löw, "Manipulating the dipolar interactions and cooperative effects in confined geometries," *New Journal of Physics*, vol. 26, no. 5, p. 055 001, 2024.

[69] R. Jones, J. A. Needham, I. Lesanovsky, F. Intravaia, and B. Olmos, "Modified dipole-dipole interaction and dissipation in an atomic ensemble near surfaces," *Phys. Rev. A*, vol. 97, p. 053 841, 5 May 2018. DOI: 10.1103/PhysRevA.97.053841. [Online]. Available: https://link.aps.org/doi/10.1103/PhysRevA.97.053841.

[70] M. B. M. Svendsen and B. Olmos, "Modified dipole-dipole interactions in the presence of a nanophotonic waveguide," *Quantum*, vol. 7, p. 1091, Aug. 2023, ISSN: 2521-327X. DOI: 10.22331/q-2023-08-22-1091. [Online]. Available: https://doi.org/10.22331/q-2023-08-22-1091.

[71] S. Cardenas-Lopez, P. Solano, L. A. Orozco, and A. Asenjo-Garcia, "Optical precursors in waveguide quantum electrodynamics," *Phys. Rev. Res.*, vol. 5, p. 013 133, 1 Feb. 2023. DOI: 10.1103/PhysRevResearch.5.013133. [Online]. Available: https://link.aps.org/doi/10.1103/PhysRevResearch.5.013133.

[72] K. M. Maller, M. T. Lichtman, T. Xia, *et al.*, "Rydberg-blockade controlled-not gate and entanglement in a two-dimensional array of neutral-atom qubits," *Phys. Rev. A*, vol. 92, p. 022 336, 2 Aug. 2015. DOI: 10.1103/PhysRevA.92.022336. [Online]. Available: https://link.aps.org/doi/10.1103/PhysRevA.92.022336.

[73] Y. Wang, A. Kumar, T.-Y. Wu, and D. S. Weiss, "Single-qubit gates based on targeted phase shifts in a 3d neutral atom array," *Science*, vol. 352, no. 6293, pp. 1562–1565, 2016, ISSN: 0036-8075. DOI: 10.1126/science.aaf2581. eprint: https://science.sciencemag.org/content/352/6293/1562.full.pdf. [Online]. Available: https://science.sciencemag.org/content/352/6293/1562.

[74] E. Shahmoon, M. D. Lukin, and S. F. Yelin, "Quantum optomechanics of a two-dimensional atomic array," *Phys. Rev. A*, vol. 101, p. 063 833, 6 Jun. 2020. DOI: 10.1103/PhysRevA.101.063833. [Online]. Available: https://link.aps.org/doi/10.1103/PhysRevA.101.063833.

[75] F. Robicheaux and S. Huang, "Atom recoil during coherent light scattering from many atoms," *Phys. Rev. A*, vol. 99, p. 013 410, 1 Jan. 2019. DOI: 10.1103/PhysRevA.99.013410. [Online]. Available: https://link.aps.org/doi/10.1103/PhysRevA.99.013410.

[76] H. Carmichael, *An open systems approach to quantum optics: lectures presented at the Université Libre de Bruxelles, October 28 to November 4, 1991*. Springer Science & Business Media, 2009, vol. 18.

[77] M. B. Plenio and P. L. Knight, "The quantum-jump approach to dissipative dynamics in quantum optics," *Rev. Mod. Phys.*, vol. 70, pp. 101–144, 1 Jan. 1998. DOI: 10.1103/RevModPhys.70.101. [Online]. Available: https://link.aps.org/doi/10.1103/RevModPhys.70.101.

[78] A. J. Daley, "Quantum trajectories and open many-body quantum systems," *Advances in Physics*, vol. 63, no. 2, pp. 77–149, 2014. DOI: 10.1080/00018732.2014.933502. eprint: https://doi.org/10.1080/00018732.2014.933502. [Online]. Available: https://doi.org/10.1080/00018732.2014.933502.

[79] J. Dalibard, Y. Castin, and K. Mølmer, "Wave-function approach to dissipative processes in quantum optics," *Phys. Rev. Lett.*, vol. 68, pp. 580–583, 5 Feb. 1992. DOI: 10.1103/PhysRevLett.68.580. [Online]. Available: https://link.aps.org/doi/10.1103/PhysRevLett.68.580.

[80] R. Dum, P. Zoller, and H. Ritsch, "Monte carlo simulation of the atomic master equation for spontaneous emission," *Phys. Rev. A*, vol. 45, pp. 4879–4887, 7 Apr. 1992. DOI: 10.1103/PhysRevA.45.4879. [Online]. Available: https://link.aps.org/doi/10.1103/PhysRevA.45.4879.

[81] K. Mølmer, Y. Castin, and J. Dalibard, "Monte carlo wave-function method in quantum optics," *J. Opt. Soc. Am. B*, vol. 10, no. 3, pp. 524–538, Mar. 1993. DOI: 10.1364/JOSAB.10.000524. [Online]. Available: https://opg.optica.org/josab/abstract.cfm?URI=josab-10-3-524.

[82] R. Dum, A. S. Parkins, P. Zoller, and C. W. Gardiner, "Monte carlo simulation of master equations in quantum optics for vacuum, thermal, and squeezed reservoirs," *Phys. Rev. A*, vol. 46, pp. 4382–4396, 7 Oct. 1992. DOI: 10.1103/PhysRevA.46.4382. [Online]. Available: https://link.aps.org/doi/10.1103/PhysRevA.46.4382.

[83] G. Lindblad, "On the generators of quantum dynamical semigroups," *Communications in mathematical physics*, vol. 48, pp. 119–130, 1976.

[84] C. W. Gardiner and M. J. Collett, "Input and output in damped quantum systems: Quantum stochastic differential equations and the master equation," *Phys. Rev. A*, vol. 31, pp. 3761–3774, 6 Jun. 1985. DOI: 10.1103/PhysRevA.31.3761. [Online]. Available: https://link.aps.org/doi/10.1103/PhysRevA.31.3761.

[85] R. T. Sutherland, "Coherent radiation in atomic systems," Ph.D. dissertation, Purdue University, 2017.

[86] D. A. Suresh and F. Robicheaux, "Photon-induced atom recoil in collectively interacting planar arrays," *Phys. Rev. A*, vol. 103, p. 043 722, 4 Apr. 2021. DOI: 10.1103/PhysRevA.103.043722. [Online]. Available: https://link.aps.org/doi/10.1103/PhysRevA.103.043722.

[87] D. A. Suresh and F. Robicheaux, "Atom recoil in collectively interacting dipoles using quantized vibrational states," *Phys. Rev. A*, vol. 105, p. 033 706, 3 Mar. 2022. DOI: 10.1103/PhysRevA.105.033706. [Online]. Available: https://link.aps.org/doi/10.1103/PhysRevA.105.033706.

[88] E. Shahmoon, M. D. Lukin, and S. F. Yelin, "Chapter one - collective motion of an atom array under laser illumination," in ser. Advances In Atomic, Molecular, and Optical Physics, L. F. Dimauro, H. Perrin, and S. F. Yelin, Eds., vol. 68, Academic Press, 2019, pp. 1–38. DOI: https://doi.org/10.1016/bs.aamop.2019.03.001. [Online]. Available: https://www.sciencedirect.com/science/article/pii/S1049250X19300011.

[89] S. J. Masson and A. Asenjo-Garcia, "Universality of dicke superradiance in arrays of quantum emitters," *Nature Communications*, vol. 13, no. 1, p. 2285, Apr. 2022, ISSN: 2041-1723. DOI: 10.1038/s41467-022-29805-4. [Online]. Available: https://doi.org/10.1038/s41467-022-29805-4.

[90] F. Robicheaux, "Theoretical study of early-time superradiance for atom clouds and arrays," *Phys. Rev. A*, vol. 104, p. 063 706, 6 Dec. 2021. DOI: 10.1103/PhysRevA.104.063706. [Online]. Available: https://link.aps.org/doi/10.1103/PhysRevA.104.063706.

[91] N. Ustimenko, D. Kornovan, I. Volkov, A. Sheremet, R. Savelev, and M. Petrov, *Nonradiant multiphoton states in quantum ring oligomers*, 2024. arXiv: 2309.14461 [quant-ph]. [Online]. Available: https://arxiv.org/abs/2309.14461.

[92] X. Zhou, H. Tamura, T.-H. Chang, and C.-L. Hung, "Coupling single atoms to a nanophotonic whispering-gallery-mode resonator via optical guiding," *Phys. Rev. Lett.*, vol. 130, p. 103 601, 10 Mar. 2023. DOI: 10.1103/PhysRevLett.130.103601. [Online]. Available: https://link.aps.org/doi/10.1103/PhysRevLett.130.103601.

[93] X. Zhou, H. Tamura, T.-H. Chang, and C.-L. Hung, "Trapped atoms and superradiance on an integrated nanophotonic microring circuit," *Phys. Rev. X*, vol. 14, p. 031 004, 3 Jul. 2024. DOI: 10.1103/PhysRevX.14.031004. [Online]. Available: https://link.aps.org/doi/10.1103/PhysRevX.14.031004.

[94] A. V. Gorshkov, A. André, M. Fleischhauer, A. S. Sørensen, and M. D. Lukin, "Universal approach to optimal photon storage in atomic media," *Phys. Rev. Lett.*, vol. 98, p. 123 601, 12 Mar. 2007. DOI: 10.1103/PhysRevLett.98.123601. [Online]. Available: https://link.aps.org/doi/10.1103/PhysRevLett.98.123601.

[95] A. Gonzalez-Tudela, D. Martin-Cano, E. Moreno, L. Martin-Moreno, C. Tejedor, and F. J. Garcia-Vidal, "Entanglement of two qubits mediated by one-dimensional plasmonic waveguides," *Phys. Rev. Lett.*, vol. 106, p. 020 501, 2 Jan. 2011. DOI: 10.1103/PhysRevLett.106.020501. [Online]. Available: https://link.aps.org/doi/10.1103/PhysRevLett.106.020501.

[96] T. Ramos, H. Pichler, A. J. Daley, and P. Zoller, "Quantum spin dimers from chiral dissipation in cold-atom chains," *Phys. Rev. Lett.*, vol. 113, p. 237 203, 23 Dec. 2014. DOI: 10.1103/PhysRevLett.113.237203. [Online]. Available: https://link.aps.org/doi/10.1103/PhysRevLett.113.237203.

[97] H. Pichler, T. Ramos, A. J. Daley, and P. Zoller, "Quantum optics of chiral spin networks," *Phys. Rev. A*, vol. 91, p. 042 116, 4 Apr. 2015. DOI: 10.1103/PhysRevA.91.042116. [Online]. Available: https://link.aps.org/doi/10.1103/PhysRevA.91.042116.

[98] T. Ramos, B. Vermersch, P. Hauke, H. Pichler, and P. Zoller, "Non-markovian dynamics in chiral quantum networks with spins and photons," *Phys. Rev. A*, vol. 93, p. 062 104, 6 Jun. 2016. DOI: 10.1103/PhysRevA.93.062104. [Online]. Available: https://link.aps.org/doi/10.1103/PhysRevA.93.062104.

[99] K. Stannigel, P. Rabl, and P. Zoller, "Driven-dissipative preparation of entangled states in cascaded quantum-optical networks," *New Journal of Physics*, vol. 14, no. 6, p. 063 014, 2012.

[100] V. Paulisch, H. Kimble, and A. González-Tudela, "Universal quantum computation in waveguide qed using decoherence free subspaces," *New Journal of Physics*, vol. 18, no. 4, p. 043 041, 2016.

[101] A. González-Tudela, V. Paulisch, D. E. Chang, H. J. Kimble, and J. I. Cirac, "Deterministic generation of arbitrary photonic states assisted by dissipation," *Phys. Rev. Lett.*, vol. 115, p. 163 603, 16 Oct. 2015. DOI: 10.1103/PhysRevLett.115.163603. [Online]. Available: https://link.aps.org/doi/10.1103/PhysRevLett.115.163603.

[102] A. González-Tudela, V. Paulisch, H. J. Kimble, and J. I. Cirac, "Efficient multiphoton generation in waveguide quantum electrodynamics," *Phys. Rev. Lett.*, vol. 118, p. 213 601, 21 May 2017. DOI: 10.1103/PhysRevLett.118.213601. [Online]. Available: https://link.aps.org/doi/10.1103/PhysRevLett.118.213601.

[103] Y.-X. Zhang, "Zeno regime of collective emission: Non-markovianity beyond retardation," *Phys. Rev. Lett.*, vol. 131, p. 193 603, 19 Nov. 2023. DOI: 10.1103/PhysRevLett.131.193603. [Online]. Available: https://link.aps.org/doi/10.1103/PhysRevLett.131.193603.

[104] Y.-X. Zhang and K. Mølmer, "Subradiant emission from regular atomic arrays: Universal scaling of decay rates from the generalized bloch theorem," *Phys. Rev. Lett.*, vol. 125, p. 253 601, 25 Dec. 2020. DOI: 10.1103/PhysRevLett.125.253601. [Online]. Available: https://link.aps.org/doi/10.1103/PhysRevLett.125.253601.

[105] S. Grava, Y. He, S. Wu, and D. E. Chang, "Renormalization group analysis of near-field induced dephasing of optical spin waves in an atomic medium," *New Journal of Physics*, vol. 24, no. 1, p. 013 031, 2022.

[106] I. S. Han, Y.-R. Wang, and M. Hopkinson, "Ordered GaAs quantum dots by droplet epitaxy using in situ direct laser interference patterning," *Applied Physics Letters*, vol. 118, no. 14, p. 142 101, Apr. 2021, ISSN: 0003-6951. DOI: 10.1063/5.0045817. eprint: https://pubs.aip.org/aip/apl/article-pdf/doi/10.1063/5.0045817/14545775/142101_1_online.pdf. [Online]. Available: https://doi.org/10.1063/5.0045817.